

Naval Environmental Prediction Research Facility
Monterey, CA 93943-5006



Contractor Report CR 88-11 June 1988

FORECASTERS HANDBOOK FOR JAPAN AND ADJACENT SEA AREAS

607483

Distribution A: Approved for
Public Release, distribution is
unlimited per Naval Meteorology
& Oceanography command memo
SER 01/011 Jan. 31, 2007, F. FURZE,
CHIEF OF STAFF

~~DISTRIBUTION AUTHORIZED TO U.S. GOVERNMENT AGENCIES AND
THEIR CONTRACTORS; ADMINISTRATIVE OR OPERATIONAL USE;
16 JUNE 1988. OTHER REQUESTS FOR THIS DOCUMENT SHALL BE
REFERRED TO COMMANDER, NAVAL OCEANOGRAPHY COMMAND.~~

Feb 01 07 01:37p

COMNAVMETOCCOM

12200003037



DEPARTMENT OF THE NAVY

COMMANDER

NAVAL METEOROLOGY AND OCEANOGRAPHY COMMAND

1100 BALCH BOULEVARD

STENNIS SPACE CENTER MS 39529-5005

5000

Ser 01/011

31 JAN 2007

From: Commander, Naval Meteorology and Oceanography Command
To: Superintendent, Naval Research Laboratory Monterey

Subj: PUBLIC RELEASE OF FORECASTERS HANDBOOK

Ref: (a) PHONCON NRL Monterey (Mr. Sam Brand) and COMNAVMETOCCOM
(Ms. Judy Dauro) of 18 Dec 06

Encl: (1) Forecasters Handbook for Japan and Adjacent Sea Areas

1. Per your request in reference (a) to convert the hardcopy publications of enclosure (1) into an electronic format, approval is granted. After reviewing the handbook that was published in 1988 with limited distribution, we have determined that information pertaining to electro-optical conditions and statistical information is no longer sensitive. This document is hereby approved for public release, distribution unlimited.

2. For further information, contact Judy Dauro, International Programs Analyst, at Commercial 228-688-4677 or DSN 828-4677.

A handwritten signature in black ink, appearing to read "Peter W. Furze".

PETER W. FURZE
Chief of Staff

UNCLASSIFIED

SECURITY CLASSIFICATION OF THIS PAGE

**Distribution A: Approved for
Public Release, distribution is
unlimited per Naval Meteorology
& Oceanography command memo
SER 01/011 Jan. 31, 2007**

REPORT DOCUMENTARY

1a. REPORT SECURITY CLASSIFICATION UNCLASSIFIED		1b. RESTRICTIONS	
2a. SECURITY CLASSIFICATION AUTHORITY		3. DISTRIBUTION / AVAILABILITY OF REPORT Distribution authorized for U.S. Government agencies and contractors; administrative or operational use; 16 June 1988. Other requests for this document shall be referred to Commander, Naval Oceanography Command.	
2b. DECLASSIFICATION / DOWNGRADING SCHEDULE			
4. PERFORMING ORGANIZATION REPORT NUMBER(S)		5. MONITORING ORGANIZATION REPORT NUMBER(S) CR 88-11	
6a. NAME OF PERFORMING ORGANIZATION Science Applications International Corporation	6b. OFFICE SYMBOL (if applicable)	7a. NAME OF MONITORING ORGANIZATION Naval Environmental Prediction Research Facility	
6c. ADDRESS (City, State, and ZIP Code) 205 Montecito Ave., Monterey, CA 93940		7b. ADDRESS (City, State, and ZIP Code) Monterey, CA 93943-5006	
8a. NAME OF FUNDING / SPONSORING ORGANIZATION Commander, Naval Oceanography Command	8b. OFFICE SYMBOL (if applicable)	9. PROCUREMENT INSTRUMENT IDENTIFICATION NUMBER N00228-84-C-3183	
8c. ADDRESS (City, State, and ZIP Code) Bay St. Louis, MS 39529		10. SOURCE OF FUNDING NUMBERS	
		PROGRAM ELEMENT NO. OM&N-1	PROJECT NO.
		TASK NO.	WORK UNIT ACCESSION NO. DN656794
11. TITLE (Include Security Classification) Forecasters Handbook for Japan and Adjacent Sea Areas (U)			
12. PERSONAL AUTHOR(S) Englebretson, Ronald E. and Gilmore, Richard D.			
13a. TYPE OF REPORT Final	13b. TIME COVERED FROM 9/15/84 TO 1/31/87	14. DATE OF REPORT (Year, Month, Day) 1988, June	15. PAGE COUNT 659
16. SUPPLEMENTARY NOTATION			
17. COSATI CODES			18. SUBJECT TERMS (Continue on reverse if necessary and identify by block number) Sea of Japan Philippine Sea East China Sea Sea of Okhotsk Yellow Sea Western North Pacific Ocean
FIELD	GROUP	SUB-GROUP	
04	02		
19. ABSTRACT (Continue on reverse if necessary and identify by block number) Weather conditions for the Sea of Japan, East China Sea, Yellow Sea, Sea of Okhotsk, Philippine Sea and western North Pacific Ocean (W of 160 deg E) are examined. Each of these regions is addressed separately with information directed toward operational forecasters. A general overview chapter provides seasonal climatology charts for the entire area. In most cases, satellite imagery examples are included in discussions of particular weather conditions. These examples provide references for various seasonal atmospheric and oceanic synoptic scale features. Also included are numerous forecast rules that have direct application to naval operational planning. Appendices provide information on local geographic terminology, tropical cyclones, and superstructure icing.			
20. DISTRIBUTION / AVAILABILITY OF ABSTRACT <input type="checkbox"/> UNCLASSIFIED/UNLIMITED <input checked="" type="checkbox"/> SAME AS RPT. <input type="checkbox"/> DTIC USERS		21. ABSTRACT SECURITY CLASSIFICATION UNCLASSIFIED	
22a. NAME OF RESPONSIBLE INDIVIDUAL Dennis C. Perryman, contract monitor		22b. TELEPHONE (Include Area Code) (408) 647-4709	22c. OFFICE SYMBOL OM&N-1

DD FORM 1473, 84 MAR

83 APR edition may be used until exhausted.
All other editions are obsolete.

SECURITY CLASSIFICATION OF THIS PAGE

UNCLASSIFIED

TABLE OF CONTENTS

Foreword	vii
Preface	ix
Record of Changes	xi
1.0 General Introduction	1-1
1.1 Objectives	1-1
1.2 Approach	1-2
1.3 Organization and Contents	1-3
2.0 Large Scale Overview	2-1
2.1 Physical Characteristics	2-1
2.1.1 Geography	2-1
2.1.2 Topography	2-3
2.1.3 Oceanographic Features	2-6
2.2 Typical Atmospheric Features	2-14
2.2.1 Seasonal Variations	2-15
2.3 Electro-Optical Conditions	2-81
2.3.1 Electro-Optics and the Atmosphere as a Medium	2-81
2.3.2 General Comments on E-O Systems and Atmospheric Interactions	2-85
2.3.3 Specific Categories of E-O Systems	2-86
2.3.4 Forecast Aids for Elevated and/or Surface Based Ducts	2-93
2.4 Ocean Acoustics	2-96
3.0 Sea of Japan	3-1
3.1 Regional Features and Their Influence on Weather Phenomena	3-1
3.2 Sea of Japan Oceanographic Features	3-12
3.2.1 Sea Straits of the Sea of Japan	3-31

3.3	Winter.	3-43
3.3.1	Climatology	3-43
3.4	Spring.	3-51
3.4.1	Climatology	3-51
3.5	Summer.	3-60
3.5.1	Climatology	3-61
3.6	Autumn.	3-67
3.6.1	Climatology	3-67
4.0	East China Sea.	4-1
4.1	Regional Features and Their Influence on Weather Phenomena.	4-1
4.2	East China Sea Oceanographic Features	4-9
4.3	Winter.	4-19
4.3.1	Climatology	4-19
4.4	Spring.	4-31
4.4.1	Climatology	4-31
4.5	Summer.	4-46
4.5.1	Climatology	4-49
4.6	Autumn.	4-55
4.6.1	Climatology	4-58
5.0	Yellow Sea.	5-1
5.1	Regional Features and Their Influence on Weather Phenomena.	5-1
5.2	Yellow Sea Oceanographic Features	5-5
5.3	Winter.	5-15
5.3.1	Climatology	5-15
5.4	Spring.	5-24
5.4.1	Climatology	5-28

5.5	Summer.	5-34
5.5.1	Climatology	5-38
5.6	Autumn.	5-44
5.6.1	Climatology	5-45
6.0	Sea of Okhotsk.	6-1
6.1	Regional Features and Their Influence on Weather Phenomena.	6-1
6.2	Sea of Okhotsk Oceanographic Features	6-10
6.3	Winter.	6-14
6.3.1	Climatology	6-14
6.4	Spring.	6-24
6.4.1	Climatology	6-24
6.5	Summer.	6-37
6.5.1	Climatology	6-37
6.6	Autumn.	6-42
6.6.1	Climatology	6-43
7.0	Philippine Sea.	7-1
7.1	Regional Features and Their Influence on Weather Phenomena.	7-1
7.2	Philippine Sea Oceanographic Features	7-4
7.3	Winter.	7-11
7.3.1	Climatology	7-11
7.4	Spring.	7-22
7.4.1	Climatology	7-22
7.5	Summer.	7-40
7.5.1	Climatology	7-40
7.6	Autumn.	7-48
7.6.1	Climatology	7-48

8.0	Western North Pacific	8-1
8.1	Regional Features and Their Influence on Weather Phenomena.	8-1
8.2	Western North Pacific Oceanographic Features.	8-5
8.3	Winter.	8-11
	8.3.1 Climatology	8-11
8.4	Spring.	8-26
	8.4.1 Climatology	8-26
8.5	Summer.	8-38
	8.5.1 Climatology	8-41
8.6	Autumn.	8-50
	8.6.1 Climatology	8-51
9.0	Forecast Aids and Thumb Rules	9-1
9.1	Synoptic Patterns	9-1
9.2	Movement and Effect of Low Pressure Systems	9-2
	9.2.1 General	9-2
	9.2.2 Winter.	9-7
	9.2.3 Spring.	9-10
	9.2.4 Summer.	9-12
	9.2.5 Autumn.	9-12
9.3	Movement and Effect of High Pressure Systems.	9-13
	9.3.1 General	9-13
	9.3.2 Winter.	9-14
	9.3.3 Spring and Summer	9-14
	9.3.4 Autumn.	9-15
9.4	Fronts, Shear Lines, and Easterly Waves	9-15
	9.4.1 General	9-15
	9.4.2 Winter.	9-17
	9.4.3 Spring.	9-21
	9.4.4 Spring and Summer	9-22
9.5	Tropical Cyclones	9-22
	9.5.1 General	9-22
	9.5.2 Spring.	9-23

9.6	Wind.	9-24
	9.6.1 General	9-24
	9.6.2 Winter.	9-26
9.7	Visibility.	9-28
	9.7.1 General	9-28
	9.7.2 Winter.	9-30
	9.7.3 Spring.	9-30
9.8	Clouds.	9-31
	9.8.1 General	9-31
	9.8.2 Winter.	9-32
9.9	Precipitation	9-32
	9.9.1 General	9-32
	9.9.2 Winter.	9-33
	9.9.3 Spring.	9-33
9.10	Temperature/Wind Chill.	9-34
9.11	Sea Surface Temperature	9-34
9.12	Electro/Optical (E/O) Forecast Aids	9-35
	9.12.1 General.	9-35
	9.12.2 Winter	9-39
	9.12.3 Spring	9-43
	9.12.4 Summer	9-44
	9.12.5 Autumn	9-46
9.13	Atmospheric Turbulence.	9-47
	9.13.1 General.	9-50
	9.13.2 Winter	9-51
9.14	Ship Superstructure Icing	9-52
9.15	Aircraft Divert Field Guidelines.	9-54
	9.15.1 Naval Air Station, Atsugi, Japan.	9-54
	9.15.2 Naval Air Facility, Misawa AFB, Japan	9-58
	9.15.3 Naval Air Facility, Kadena AB, Japan.	9-60
	9.15.4 Marine Corps Air Station, Iwakuni, Japan.	9-70
	9.15.5 Korean airfields.	9-71
	9.15.6 Naval Air Station, Agana, Guam.	9-87

9.15.7	Naval Air Station, Cubi Pt., Republic of the Philippines.	9-90
9.15.8	Naval Station, Adak, Alaska	9-95
9.16	Oceanographic Forecast Aids	9-100
9.16.1	General	9-100
9.16.2	Winter.	9-104
9.16.3	Spring.	9-104

REFERENCES

APPENDICES

- Appendix A Glossary of Geographic Equivalents for Japan and Adjacent Seas Handbook
- Appendix B Tropical Cyclones
- Appendix C Equivalent Wind Chill and Vessel Superstructure Icing

FORWORD

The Japan and Adjacent Seas handbook is one of a series of regional forecaster handbooks produced by the Naval Environmental Prediction Research Facility (NEPRF). This publication has been developed in response to Commander, Naval Oceanography Command requirement PACMET 84-10, validated by the Chief of Naval Operations (OP-096).

The primary objective of this publication is to provide fleet forecasters and other decision makers with a single, comprehensive reference on environmental conditions for the Far East. Included are several satellite pictures, which provide reference images for various seasonal phenomena, and specific examples of satellite imagery interpretation.

This handbook should be regarded as a flexible document, capable of being updated and revised as applicable. Fleet users are urged to submit comments and suggested changes which can be incorporated into the handbook to increase its usefulness.

W. L. SHUTT
Commander, U.S. Navy

PREFACE

This handbook examines environmental conditions for the Sea of Japan, East China Sea, Yellow Sea, Sea of Okhotsk, Philippine Sea and western North Pacific (west of 160 deg East) and is organized by region for easy access.

A general overview chapter follows the introductory chapter. The overview includes seasonal climatology charts for the entire Far East area. In the regional chapters, references are made to these charts to assist the reader in differentiating seasons and sub-areas.

Chapters 3 through 8 are dedicated to the six sub-areas of interest. Each of these chapters follows a similar format in that information is presented by seasons. Generous use of actual satellite pictures (similar to those used in the NEPRF NTAG series of publications) is made to give the forecaster guidelines to follow in predicting specific conditions based on these data.

The final chapter contains forecast aids and rules of thumb for the sub-areas. In most cases, these aids have direct applications to naval operations. Most of the rules and aids were obtained from forecaster handbooks produced locally by both the U.S. Air Force and the U.S. Navy at various airfields and bases in the Far East region.

The appendices include a glossary (Appendix A) of applicable terms used by the various countries in the region. Appendix B presents statistics and climatology on typhoons in the region while Appendix C contains information on superstructure icing.

1.0 GENERAL INTRODUCTION

1.1 Objective

The Objectives of this Handbook are to:

a. Provide operational forecasters with a single reference text of information on the Sea of Japan, East China Sea, Yellow Sea, Sea of Okhotsk, Philippine Sea, and western North Pacific west of 168°E.

b. Organize the material for easy access to a general overview chapter with seasonal climatological charts and successive chapters on regional environmental conditions within the area of each of the above named marginal seas or oceanic areas.

c. Employ satellite imagery and graphics to illustrate discussions of operationally important phenomena, to provide reference images for various seasonal atmospheric and oceanic synoptic scale features, and present specific examples of imagery interpretation and deduction of environmental conditions.

d. List FORECAST RULES/AIDS which may have direct application to naval operational planning, tactics, and daily operations.

e. Identify pertinent and more detailed sources of information in the Reference Section.

f. Attach supplemental data/information from various sources as Appendices.

1.2 Approach

The following approach was used in development of this Handbook:

a. An operationally-oriented outline was stratified by: (1) A Large Scale Overview, (2) Regional Area Conditions, and (3) Seasonal Sections on Environmental Conditions.

b. Pertinent reference material from the technical libraries at the Naval Environmental Prediction Research Facility (NEPRF) and the Naval Postgraduate School (NPS) Monterey was collected and reviewed.

c. Operational reports of significant environmental events/conditions were reviewed.

d. Naval Oceanographic Command personnel who have had recent WESTPAC experience were interviewed.

e. Satellite imagery from the area was reviewed for specific illustrations of key phenomena.

f. FORECAST RULES/AIDS which have been developed by area forecasters were collected, screened, and selected for use in forecasting both local airfield and large area conditions.

g. The general reference information, satellite imagery, and forecast rules/aids were merged to provide a comprehensive reference text.

1.3 Organization and Contents

The Handbook is organized to provide large area general information, regional information, and specific location/condition information. Because of the extensive latitudinal range of the regions addressed, plus the unique monsoonal influences a simple four season year was not always appropriate. However, the four seasonal approach was generally retained with modification where necessary for regional variations.

Because of the varied countries and languages inclusive in the area covered an appendix of geographic terms was included. Information on such varied subjects as tropical cyclones and superstructure icing are included. The general text and appendix material is taken from the various references provided. The satellite imagery interpretation is based on references from the NEPRF NTAG series, Air Force interpretation manuals, various journal articles that made use of satellite imagery, and the Authors interpretation.

2.0 LARGE SCALE OVERVIEW

2.1 Physical Characteristics

The physical makeup of eastern Asia and adjacent ocean areas exerts a significant influence on the weather of the region. Many meteorological conditions described herein are the result of airmass trajectory coupled with modifications imposed by the land and water areas over which the airmass travels. Steep sea surface temperature gradients may cause markedly different weather conditions in some adjacent water areas with similar flow patterns. A careful study of the topography of eastern Asia and the bathymetry of adjacent water areas is essential to successful forecasting.

Appendix A contains a glossary which lists the non-English words for geography, topography, and bathymetry features most commonly encountered in the western North Pacific Ocean and marginal seas.

2.1.1 Geography

Figure 2-1 shows the geography of the land masses which border the water areas addressed in this handbook. The figure has been expanded westward to include central and western China, which contain the highest land elevations in the world and exert a significant influence on the large scale weather patterns which occur.

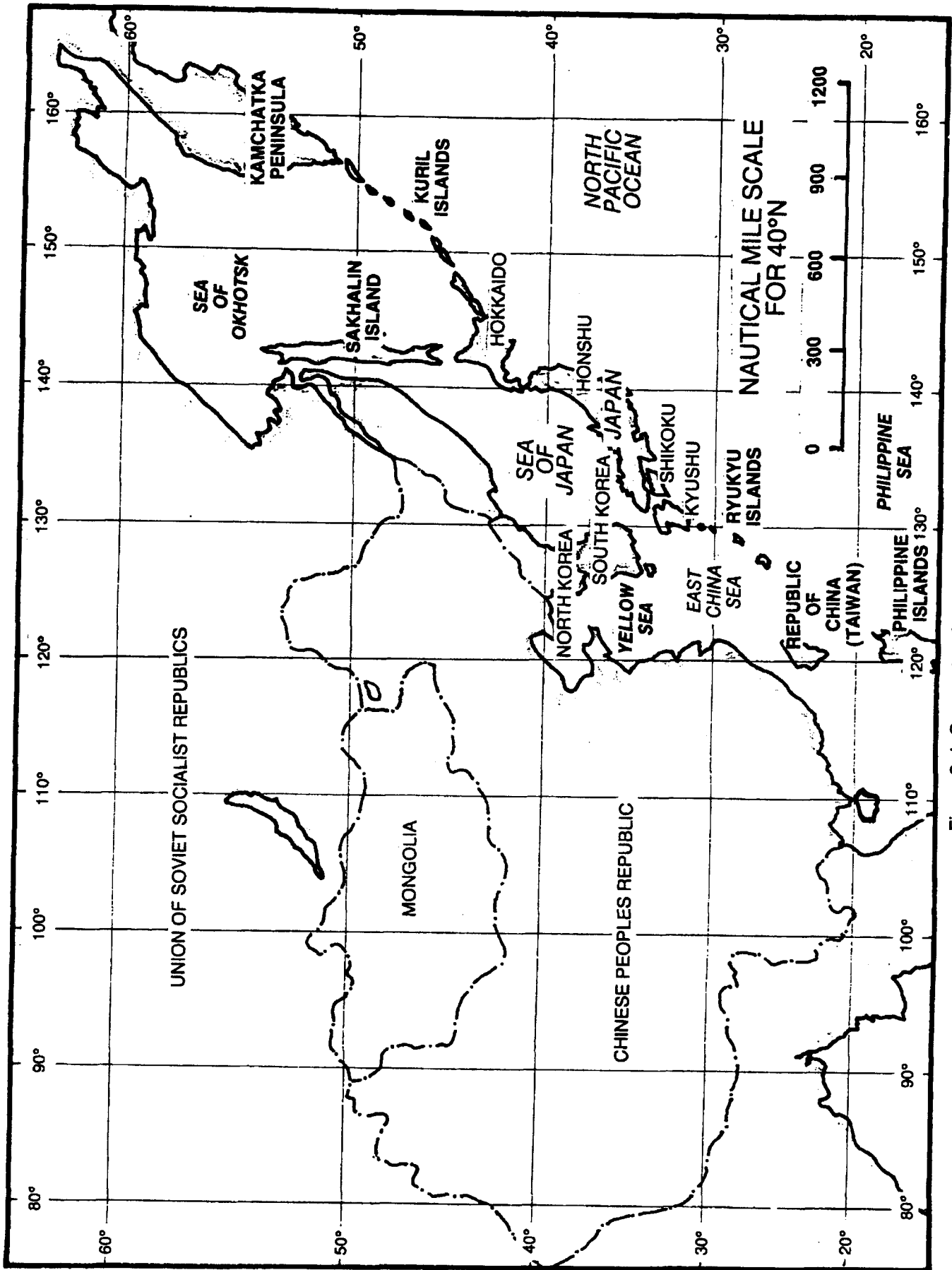


Figure 2-1. Geography of Eastern Asia.

2.1.2 Topography

Figure 2-2 depicts some of the major topographic features of the Asian continent. Asia contains some of the most rugged terrain in the world, with elevations ranging from the 29,028 ft (8,848 m) of Mt. Everest to the -154 ft (-47 m) of the Turpan Depression. The topography of eastern Asia can be classified by three major physical features: (1) the volcanic area, (2) the eastern ridge line of the continent, and (3) the mountains of Central China and Mongolia, an area commonly referred to as the Tibetan Plateau.

The volcanic area is composed of a mountainous chain, formed by the Kamchatka Peninsula and three island chains, the Kuril, Japan, and the Ryukyu Islands. Japan is the most significant of the three island chains because it poses the greatest barrier to air flow. The Japanese Alps average near 7874 ft (2,400 m) in elevation and cause frequent strong dynamic troughs which form in their lee to the southeast and east of the country.

The eastern ridge line of the Asian continent is composed of mountains averaging some 3,281 to 4,921 ft (1,000 to 1,500 m) in elevation with some peaks exceeding 8,202 ft (2,500 m). Included in the ridge line are the Sikhote Alin range which is most prominent along the northwest coast of the Sea of Japan but continues southward into the Korean peninsula, the Dzugdzhur and Kolyma ranges

along the west and north coasts of the Sea of Okhotsk, and other less significant coastal mountains in eastern China which seldom reach more than 2,953 ft (900 m) in elevation.

The Tibetan Plateau in central and western China has elevations commonly ranging from 9,843 to 19,685 ft (3,000 to 6,000 meters) with many peaks exceeding the 6,000 m level. The plateau is irregular in shape and is comprised of several mountain ranges, the most prominent of which is the Himalayas. Also included are the Kunlun Mountains, Tian Shan, Qilian Shan, and Altun Shan. Immediately north of the Tibetan Plateau lie the extensive wastelands of the Taklimakan Desert and the Dzungarian Basin. The eastern extension of the wastelands forms the famous Gobi Desert, where strong winds are frequent and the annual rainfall averages just four inches (FWC/JTWC, Guam, 1978).

The remainder of eastern Asia is a complex mixture of mountain ranges and extensive plains and valleys. The more prominent mountain ranges include the 2,953 to 5,906 ft (900 to 1,800 m) Greater Khingan Range just east of the Gobi Desert, and the Koryak Range which lies along the eastern coast of Siberia north of the Kamchatka Peninsula. Elevations in these ranges are predominantly in the 2,953 to 6,562 ft (900 to 2,000 m) range with some peaks exceeding 7,874 ft (2,400 m). An extension of the Koryak Range runs the length of the Kamchatka Peninsula and has elevations frequently exceeding 9,843 ft (3,000 m), with one peak reaching 15,584 ft (4,750 m).

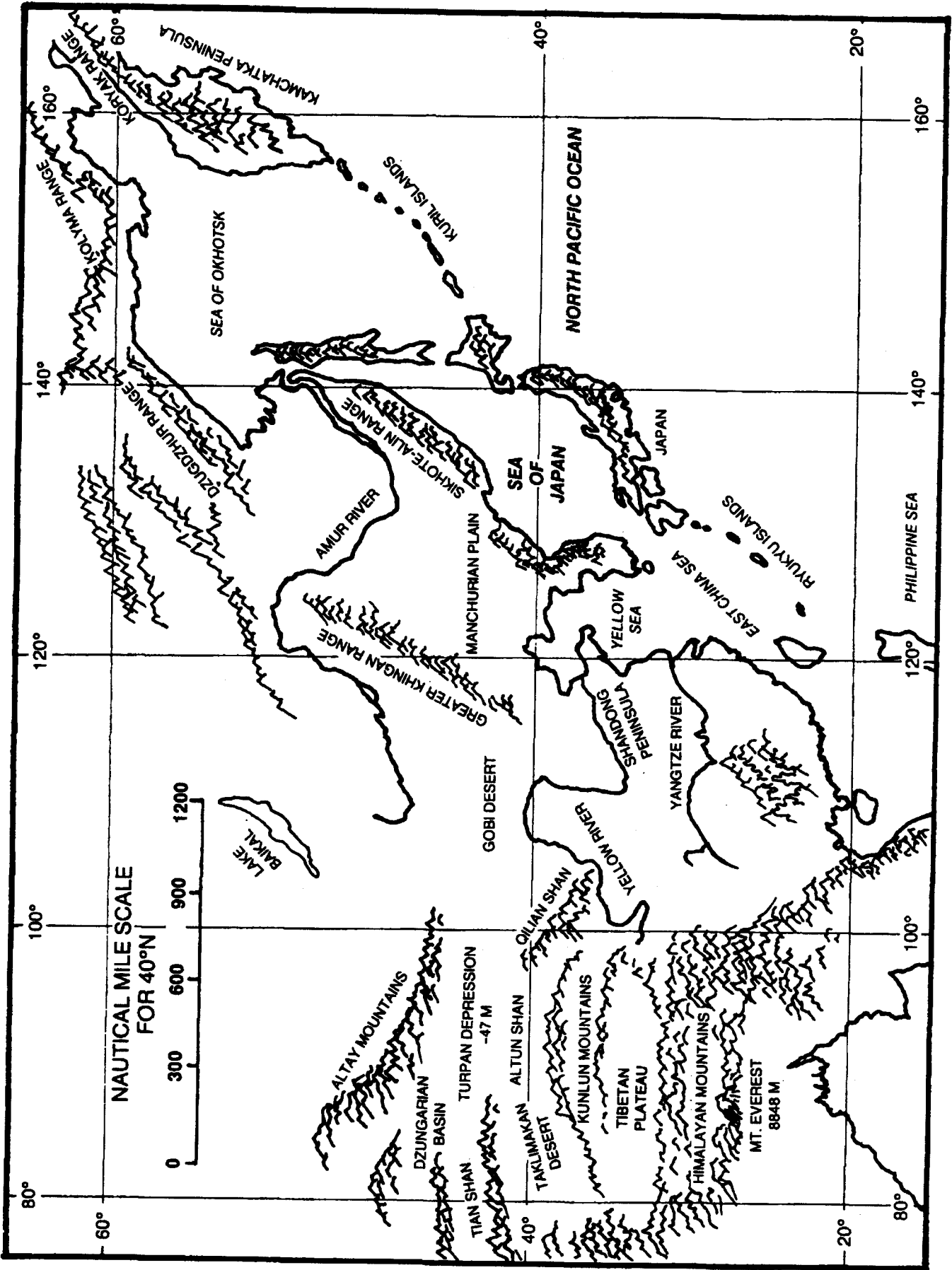


Figure 2-2. Major topographical features of eastern Asia.

2.1.3 Oceanographic Features

This handbook addresses oceanic regions that include both marginal seas and deep ocean areas of the western North Pacific Ocean. Significant differences in physical properties exist between the marginal seas and deep ocean regimes that impact temperature and salinity structures and bottom characteristics and, therefore, sound speed profiles critical to acoustic propagation. Critical physical properties of interest are:

- (1) bathymetry and bottom topography features
- (2) ocean fronts and current structures
- (3) temperature and salinity change due to precipitation, river inflow, and fluctuations in evaporation due to variations in atmospheric circulations

A large-scale overview of each of these critical properties for the region addressed in this handbook follows. Detailed discussions addressing interrelated facets of these and other properties will be provided in the individual sea and oceanic area sections.

2.1.3.1 Bathymetry and Bottom Topography

The bottom features of the western North Pacific and adjacent seas range from deep ocean trenches, troughs, ridges, and basins to regions of extensive continental shelf (Figure 2-3).

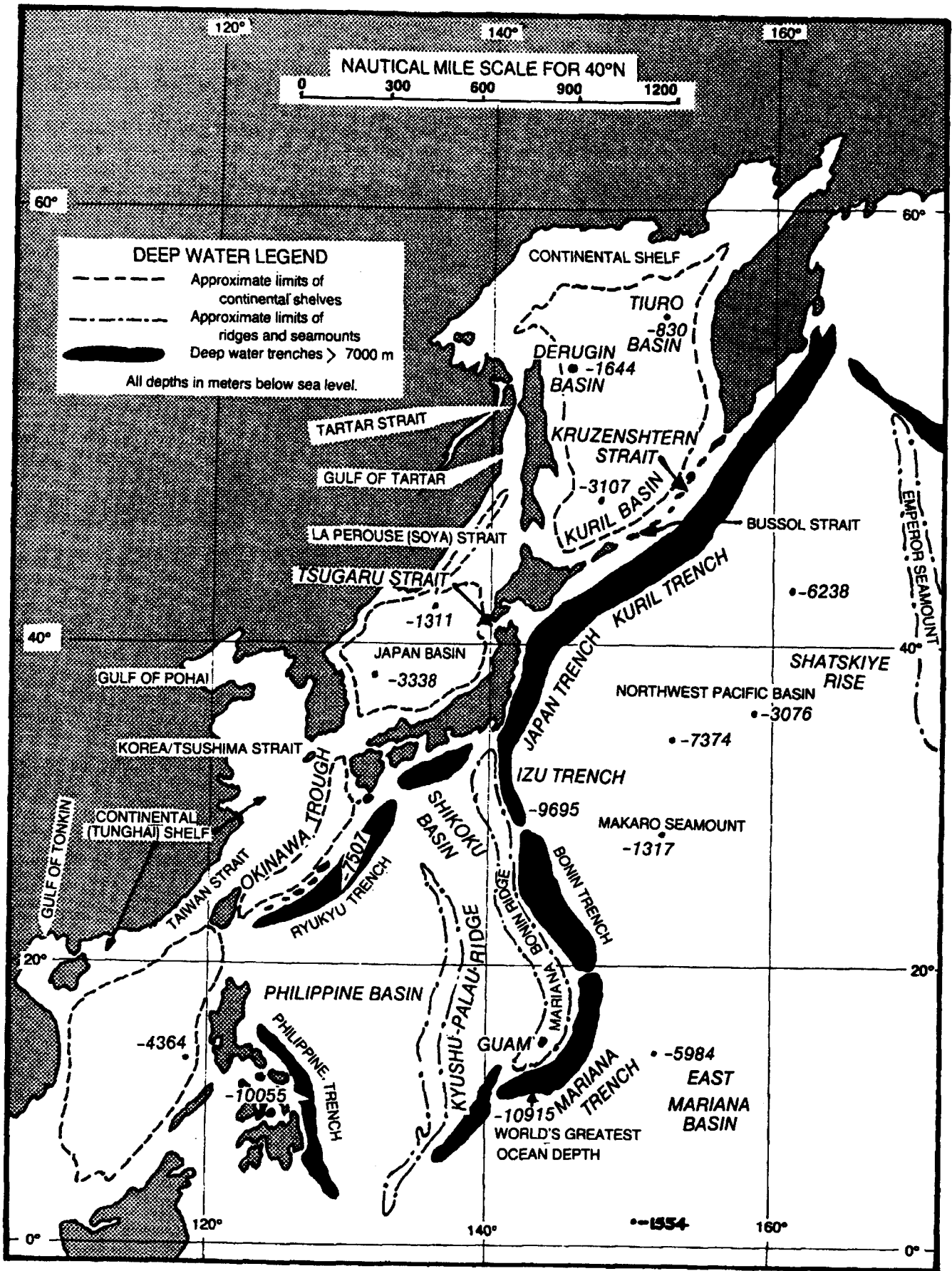


Figure 2-3. Major bathymetric features of the Sea of Japan, Yellow Sea, East China Sea, Sea of Okhotsk, Philippine Sea and western North Pacific Ocean.

The Philippine Sea is an abyssal zone (depths generally greater than 2,000 m). The bottom topography is complicated by deep trenches (greatest depth over 6,000 m), belts of seamounts, deep basins, and a number of island arcs. The sea is separated on the east from the Pacific Basin proper by a number of oceanic island arcs and on the west from the marginal seas by the continental arcs of Japan, the Ryukyu Islands, and the Philippines (Figure 2-3). The abyssal deep basin is separated into east and west basins by the Kyushu-Palau Ridge. The bottom sediments are pelagic red clays and oozes with volcanic material along the island arcs.

The East China Sea has two contrasting bathymetric zones, a broad continental shelf and the Okinawa Trough. The shelf, known as the Tunghai Shelf, is part of one of the largest in the world extending from the Yellow Sea south through the Taiwan straits to the South China Sea and the Gulf of Tonkin. The shelf width is about 150 n mi at the southern boundary of the East China Sea (near the northern end of Taiwan) and broadens northward to about 400 n mi near the northern boundary (near 33°N). The majority of the shelf has depths less than 100 m with the shelfbreak near 150 to 170 m. The shelf bottom consists of terrigenous sediment primarily from the Yangtze (Changjiang) River (Figure 2-2) with 400 million tons of sediment deposited annually (as compared to 500 million by the Mississippi River).

The Okinawa Trough extends from Taiwan to Kyushu (the southernmost island of Japan) along the inner side of the Ryukyu Islands arc. A large area of the trough has depths of 1,000 m with a maximum of over 2,700 m. The trough bottom is composed of a mixture of terrigenous muds and pelagic oozes.

The Yellow Sea and Gulf of Pohai form a broad semi-enclosed sea with maximum depths of 60-80 m in the central and southeastern parts (Fairbridge, 1966). The entire sea floor is part of the continental shelf and is comprised of terrigenous sediments brought down from the eastern watershed region of China via such rivers as the Yellow, Liao, White, and Yangtze (Changjiang). The westward flowing rivers of Korea, Yalu, Han, and Kum also carry large amounts of sediment into the Yellow Sea. Broad tidal mudflats are typical coastal features of the Yellow Sea.

The Sea of Japan contains both continental shelf and deep basin regions. The shelf is very narrow except in the extreme southern and northern narrows. The majority of sea depths exceed 1,000 m with a large area of the basins greater than 3,000 m. The Japan Sea Basin is separated from the Pacific floor by the Japanese Island Arc on the southeast side and bounded by the continental shelf elsewhere. The Sea of Japan is connected on the south and north to marginal seas by the Tsushima (Korea) Strait, and La Perouse (Soya) and Tartar straits respectively. Only the Tsushima (Korea) Strait has a sill depth greater than 100 m. The Tsugaru Strait located between Honshu and Hokkaido on the northeastern side of the Sea of Japan connects it with the main Pacific Ocean.

The Sea of Okhotsk has three main categories of bottom topography: (a) continental and island shelves, (b) the bottom of the central part of the sea, and (c) the bottom of the southern deep-water basin. The shelf area occupies more than 40% of the entire sea area and is composed primarily of sands or silts. The widths, outer margin depths, and slopes toward the basins vary widely (see section on the Sea of Okhotsk for details). The central

floor area has several systems of elevations and troughs. Depths over the systems range from 200 m to near 1,750 m. The Kuril Basin runs along the inner side of the Kuril Islands and has a greatest depth of over 3,000 m. The basin is surrounded on all sides by steep slopes (15-20°). The sediments range from pebbly gravel and sand in the nearshore and over open sea summits and slopes, through bands of silts and clays to ooze over the majority of the central part and abyssal plain of the Kuril Basin. In contrast to the Sea of Japan, which is nearly landlocked, the Sea of Okhotsk has free exchange of water with the Pacific. Bussol (Boussole) Strait accounts for over 40 percent of the cross sectional opening of the straits and has a sill depth of over 2,300 m. Kruzenshtern Strait accounts for about 25 percent more of the total opening and has a sill depth over 1,900 m.

2.1.3.2 Currents

An overview of the major currents is provided here. Additional details on these currents as well as on local currents are presented in the regional sections.

The Kuroshio Current is the dominant ocean current of the western North Pacific and resembles the Gulf Stream of the western Atlantic. The Kuroshio begins east of northern Luzon, the northernmost of the Philippine Islands, (Strommel and Yoshida, 1972) and flows close to the east coast of Taiwan and then into the East China Sea (Figure 2-4 and see Figures S-3-7, page 3-36 and S-3-8, page 3-52). In the East China Sea the Kuroshio follows the Okinawa Trough between the continental shelf and the Ryukyu Ridge. The current splits in two parts southwest of Kyushu. The major part flows east

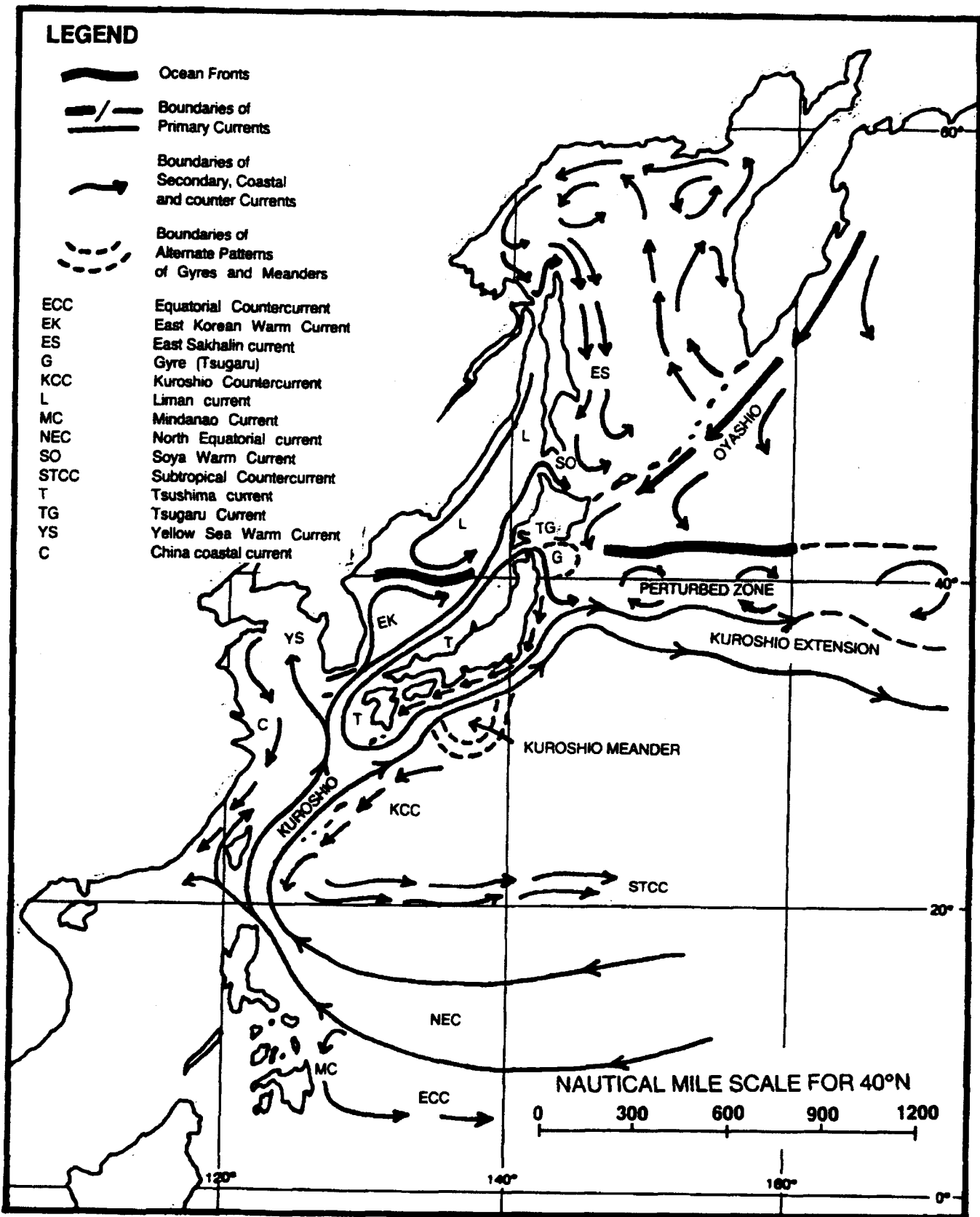


Figure 2-4. Schematic Distribution of currents, ocean fronts, gyres, meanders and perturbed areas.

to south of Shikoku and then northeastward along southern Japan. The minor branch flows north as the Tsushima Current west of Kyushu through the Tsushima (Korea) Strait into the Sea of Japan. The Kuroshio Current south of Japan either flows northeastward close to the continental slope, or makes a large meander to near 31°N south of Honshu. Once formed, this large meander tends to persist for several years. The Kuroshio leaves the Japan coast near 36°N and flows generally east but with a meandering path. This portion of the current flowing eastward from Japan is called the Kuroshio Extension. (See Figure S-8-2, page 8-23). The Kuroshio retains its form of a relatively narrow concentrated current until about 160°E where it transforms into the weak, broad North Pacific Current.

The Tsushima Current is a major feature of the Sea of Japan (See Figure S-3-3, page 3-15). It has been defined by Sverdrup et al. (1942) as the warm current that branches off on the left-hand side of the Kuroshio and enters the Sea of Japan through the Tsushima Strait. The Tsushima Current splits just south of the Strait with one branch following the western coast of Japan to the north and a second weaker branch entering the central Yellow Sea. The Tsushima carries water of high temperature and high salinity northward. The major portion of the Tsushima Current transport (about 75 percent) flows out of the Sea of Japan through the Tsugaru Strait as the warm Tsugaru Current (See Figure S-3-4, page 3-22). The remainder continues northward along the west side of Hokkaido and then splits. One branch turns eastward through the Soya (La Perouse) Strait and returns southward as the warm Soya Current along the northeast coast of Hokkaido. The other branch continues northward as a warm current off western Sakhalin Island. The cold

Liman Current has a southerly set in the western portion of the Sea of Japan (See Figure S-3-3, page 3-15).

The Oyashio Current is a cold current that originates in the Bering Sea and flows southwest along the Kamchatka Peninsula, the Kuril Islands, and Hokkaido, meeting the Kuroshio off the north-eastern coast of Honshu near 37-40°N (See Figure S-8-2, page 8-23). This region, where arctic waters meet warm waters, is called the Perturbed Area. Numerous eddies and thermohaline fronts are irregularly distributed in the Perturbed Area causing complicated hydrographic conditions (Strommel and Yoshida, 1972). The major features of this area have been theoretically described as four parallel rows of stationary vortices or eddies that rotate in alternate directions (Barkley, 1968). A review of Japanese Hydrographic Division quarterly isotherm analyses for 1955-64, by Barkley (Marr, 1970) provides empirical support for the theoretical configuration. The Perturbed Area extends from near the Japanese coast eastward to beyond 160°E and north-south from about 37°N to near 50°N. The area has a north-south dimension of 200-300 n mi in the near-shore region and increases eastward. There is also a normal north-south seasonal displacement.

2.1.3.3 Temperature and Salinity

The seasonal variations in near-surface temperature and salinity differ throughout the region. For a given location the near-surface temperature values are affected by two principal heating processes. First is the seasonal variation in solar heating, with the typical oceanic lag resulting in a maximum in August and minimum in February/March. Second, the advection process

due to shifting ocean currents can modify the seasonal cycle at a given point. The extreme minimum and maximum temperatures discussed in the text for each sea refer to the value for which 1% of all reported are lower or higher. Near the surface, salinity values reflect the effects of additional fresh water due to precipitation or run-off (reduces salinity) and evaporation processes (increases salinity). The shifting ocean currents also play a role in changing salinity values at a given location, reflecting the values of their source regions. Local variations in precipitation, evaporation, and currents result in salinity minimums in late summer and fall (following the rain and tropical cyclone season) and maximums in late winter and spring as a result of high evaporation rates.

2.2 Typical Atmospheric Features

The water areas discussed in this handbook span more than 50 degrees of latitude, from the southern reaches of the Philippine Sea to the northern limit of the Sea of Okhotsk. The weather over these diverse areas ranges from tropical to sub-arctic, making it difficult, if not impossible, to address in general terms a "typical" atmospheric feature that would apply to or impact all of the areas discussed herein. Consequently, this section addresses only large scale events that normally occur in the course of the seasons, without regard for their effects, or lack thereof, on a particular area.

2.2.1 Seasonal Variations

In the mid-latitudes, one would normally expect to find four reasonably distinct seasons: the traditional spring (mid-March to mid-June), summer (mid-June to mid-September), autumn (mid-September to mid-December), and winter (mid-December to mid-March). Not all of the areas discussed in this handbook are in the mid-latitudes however, and even those that are do not all have the standard seasons.

Because this section is intended only as an overview of the whole of eastern Asia, it will address the four traditional seasons, and leave the discussions of regional differences to those sections that apply to each specific region. The selection of individual months that best represent each season was made after considering several factors, the most significant of which was to best describe the majority of the covered areas. Ultimately, the months of February, May, August, and November were chosen. They fall within the traditional quarterly seasons and also fit reasonably well into the more detailed seasonal breakdown of southern Japan and adjacent areas.

Although the start and end of the seasons usually occur in the middle of calendar months, most available climatology reference documents have data grouped and summarized by whole months. Consequently, unless otherwise indicated, it has been necessary to treat each season as a four-month period when describing the conditions that prevail at its start or end. For example, to

present the conditions that exist at the start and end of winter in the East China Sea, the whole months of December and March are considered.

2.2.1.1 Monsoons

A significant portion of eastern Asian weather is controlled by the Asiatic monsoon. The term "monsoon" originated with the Arabic "mausim", a season, and was originally applied to the wind regimes of the Arabian Sea where winds blow for six months from the northeast (winter monsoon) and six months from the southwest (summer monsoon). Monsoon and monsoonal areas have been defined in many ways, but most have a central theme -- seasonality -- surface winds which blow persistently from one general direction during one season and just as persistently from a markedly different direction during another season (FWC/JTWC, 1978).

In winter, the Siberian high, a large, shallow high pressure cell, dominates the eastern USSR. The cold, snow covered surface absorbs little solar radiation because of a high albedo, and subsequent cooling and light surface winds allow a massive pool of shallow but intensely cold air to develop. Surface pressures of 1050 mb are not uncommon, and pressures of 1082 mb were analyzed on surface pressure charts over Siberia during 1974 and 1975 (FWC/JTWC, 1978). The high pressure cell creates the winter monsoon, also called the Northeast Monsoon, resulting in a strong north or northeasterly airflow predominating over eastern Asia and adjacent waters.

Conversely, in summer, the warming landmass causes a large thermal low to form over Asia, creating the summer monsoon, also

known as the Southwest Monsoon. It transports warm, moist air northward along the coastal area of eastern Asia. The summer monsoon of the western North Pacific is relatively weak compared to the summer monsoon of India. Gale force winds seldom occur, and then only when they are associated with strong inflow near a large tropical cyclone or with channeling (Venturi effect) through restricted waters such as the Taiwan Strait between mainland China and Taiwan (Figure 2-3). The summer monsoon of Asia is less intense than that of India and Asia Minor due to:

- (1) less intense heating at higher latitudes and periodic invasions of cool air from the north
- (2) a wider range of sea surface temperatures
- (3) clouds associated with the periodic formation of an extratropical or tropical cyclone reduces the incoming solar radiation that reaches the surface and eliminates the heat low
- (4) the more northerly position of the Polar Front (FWC/JTWC, 1978).

In the mid-latitude coastal areas the local meteorological conditions are controlled by the seasonal advance and retreat of the Polar Front, the boundary between continental polar and maritime tropical airmasses. The autumn transition from the summer to winter monsoon occurs rapidly. It involves a shift from light and variable southerly winds to stronger, steadier northerly winds as the mean position of the Polar Front migrates rapidly from near 40°N southward to 20-25°N (Figure 2-5).

The winter monsoon season dissipates as the Siberian high weakens during the spring, resulting in a northward migration of the Polar Front to its summer position and the establishment of the summer monsoon over the coastal waters of eastern Asia (Huh, 1982). This spring transition usually results in many vacillations between

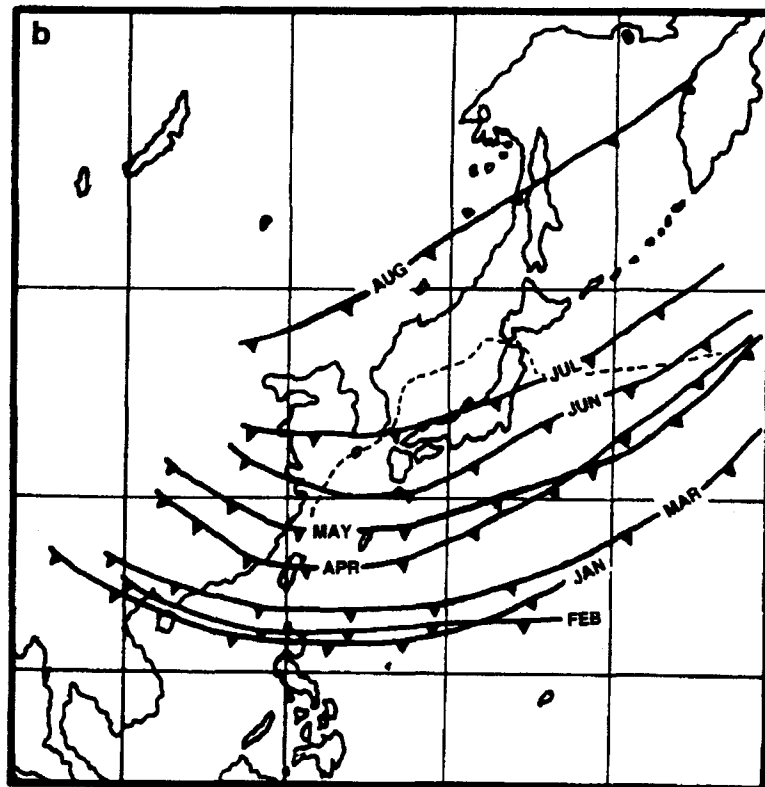
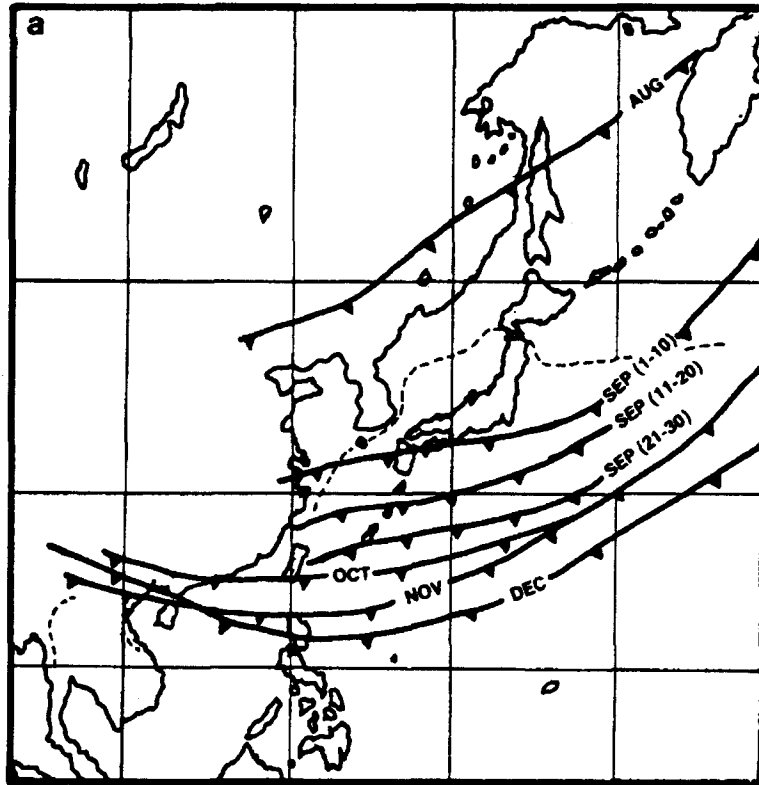


Figure 2-5. Seasonal migration of the primary polar front/polar trough system. (a) Summer to mid-winter seaward advance. (b) Spring to summer landward retreat. (Adapted from Huh (1982), with U.S. Air Force (1970) as original data source)

northeast and southwest flow in the mid-latitudes before the thermal low becomes firmly established over central Asia.

The transitions from one monsoon regime to the other occur during the traditional late spring, summer and early autumn months and, in some areas, cause such pronounced changes in the climate that the transition periods are treated as separate seasons. For example, the southern half of Japan experiences six distinct seasons plus a typhoon season that overlaps three of the other seasons. These seven seasons, as outlined by NOCD, Atsugi, (1980) and NOCF, Yokosuka, (1981) are:

- (1) Winter - - - - - December to mid-March
- (2) Spring - - - - - mid-March to mid-June
- (3) Bai-U (wet season)
also called Mei-Yu
Plum Rain in China - - - mid-June to mid-July
- (4) Summer - - - - - mid-July to mid-September
- (5) Typhoon - - - - - July, August, September
- (6) Autumn Bai-U (Shurin)- - mid-September to mid-October
- (7) Autumn - - - - - mid-October through November

Korea, however, a country close to southern Japan, has four "traditional" seasons, but experiences a shortened autumn season and a longer winter season (U. S. Navy, 1965):

- (1) Winter - - - - - November through February
- (2) Spring - - - - - March through May
- (3) Summer - - - - - June through August
- (4) Autumn - - - - - September and October

2.2.1.2 Mei-Yu/Bai-U Spring Front of the Far East

The spring rainy season is a unique climatological feature. The circulation feature is known as the Mei-Yu front (plum rain) over China and Taiwan and as the Bai-U front in Japan. The front has a near stationary nature and occurs during the transition period between the Northeast Monsoon in the winter and the Southwest Monsoon in the summer. The front initially develops in mid to late May over southern China and Taiwan in response to the westward extension of the subtropical Pacific high. The duration of the rainy season is about one month over the southern areas and increases to about two months over central China and southern Japan. The nature of the precipitation is continuous or intermittent light rain mixed with frequent heavier rainshowers or thunderstorms. The entire cloud band and rainy area moves slowly northward throughout June and July and may influence areas of northern China and Japan until well into August. However, as pointed out by Kuo and Anthes (1982), the front tends to move back and forth, thus creating a difficult short-term forecasting problem.

The Mei-Yu/Bai-U front is a subtropical front and therefore has different characteristics than a Polar Front. The Mei-Yu/Bai-U front is characterized by a narrow steady precipitation zone, strong gradient of equivalent potential temperature, thick moist neutral layer, and a steady generation of convective instability (Ninomiya, 1984). However, model studies (Kuo and Anthes, 1982) as well as empirical studies by various far-east investigators indicate that the eastern section of the front (east of about 135°E) is similar to a mid latitude cold front while the western section (west of about 130°E) resembles a semi-tropical system. The Mei-Yu/Bai-U front is

a relatively shallow feature and develops only in the lower troposphere, unlike the mid latitude fronts which typically have a supporting trough that extends to the upper troposphere.

The structure of the Mei-Yu/Bai-U front is marked by a significant low level jet (LLJ) which exhibits ageostrophic flow in the near surface to 600 mb layer. The winds are generally 20% to 50% stronger than indicated geostrophic winds. The LLJ maximums are located near the 700 mb level and are typically found about 180 n mi southeast of the areas of most active convection (Ushijima, 1968).

The circulation pattern of the frontal structure is composed of weak mesoscale cyclones with embedded clusters of convective cells. In the vicinity of Taiwan, the mesoscale disturbances have a periodicity on the order of 17 to 20 hours, a wavelength of about 180 n mi, and a phase speed of near 10 kt. The embedded convective clusters have periods of about 3 to 7 hours, wavelengths of 35 to 100 n mi, and speeds of 12 to 15 kt. In the vicinity of southern Japan, the wavelengths of the mesoscale features are on the order of 600 n mi or less, while the phase speeds increase to 30 to 40 kt (Chen and Tsay, 1978). The periodicity of the mesoscale remains near 20 hours (Matsumoto et al, 1970) while the mesoscale disturbances are characterized by cyclonic circulation that show little tendency to deepen as they move eastward (Matsumoto and Tsuneoka, 1970). Deepening is likely to occur if the Mei-Yu/Bai-U front is interacting with a mid latitude upper level trough east of about 135°E.

The Mei-Yu/Bai-U cloud band has different characteristics in its northern and southern portions. In the northern portion, low and/or middle clouds generally prevail while in the southern portion well organized cumulonimbus clusters are found, especially to the

west of 130°E (Chen, 1980). The northern portion of the frontal zone is marked by a dry area with light winds in the mid troposphere (500 mb) and above.

2.2.1.3 Migratory Lows

Seasonal meteorological conditions affect the likelihood of cyclogenesis and cyclone trajectory cycle. Most discussions of migratory lows in the Far East identify six basic types, based on the location of their formation and/or track. Figure 2-6 depicts the tracks of the six types. The following descriptions are taken from the Area of Responsibility Forecasters Handbook, by NOCD, Atsugi, (1980).

The "northern lows" (Types A, B and C) generally form in northern China or southern USSR and move from their source region into the Sea of Okhotsk or into the northern Pacific. They are all formed by movement of short-wave troughs through the low pressure source region, and all are enhanced by downslope adiabatic warming as the systems traverse from their mountainous source regions to the Sea of Japan. Northern lows include:

Type A - Manchurian Low. Maximum occurrence is during the autumn and spring. The system generally tracks over Sakhalin Island and into the Sea of Okhotsk.

Type B - Lake Baikal Low. Maximum occurrence is during spring, but may occur throughout the year. The track is somewhat south of the Manchurian Low, moving instead over the Sea of Japan and northern Japan. Average speed of movement is 22 kt.

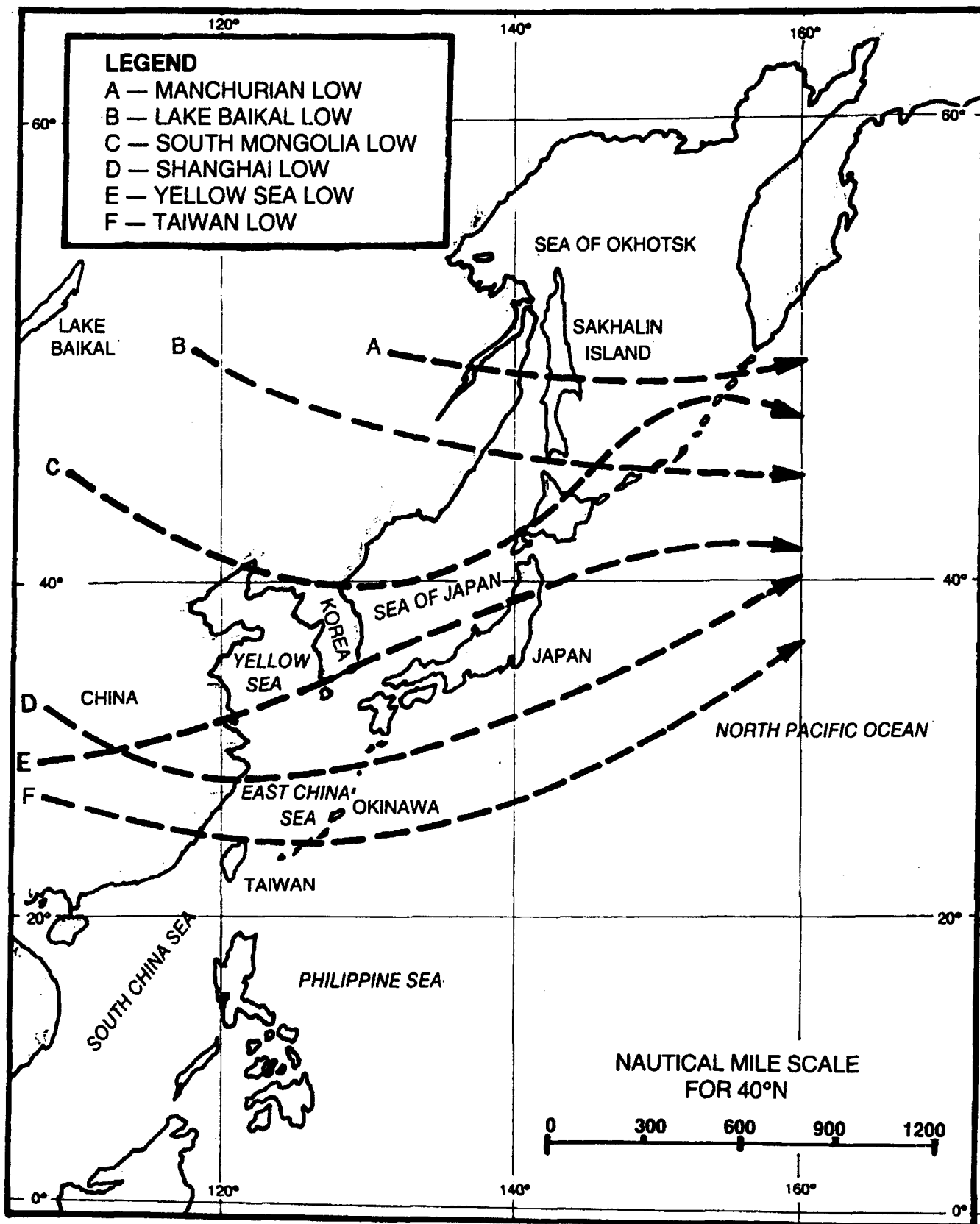


Figure 2-6. Storm tracks (adapted from Naval Oceanography Command Detachment, Atsugi, Japan, 1980).

Type C - South Mongolia Low. South Mongolia lows can occur during any season. The track is more southerly than the two previously discussed, and may generate a Yellow Sea Low (Type E) as it passes through that region. Its trajectory is normally over the Yellow Sea, Korea, the Sea of Japan, northern Japan, and into the southern Sea of Okhotsk with a mean speed of about 20 kt.

The "southern lows" (Types D, E, and F) generally form over central and southern China, then track over the Yellow Sea, Sea of Japan, and northern Japan, or track over the East China Sea and remain south of Japan. They occur year-round and produce widespread precipitation, low ceilings, poor visibility and occasional thunderstorms or high winds. There are three major systems in the southern group.

Type D - Shanghai Low. Also called the Hwang Ho Low, this system occurs most frequently during spring. Similar to the "Hatteras Low" of the United States' east coast, it is notorious for rapid intensification as it moves over the warm waters of the Kuroshio Current. Moving from its source region over central China, it tracks east to northeast at a mean speed of about 18 kt, and then eastward between the Japanese islands of Kyushu and Okinawa. This low is generated by a deepening of the China thermal low. If the thermal low is deepened by a short-wave trough moving north of the Himalaya Mountains, a central pressure of less than 1012 mb will generate a Shanghai Low. If the low is deepened by a short-wave trough moving from the south of the Himalayas, a central pressure of less than 1000 mb will generate a Shanghai Low. An empirical rule

states that when a low is generated over China and passes 120°E south of 30°N, it will be a Shanghai Low and should pass south of the Japanese island of Honshu.

Type E - Yellow Sea Low. Sometimes referred to as a Central Basin Low. Primarily a summer and autumn phenomena, Yellow Sea Lows move from their source region at a mean speed of 21 kt and track over South Korea into the Sea of Japan. They frequently produce a secondary low south of the Japanese islands of Khushu or Shikoku 12 to 18 hours after entering the Yellow Sea.

Type F - Taiwan Low. Sometimes called Yangtze Lows. Taiwan Lows are initially generated over China near 25°N 100°E, and occur most frequently from autumn through spring. They track northeastward from the Taiwan/China coast region at a mean speed of 24 kt, and will always track south of Japan.

2.2.1.4 Cold Fronts

The majority of cold fronts approaching the eastern coast of Asia are the result of old, occluded fronts coming from Europe. Circumventing the Tibetan Plateau, they follow a southeastward and eastward track toward Korea and Japan, causing invasions of intensely cold air. The flow pattern at 500 mb through 200 mb influences the direction the cold air will follow, and the availability of moisture determines weather in terms of precipitation and clouds. The document Forecaster's Handbook Volume 1 (FWC/JTWC, 1969) theorizes that in the Far East there are basically three types of cold fronts with respect to origin and movement (Figure 2-7). It was also found that anticyclones will follow the same trajectories as the cold fronts.

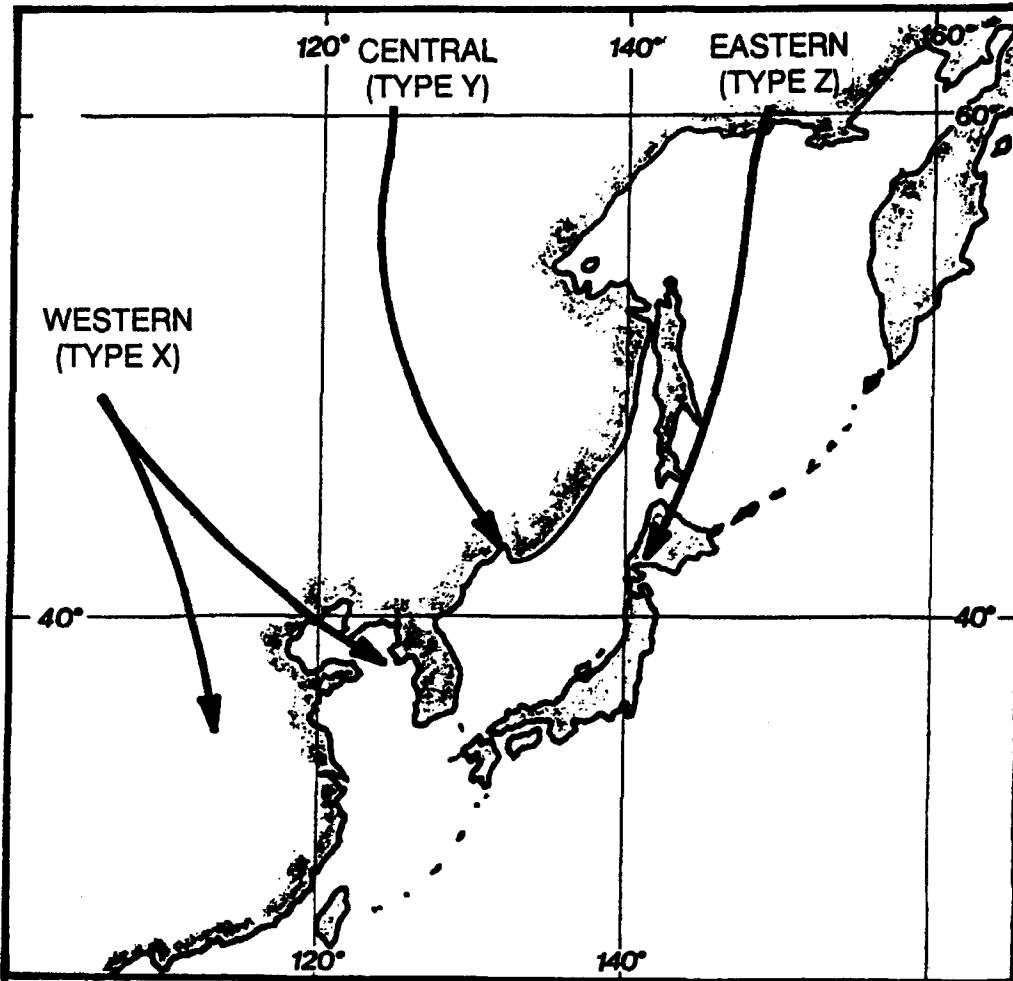


Figure 2-7. Tracks of cold fronts over Asia as categorized by Sjan-Zsi Li, adapted from Fleet Weather Central, Guam (1969).

The vertical extent of cold fronts is not believed to extend much above 6,500 ft (1,981 m). However, A. Lee in his study The Cold Waves of China, found that they may reach 10,000 ft (3,048 m) during a severe, cold outbreak.

Type X - Western Cold Front. Western cold fronts occur most frequently of the three types hypothesized, originating on the shores of the Arctic Ocean in the western USSR between 30°E and

90°E. They occur throughout the year and usually follow one of two trajectories. After leaving their source region, most Western fronts travel into north China, reaching the coast about 40°N. The other, less frequent, trajectory has the cold front moving southward as far as Indo-China. Western fronts are quite shallow and only in intermediate latitudes do they cause severe drops in temperature. Frontal precipitation is associated with them. Cyclogenesis along these fronts over the Shandong Peninsula in the western Yellow Sea will also cause widespread frontal weather. Western cold fronts are produced by relatively strong meridional flow at 500 mb with a long wave trough position over Korea.

Type Y - Central Cold Front. Central cold fronts occur frequently and are especially severe in northern and central China, Manchuria, Mongolia, Korea, and Japan. Originating in eastern Siberia between 100°E and 140°E at 55°N to 70°N, they have more vertical extent than the Western type, and are associated with very dry and cold air, resulting in pronounced drops in temperature. Central fronts are most often observed during mid-winter and are produced by strong meridional flow, or a block north of Mongolia and a long wave trough over Japan.

Type Z - Eastern Cold Front. Eastern cold fronts are formed from 140°E eastward between 55°N and 70°N and travel toward the south-southwest along the east coast of Siberia and into Korea. They do not occur as frequently as Western and Central cold fronts and are primarily spring and summer phenomena, with a secondary frequency maximum in November.

2.2.1.5 Winter (mid-December to mid-March)

At the surface, Eastern Asia is under the influence of the Siberian high pressure cell which is resident in the Lake Baikal region of the USSR. This continental, cold high is at its maximum intensity in January and February. The Siberian high fluctuates in position and intensity in response to migratory mid-tropospheric disturbances and sends cold surges eastward from the Asian mainland. During winter, the oceanic, warm mid-Pacific high is at its weakest and has receded southeastward. The westward extension of this oceanic high is also weakened and shifted southeastward, resulting in an area of lower pressure between the two high pressure systems. The Polar Front lies between the two high pressure cells and is oriented east-west near 20°N over the waters adjacent to eastern Asia.

In the upper atmosphere, the jet stream is at its southernmost position and at its greatest strength in winter. A significant feature of the jet stream is that it splits as it passes the Tibetan Plateau in its eastward journey across western China. Murakami (1981) states that, based on a limited data study performed by Chinese scientists, during winter the low-level (below 500 mb) westerlies split into two branches (northern and southern) and flow around, rather than up and over, the high mountains of the Tibetan Plateau and that "a strong upper level (200-300 mb) jet stream flows along the southern periphery of the Tibetan Plateau...." The splitting effect is seen in Figure 2-8. The two branches of the jet stream then merge into a single flow over southwestern Japan.

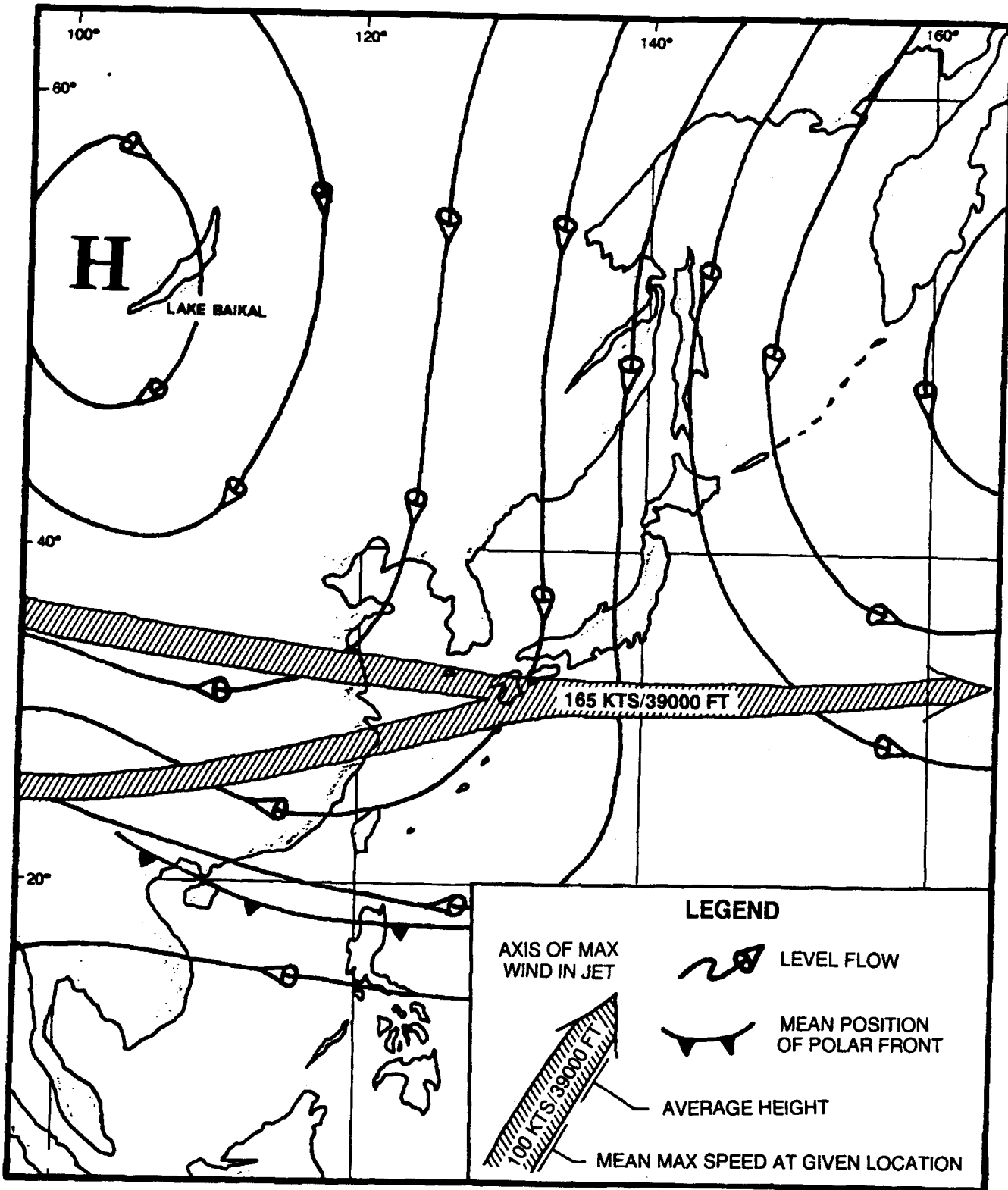


Figure 2-8. Typical atmospheric features during February: mean low level flow, mean position of polar front, and mean jet stream position (adapted from U.S. Marine Corps, 1967 and U.S. Air Force, 1968).

The Aleutian low is well established near 53N 170E and is at its strongest during the months of January and February. An area of low pressure, sometimes evident only as a trough, becomes a semi-permanent feature over the eastern Sea of Okhotsk during the winter and forms an anchor for a semi-permanent thermal trough that extends into the Sea of Japan. The thermally induced trough is a result of the temperature difference between the frigid air of the Asian landmass and the relatively warmer waters of the Sea of Japan.

The most probable winter migratory low pressure systems are Lake Baikal Lows, South Mongolia Lows, and Taiwan Lows. Records for the years 1951 and 1952 from Fleet Weather Facility, Yokosuka, Japan showed an average of about 57 cold fronts per year in the Far East. Of these, about 18 (32%) occurred during the winter (mid-December to mid-March) a frequency of about one every five days (FWC/JTWC, 1969).

During the winter months, significant tropical cyclone activity is limited to the Philippine Sea and the western North Pacific Ocean south of about 20°N. Although tropical cyclones have been known to form during all months of the year, few form during winter, and of those that do, even fewer still reach typhoon strength. In the western Pacific approximately one typhoon per four years occurs in January and one per five years in February and March (Crutcher and Quayle, 1974). All of the storms of record during January and February have stayed well south of 30°N, with the primary track westward over the central Philippine Islands, or recurving northeastward and passing 140°E south of 20°N. Refer to Appendix B for tropical cyclone tracks.

Figures 2-9 through 2-21 depict various average climatic conditions that prevail over eastern Asia and adjacent waters during

the month of February. A brief discussion of each of the parameters is presented in the climatology sections of the regional chapters in this handbook.

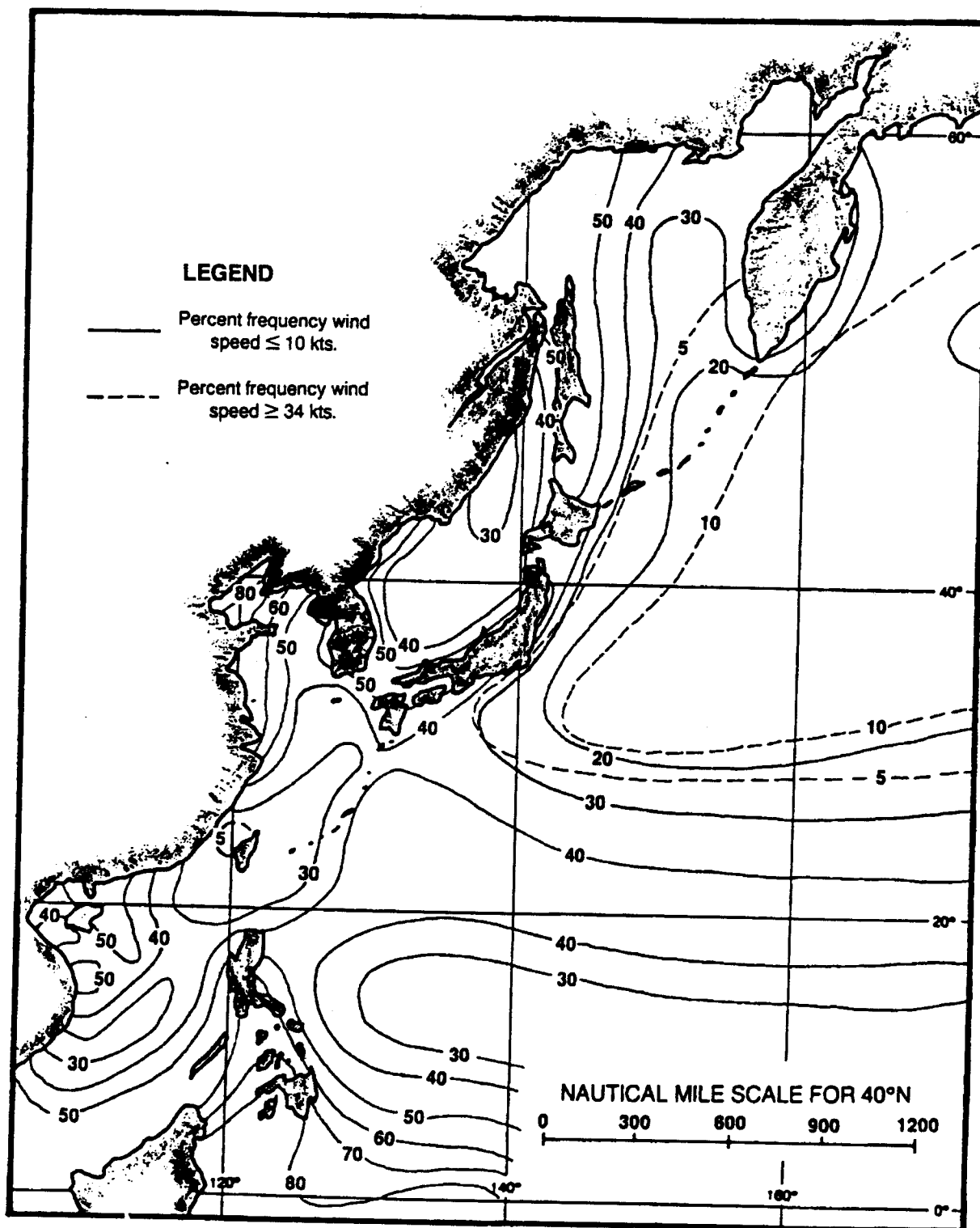


Figure 2-9. Surface winds during February (adapted from U.S. Navy, 1977).

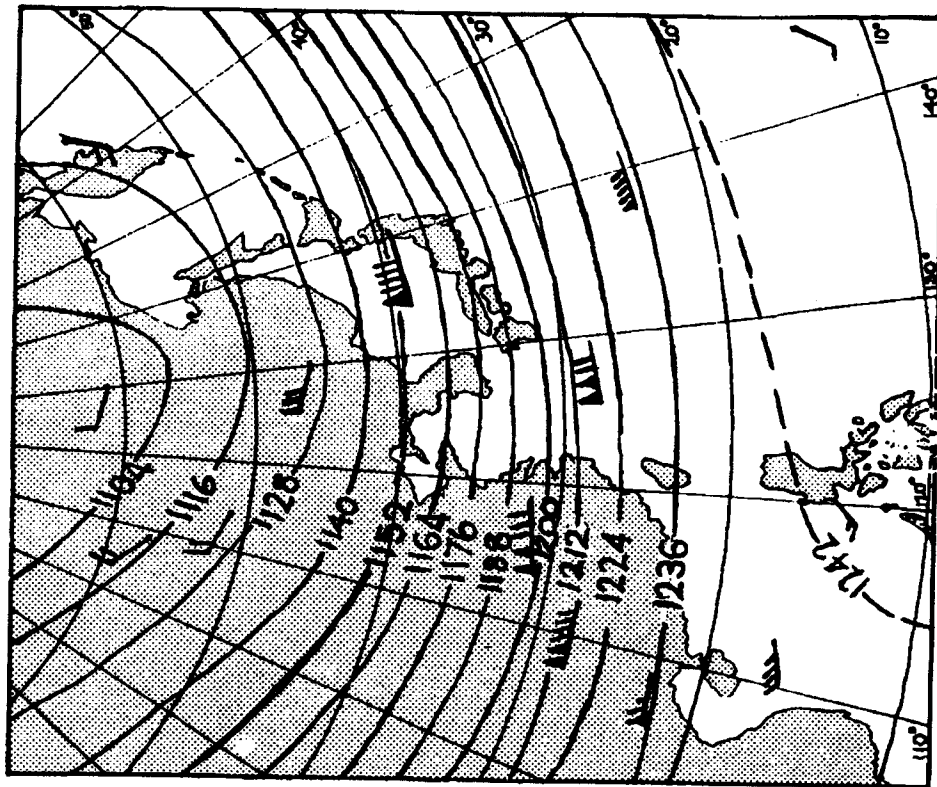


Figure 2-11. 200mb heights and winds for February. All heights in tens of gpm. (adapted from Crutcher & Meserve, 1970)

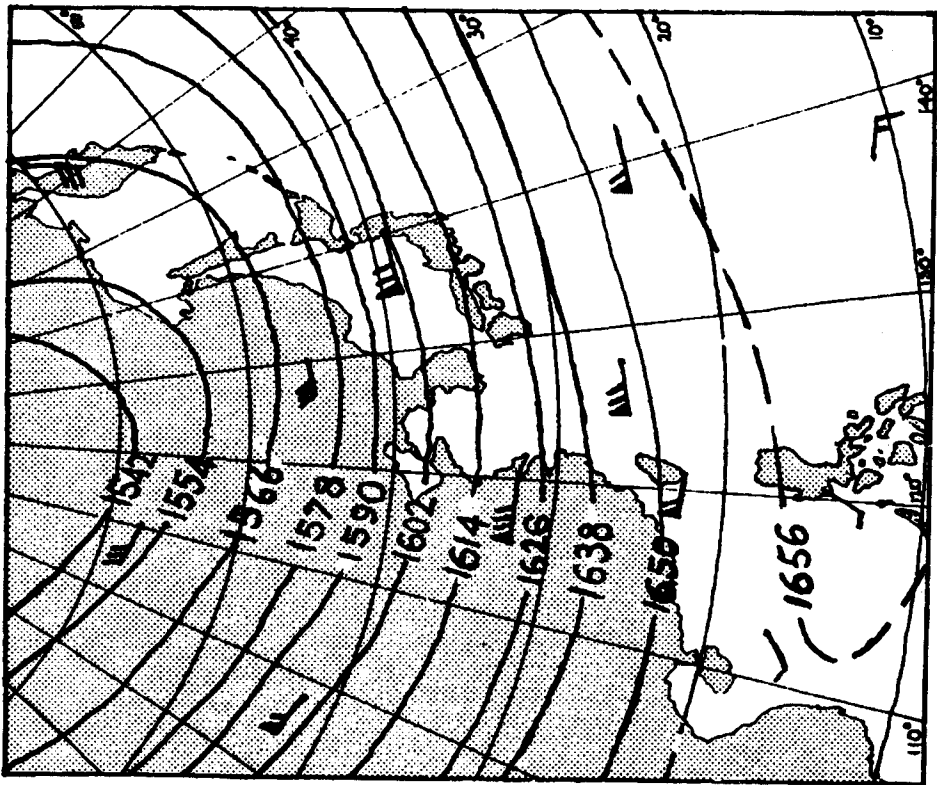


Figure 2-10. 100mb heights and winds for February. All heights in tens of gpm. (adapted from Crutcher & Meserve, 1970)

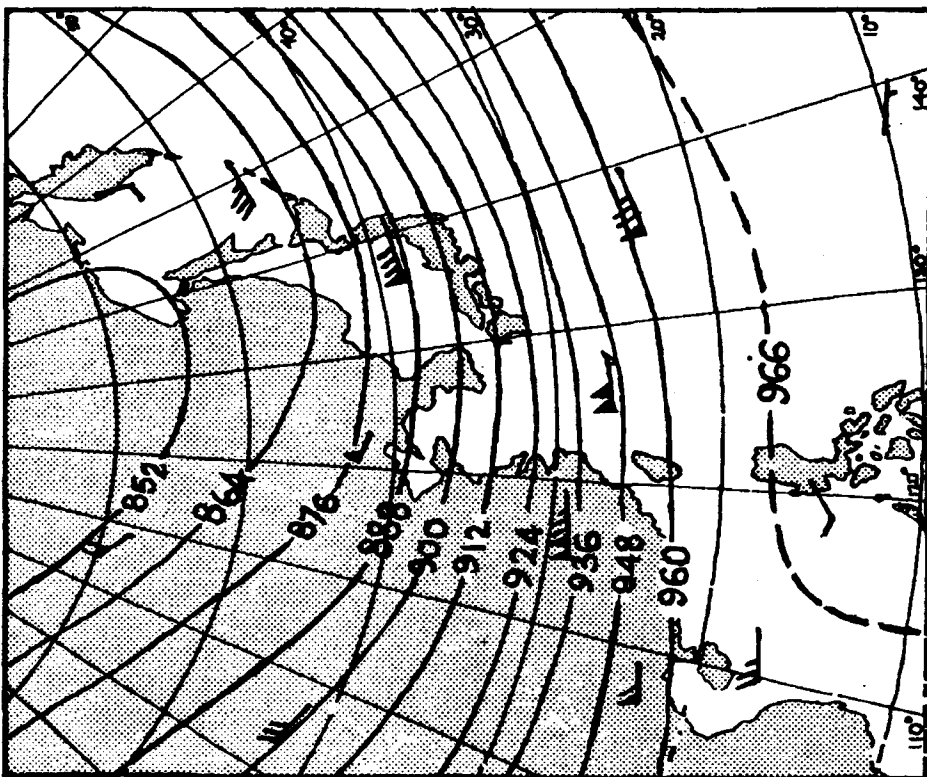


Figure 2-12. 300mb heights and winds for February. All heights in tens of gpm. (adapted from Crutcher & Meserve, 1970)

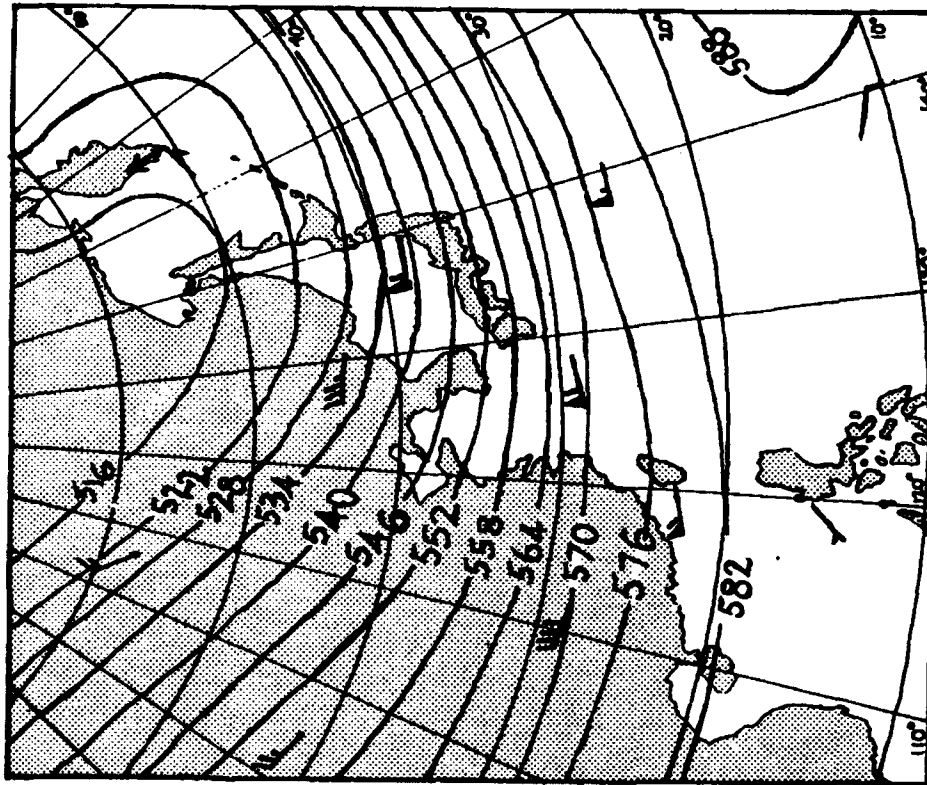


Figure 2-13. 500mb heights and winds for February. All heights in tens of gpm. (adapted from Crutcher & Meserve, 1970)

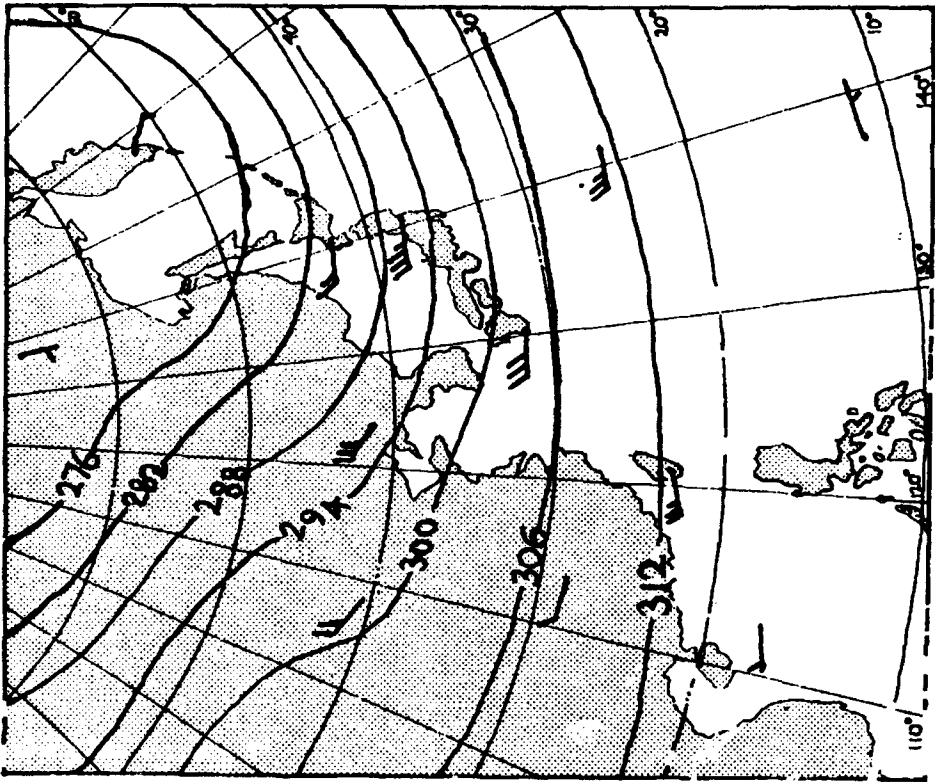


Figure 2-14. 700mb heights and winds for February. All heights in tens of gpm. (adapted from Crutcher & Meserve, 1970)

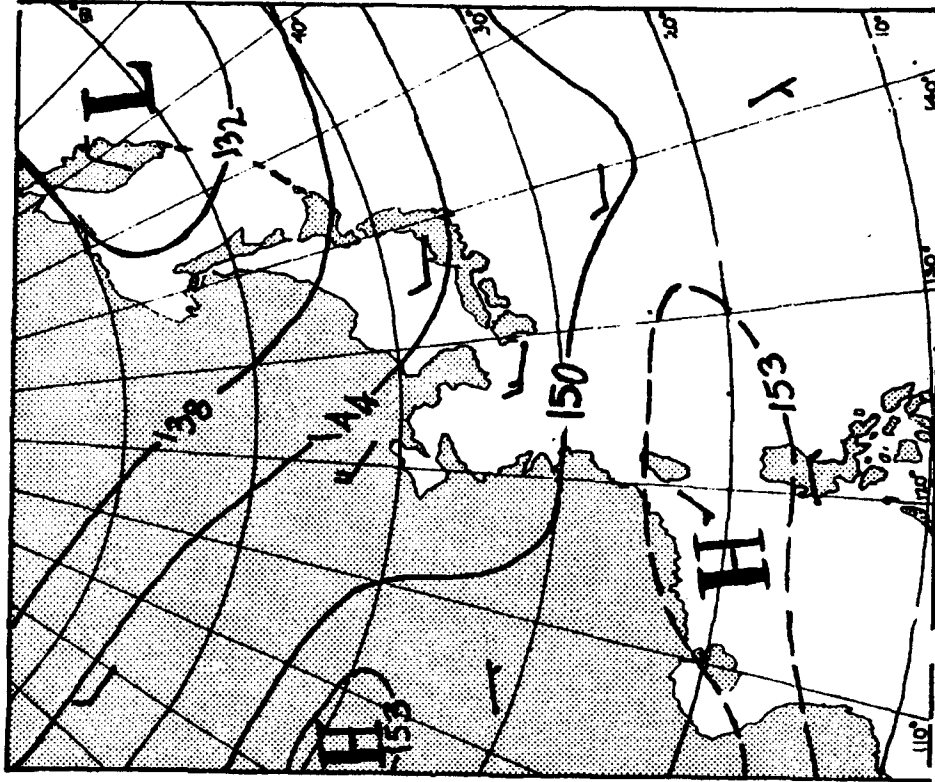


Figure 2-15. 850mb heights and winds for February. All heights in tens of gpm. (adapted from Crutcher & Meserve, 1970)

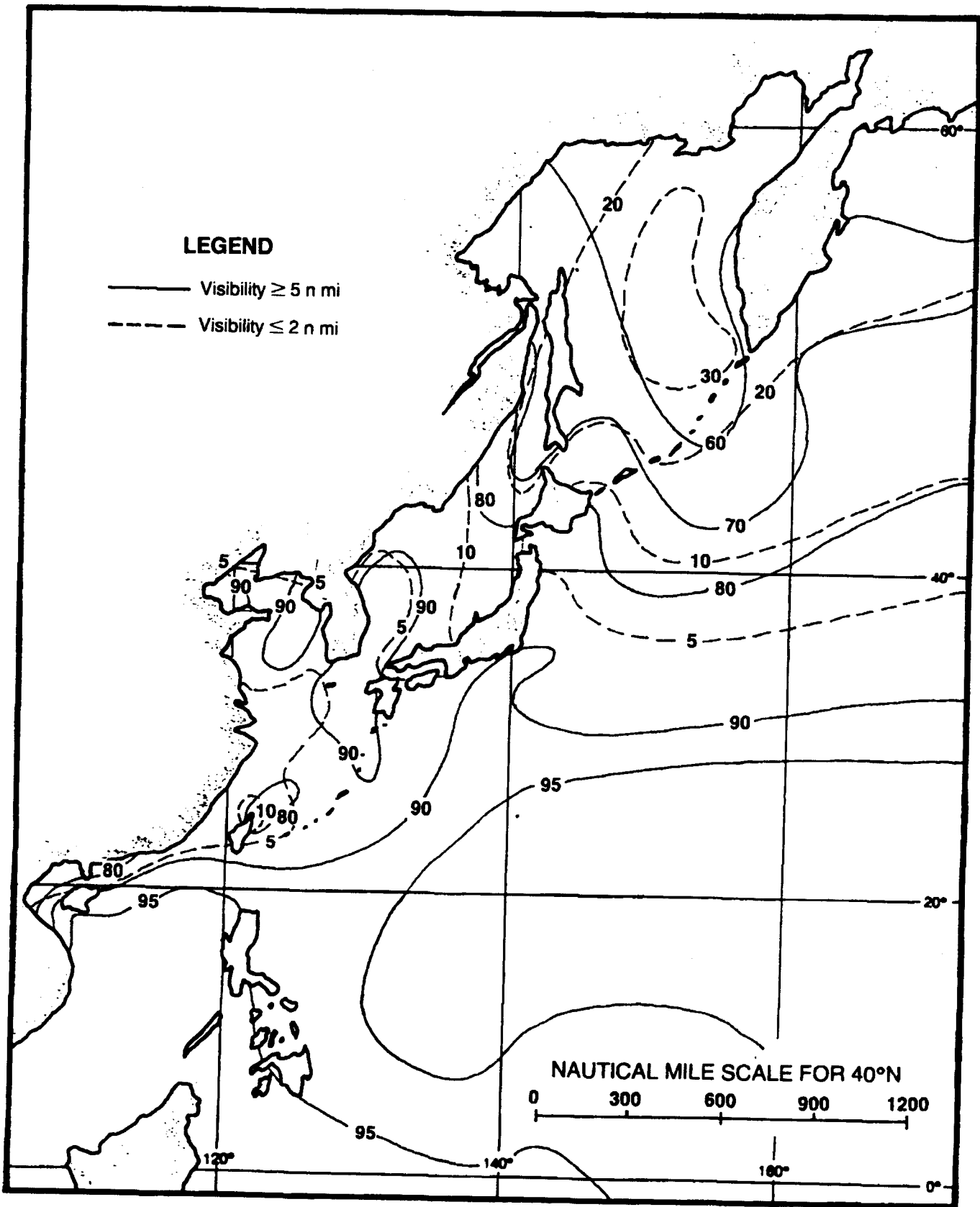


Figure 2-16. Percent frequency of occurrence of visibility limits during February (adapted from U.S. Navy, 1977).

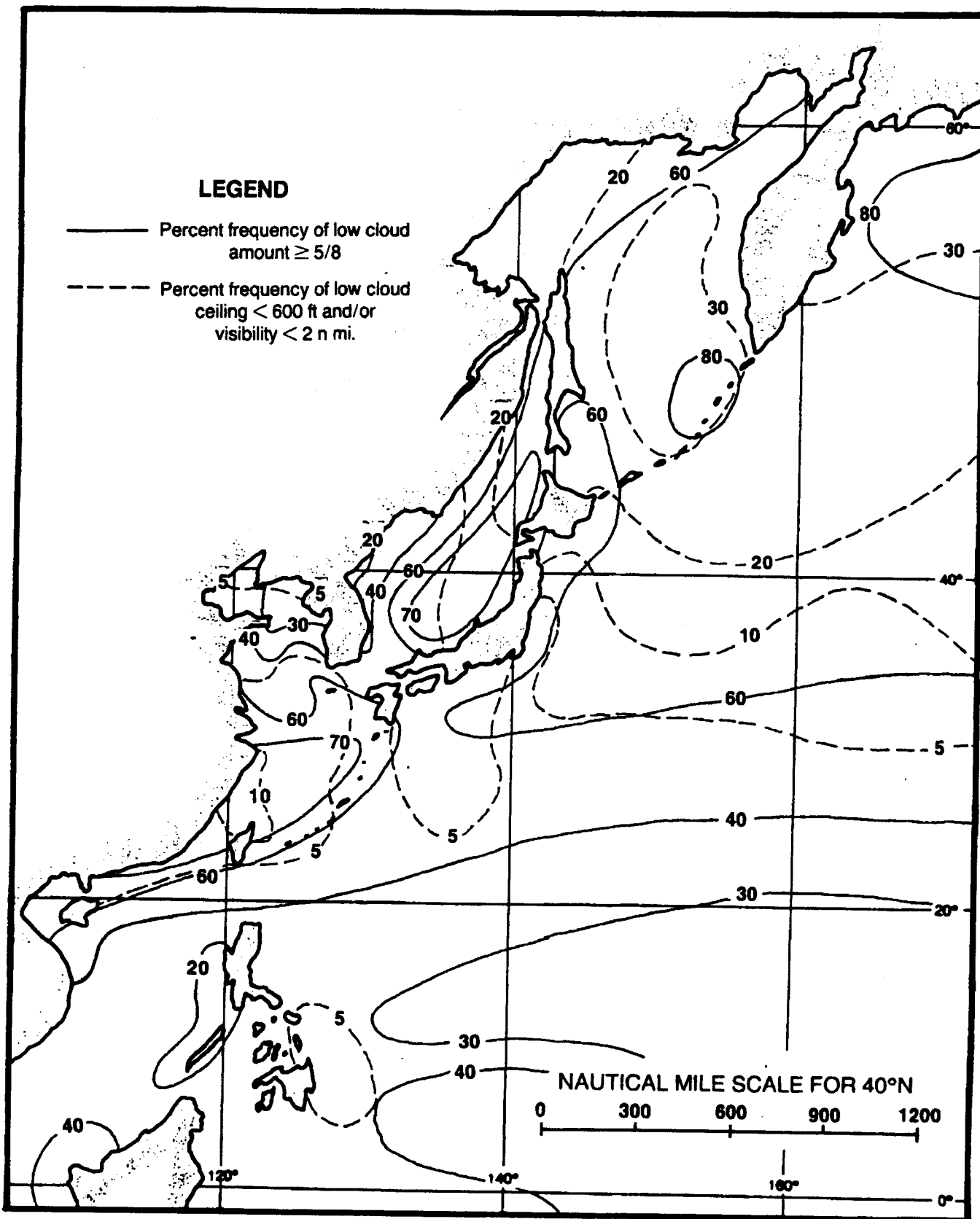


Figure 2-17. Low cloud amounts vs. ceiling and visibility during February (adapted from U.S. Navy, 1977).

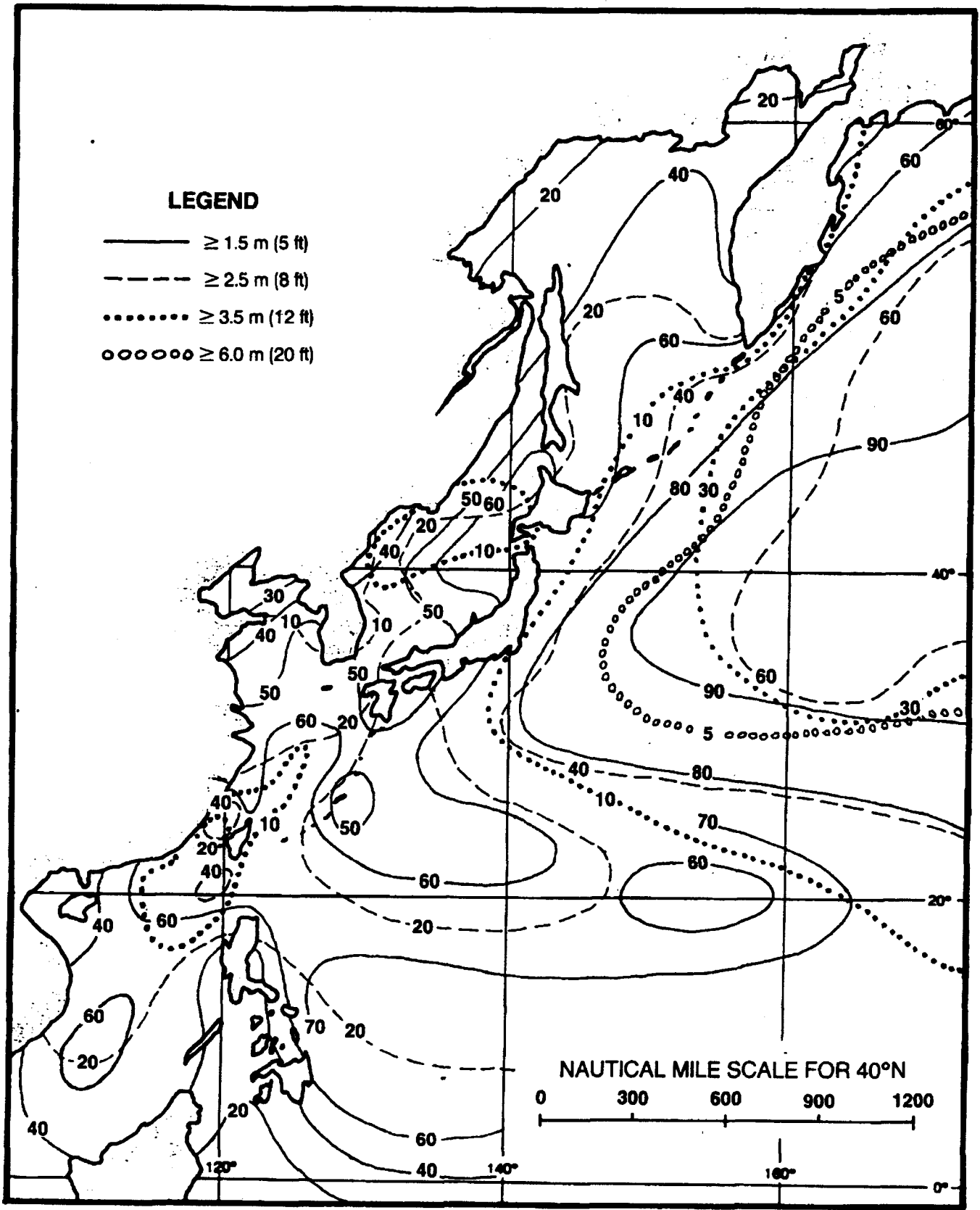


Figure 2-18. Percent frequency of occurrence of wave heights during February (adapted from U.S. Navy, 1977).

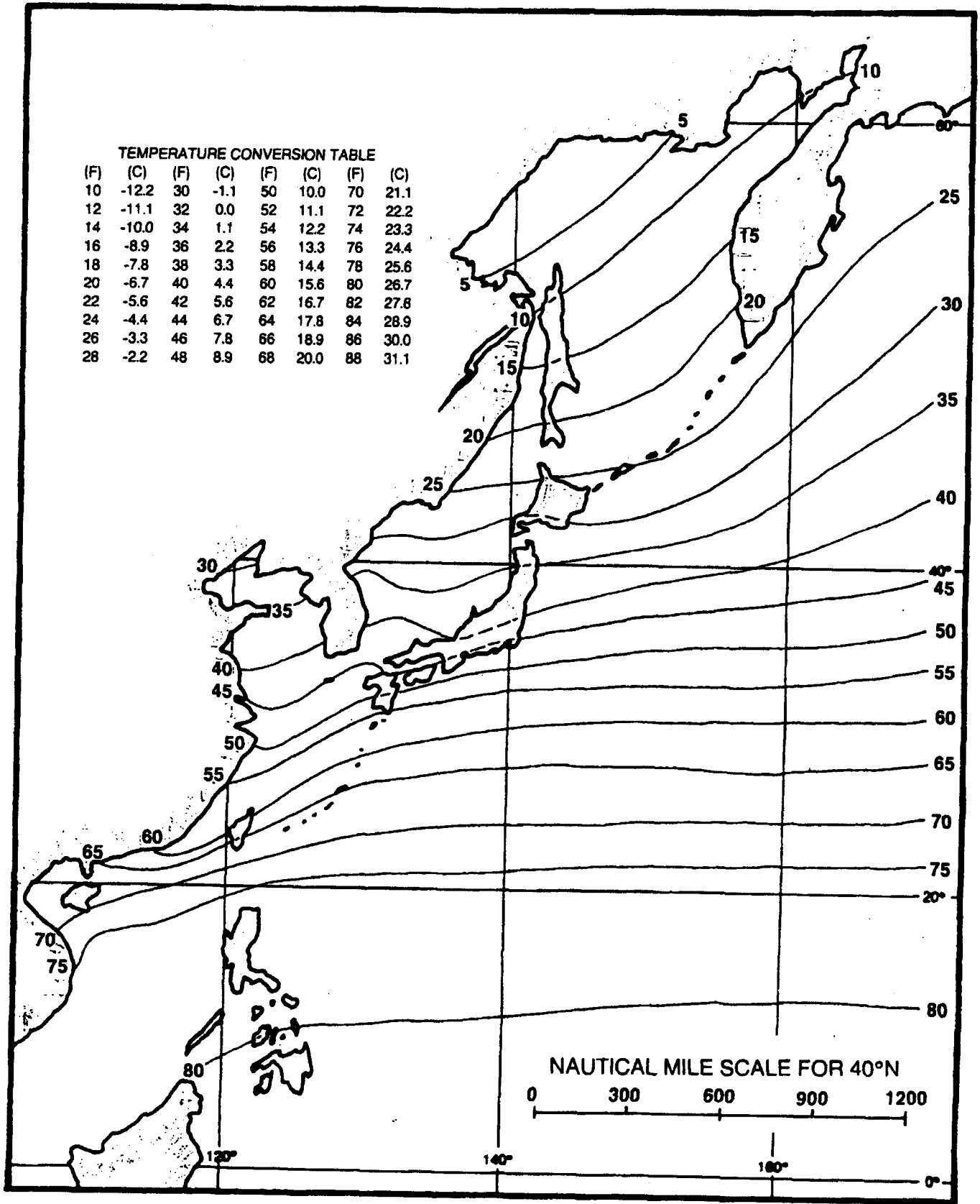


Figure 2-19. Mean surface air temperature in degrees Fahrenheit during February (adapted from Ownbey, 1973 and U.S. Navy, 1977).

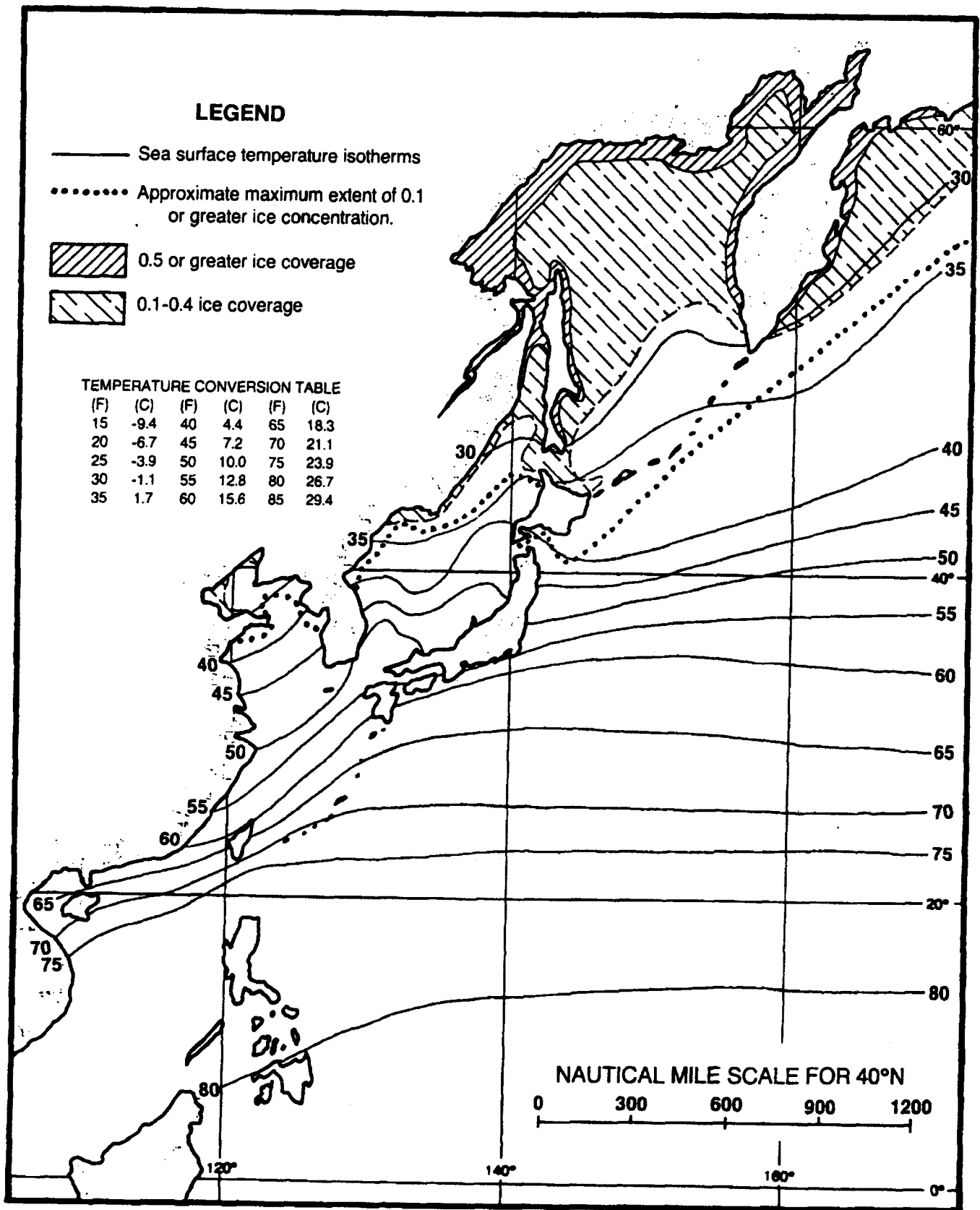


Figure 2-20. Mean sea surface temperature in degrees Fahrenheit during February, with approximate ice limits (adapted from U.S. Navy, 1967 and U.S. Navy, 1977).

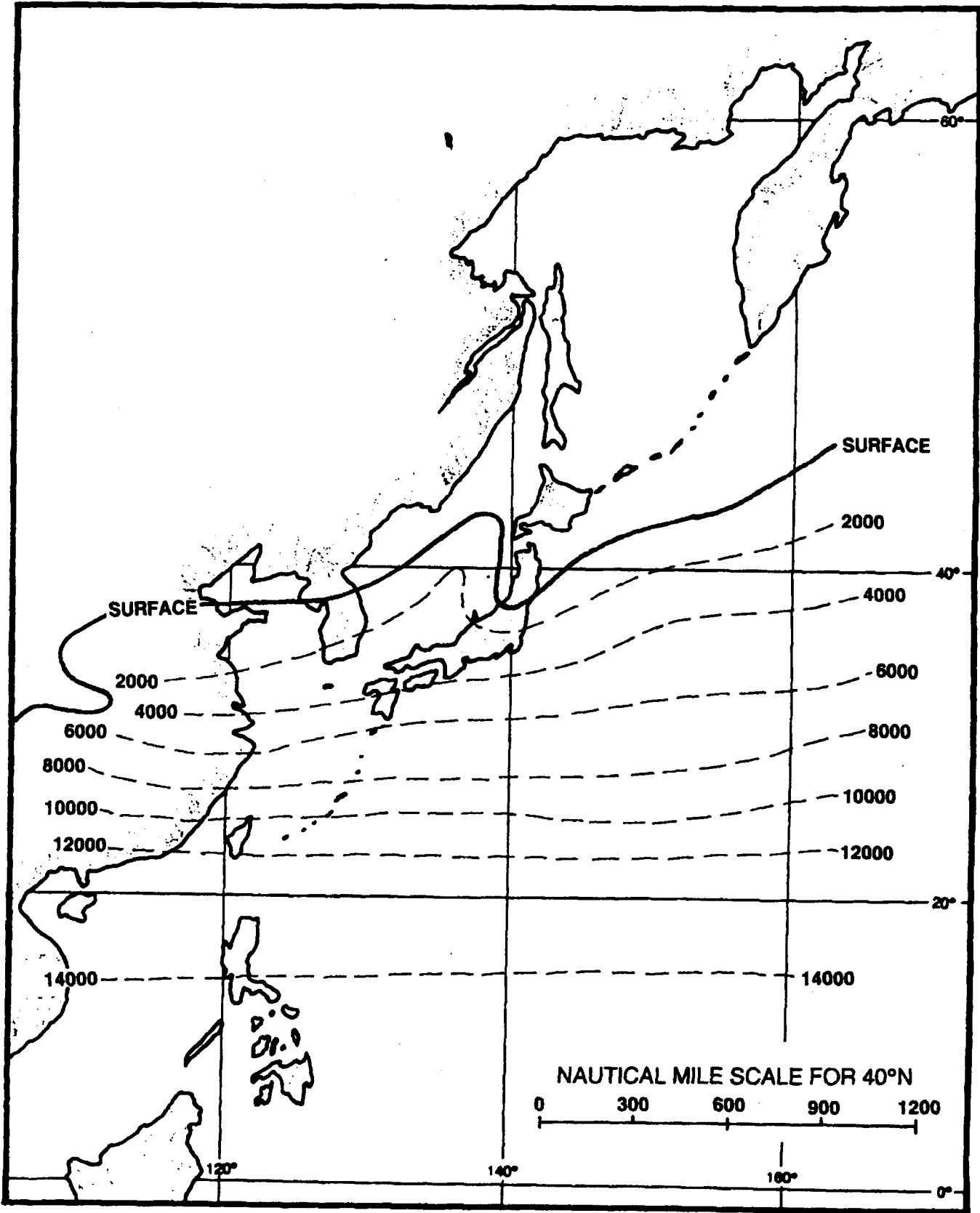


Figure 2-21. Mean altitude of the freezing level for February in feet (adapted from U.S. Air Force, 1965).

2.2.1.6 Spring (mid-March to mid-June)

The Siberian high weakens considerably and gradually shifts from the Lake Baikal position to near 45N 95E during spring. A low pressure area forms over Indochina and the low pressure center that is resident over the Sea of Okhotsk in winter retrogrades to a position over northern Mongolia. Thermal lows may begin to form over China and northeast Mongolia. As the Siberian high weakens, occasional "bubble highs" break off from the main high pressure cell and move eastward across the Sea of Japan. As the small high moves rapidly eastward it is usually followed by cyclogenesis and bad weather in the coastal Asian waters. As documented by George and Wolff (1953), "The reliability of this sequence of events leads directly to the adoption of the appearance of this surface bubble as the predictor for cyclogenesis and bad weather to follow."

The Aleutian low is still in evidence but, after April, is more diffuse and migratory in nature. The Polar Front starts to retreat northward, extending southwestward from the Aleutian low to a position south of Japan then westward across the Okinawa area and into China. Figure 2-22 shows the mean position of the front during May. It can be seen by comparing Figures 2-8 (page 2-29) and 2-22 that by May the jet stream has weakened and moved northward from its winter position. The north-south seasonal fluctuations of the Polar Front are directly tied to the movement of the southerly jet stream as it shifts from south of the Himalayan Plateau (winter position) to north of the plateau (summer position). Yoshino, (1965) shows

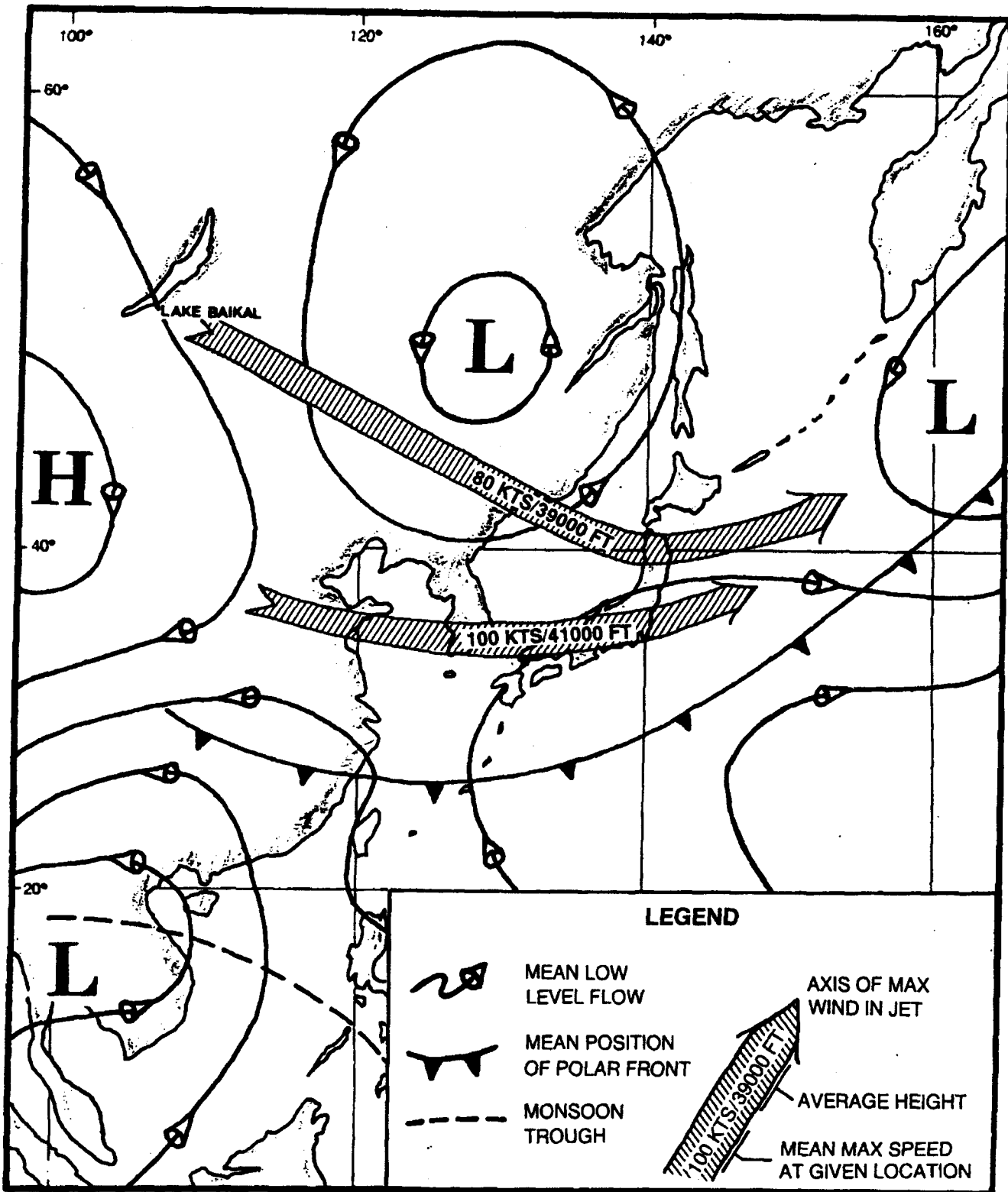


Figure 2-22. Typical atmospheric features during May: mean low level flow, mean position of polar front, mean position of monsoon trough and mean jet stream position (adapted from U.S. Marine Corps, 1967 and U.S. Air Force, 1968).

the relationship of the latitude of the upper wind maximum to the beginning and end of the Bai-U season in Japan and the Mei-Yu season in the Yangtze (Changjiang) region of China, as the Polar Front moves northward in concert with the northward displacement of the upper wind maximums.

Figure 2-22 shows there are two mean jet stream cores. The southernmost core crosses the Yellow Sea, southern Korea and southern Honshu before proceeding east-northeastward across the Pacific Ocean. The northern core extends southeastward from Lake Baikal and crosses the northern tip of Honshu before moving eastward across the Pacific. Some studies show the two cores merging into a single core just east of Japan.

The most probable spring migratory low pressure systems include Manchurian Lows, Lake Baikal Lows, South Mongolia Lows, Shanghai Lows, and Taiwan Lows. The average tracks for each of the systems are presented in Figure 2-6 (page 2-23).

Of the yearly average of about 57 cold fronts occurring in the Far East, 14 (25%) occur during spring (mid-March to mid-June), a frequency of about one each six days (FWC/JTWC, 1969).

From a minimum in February, tropical cyclone activity starts to show a marked increase by June, although an average of only one typhoon can be expected to form in the western North Pacific during June. The northward limit of tropical cyclones during March and April (combined statistics) encompasses the East China Sea, extreme

southern Sea of Japan, the western North Pacific Ocean south of 36°N, and the Philippine Sea. During June, the tracks start to show incursions across all of the water areas addressed in this handbook, except for the Sea of Okhotsk (Crutcher and Quayle, 1974). Refer to Appendix B for tropical cyclone tracks.

Figures 2-23 through 2-35 depict the average climatic conditions that prevail over eastern Asia and adjacent waters during the month of May. A brief discussion of each of the parameters is presented in the climatology sections of the regional chapters in this handbook.

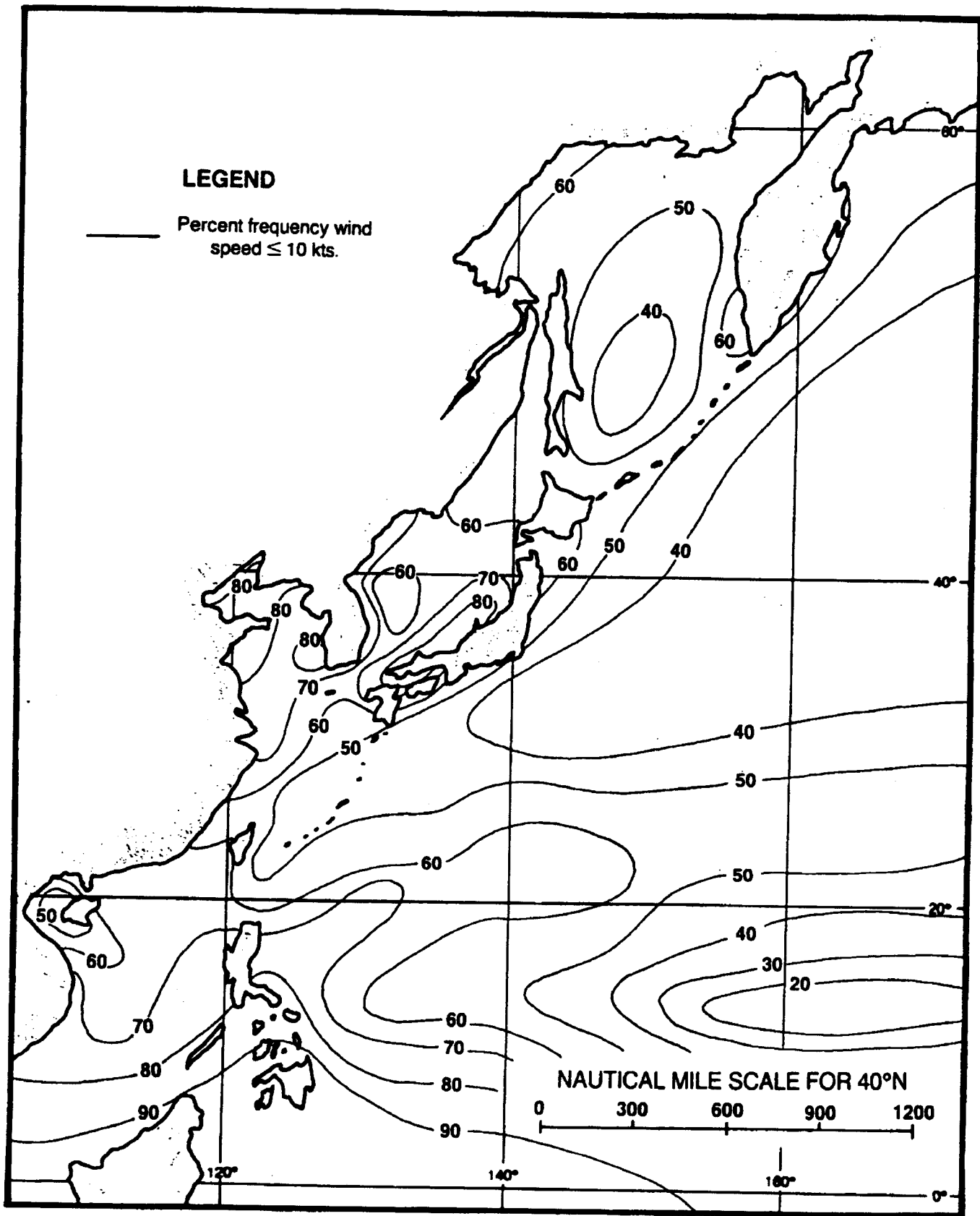


Figure 2-23. Surface winds during May (adapted from U.S. Navy, 1977).

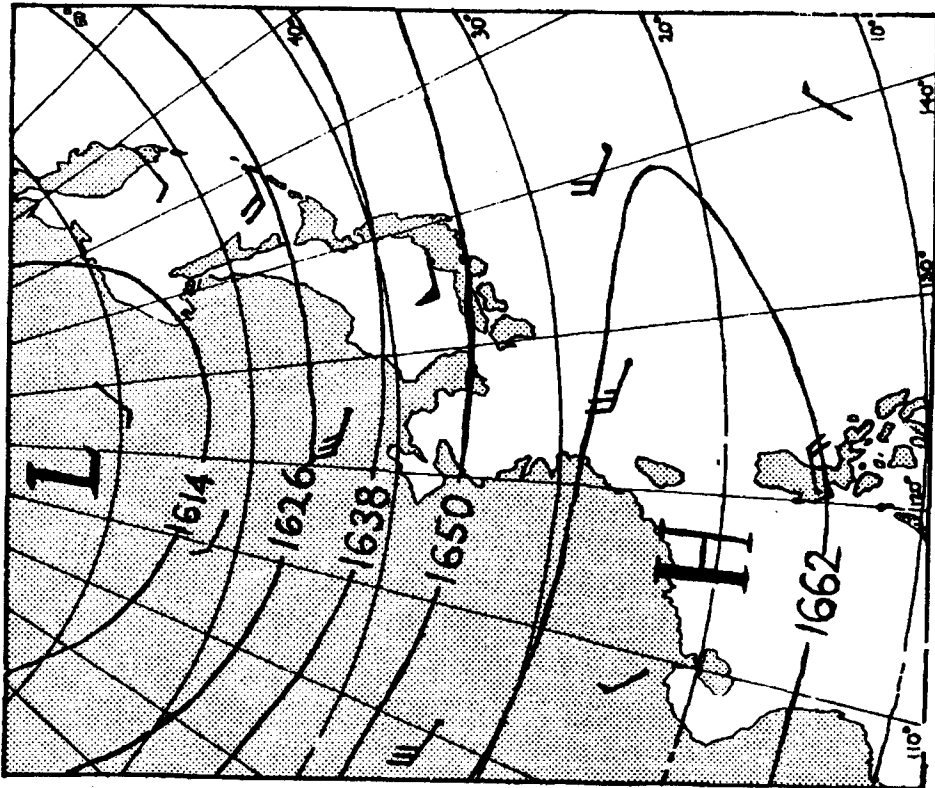


Figure 2-24. 100mb heights and winds for May. All heights in tens of gpm. (adapted from Crutcher & Meserve, 1970)

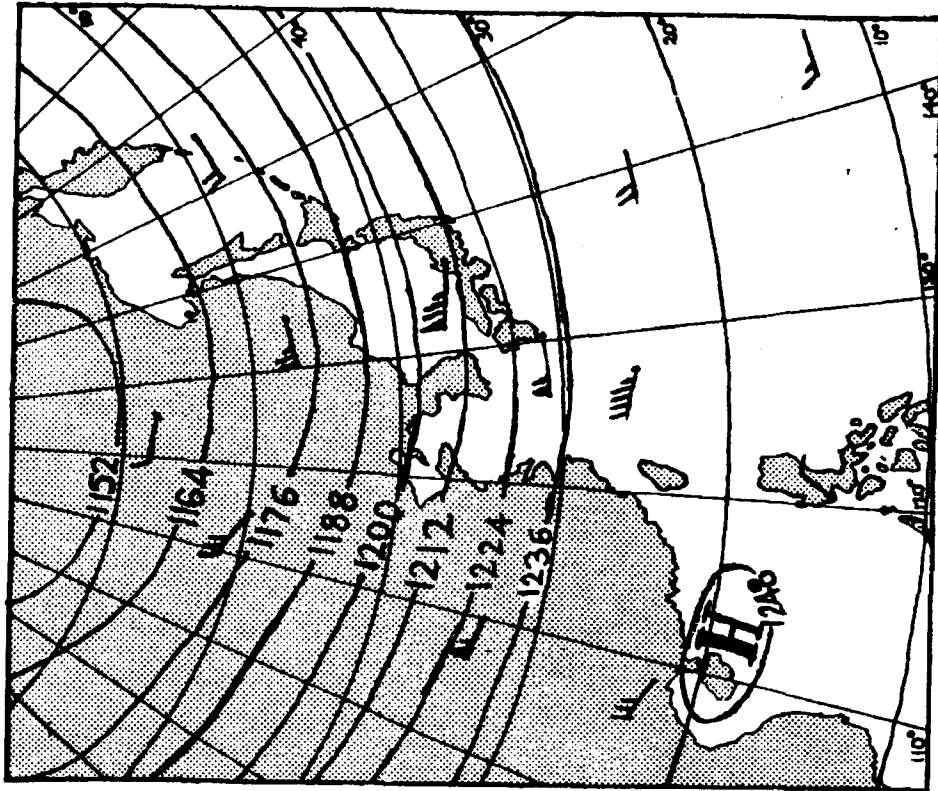


Figure 2-25. 200mb heights and winds for May. All heights in tens of gpm. (adapted from Crutcher & Meserve, 1970)

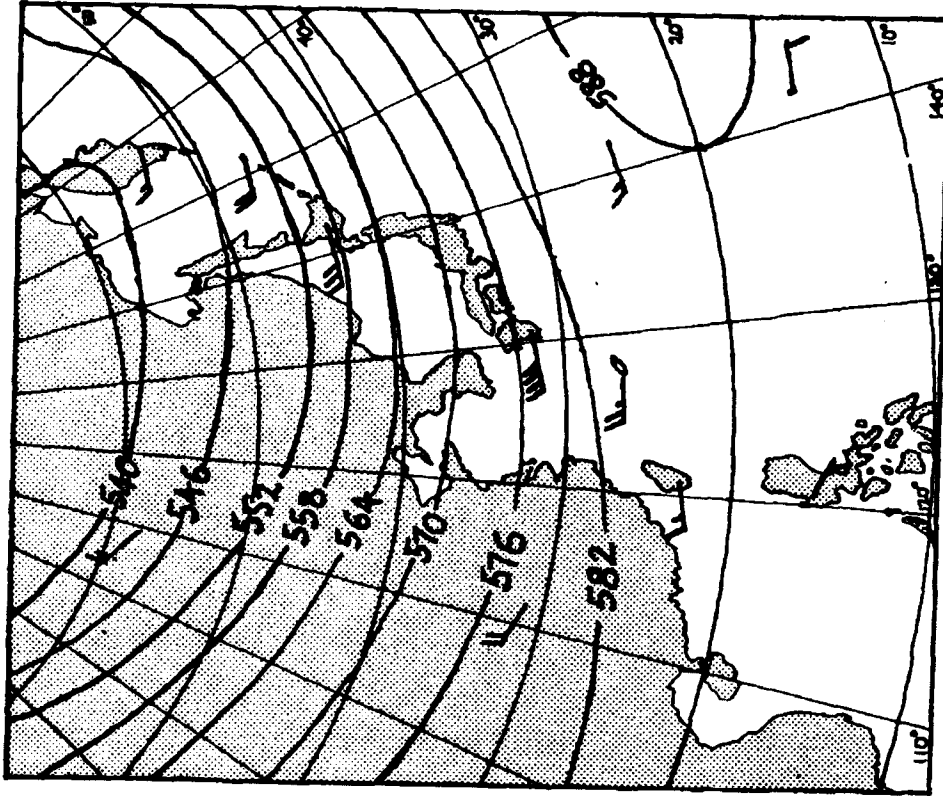


Figure 2-27. 500mb heights and winds for May. All heights in tens of gpm. (adapted from Crutcher & Meserve, 1970)

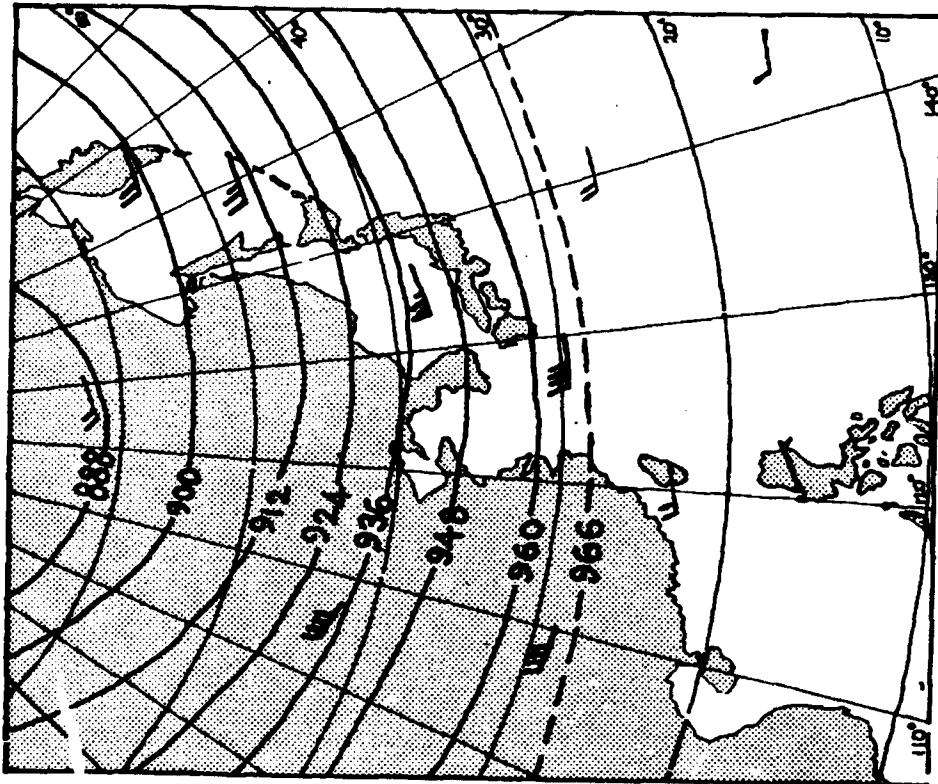


Figure 2-26. 300mb heights and winds for May. All heights in tens of gpm. (adapted from Crutcher & Meserve, 1970)

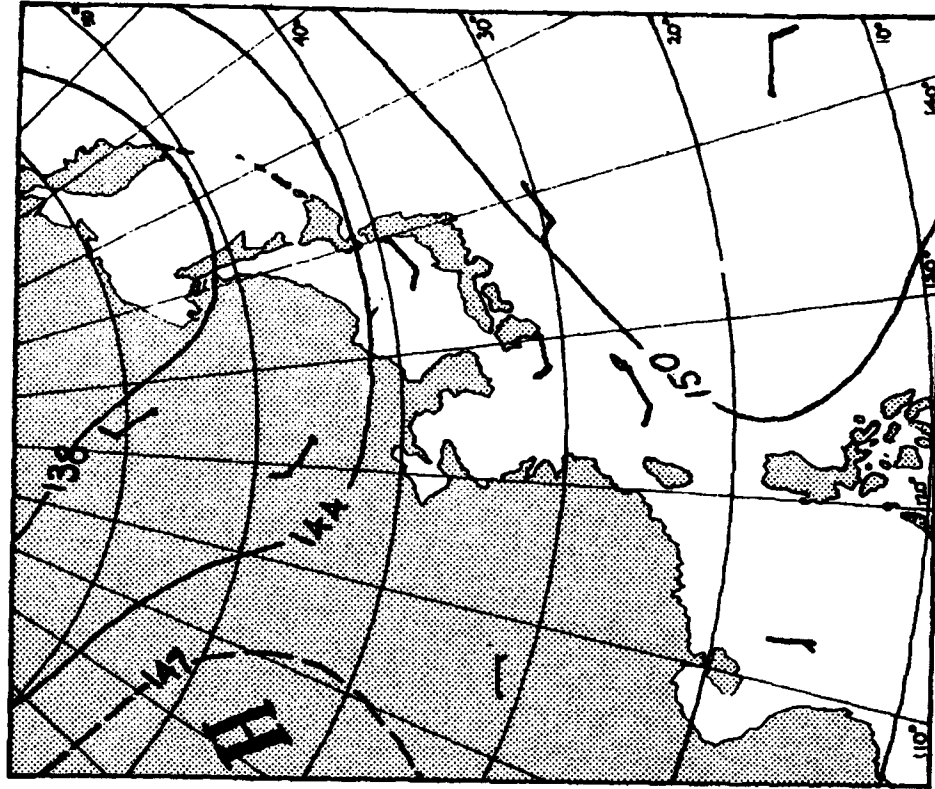


Figure 2-29. 850mb heights and winds for May. All heights in tens of gpm. (adapted from Crutcher & Meserve, 1970)

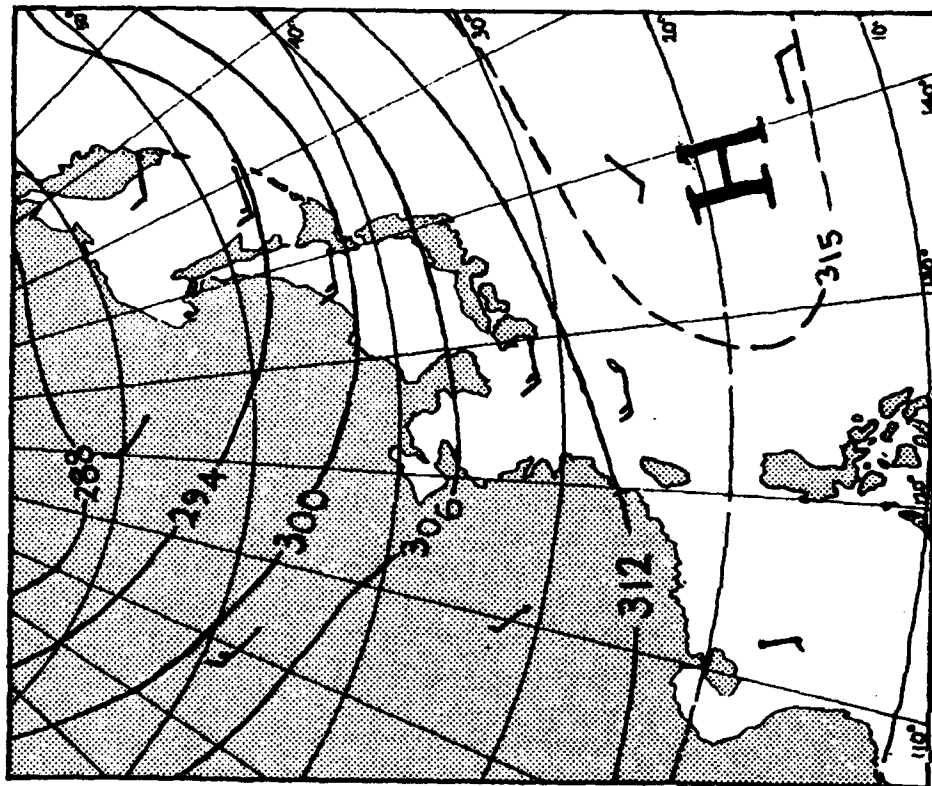


Figure 2-28. 700mb heights and winds for May. All heights in tens of gpm. (adapted from Crutcher & Meserve, 1970)

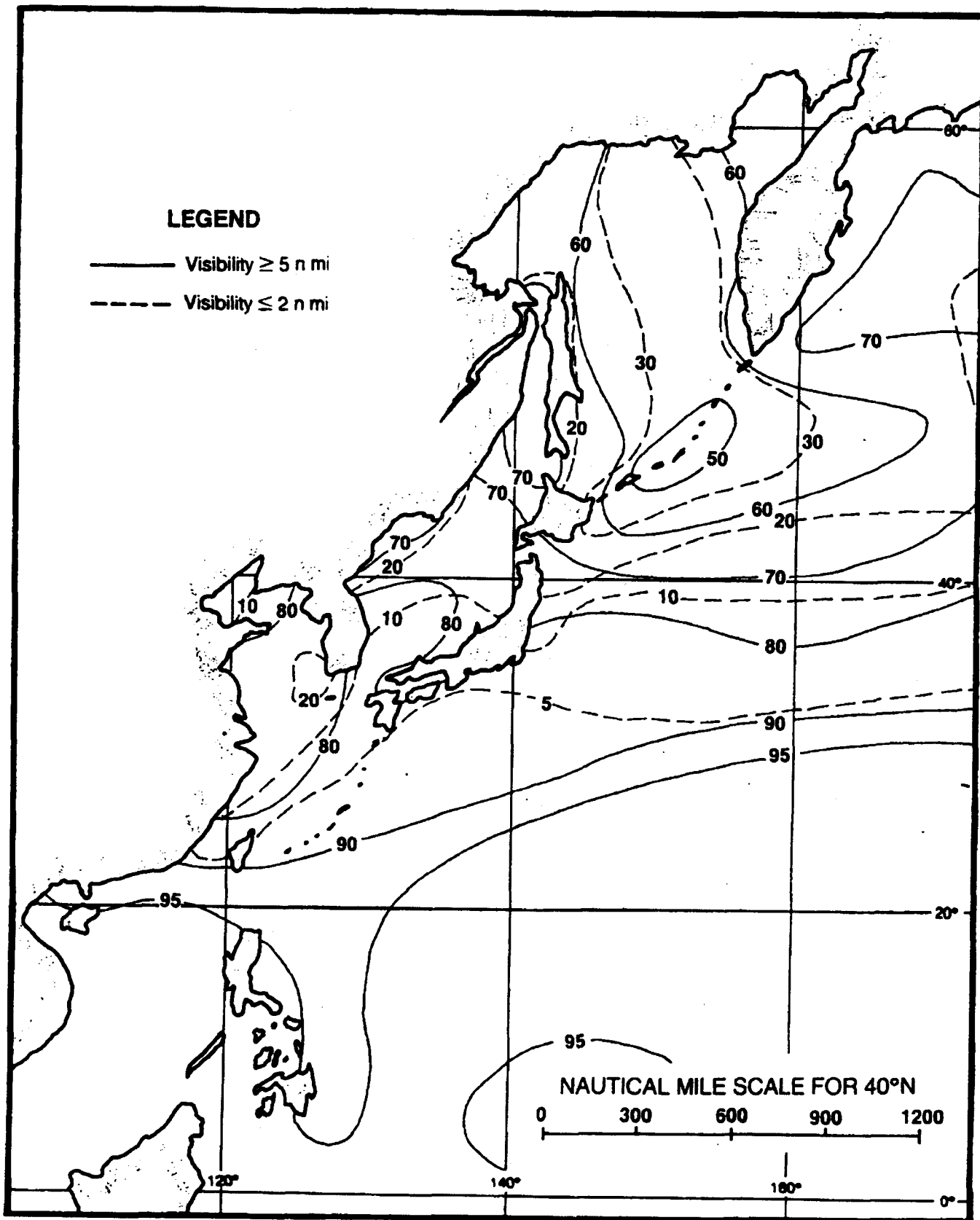


Figure 2-30. Percent frequency of occurrence of visibility limits during May (adapted from U.S. Navy, 1977).

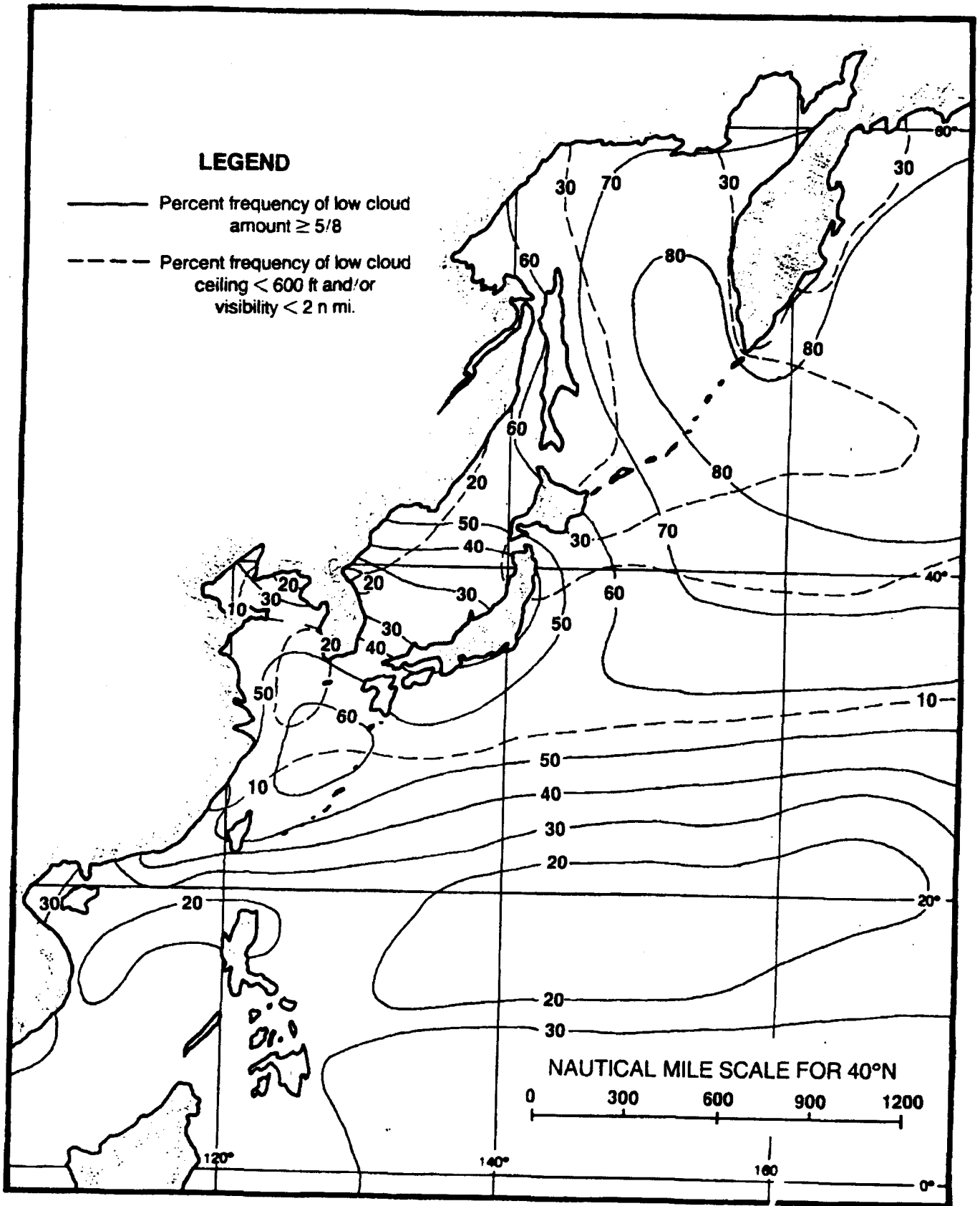


Figure 2-31. Low cloud amounts vs. ceiling and visibility during May (adapted from U.S. Navy, 1377).

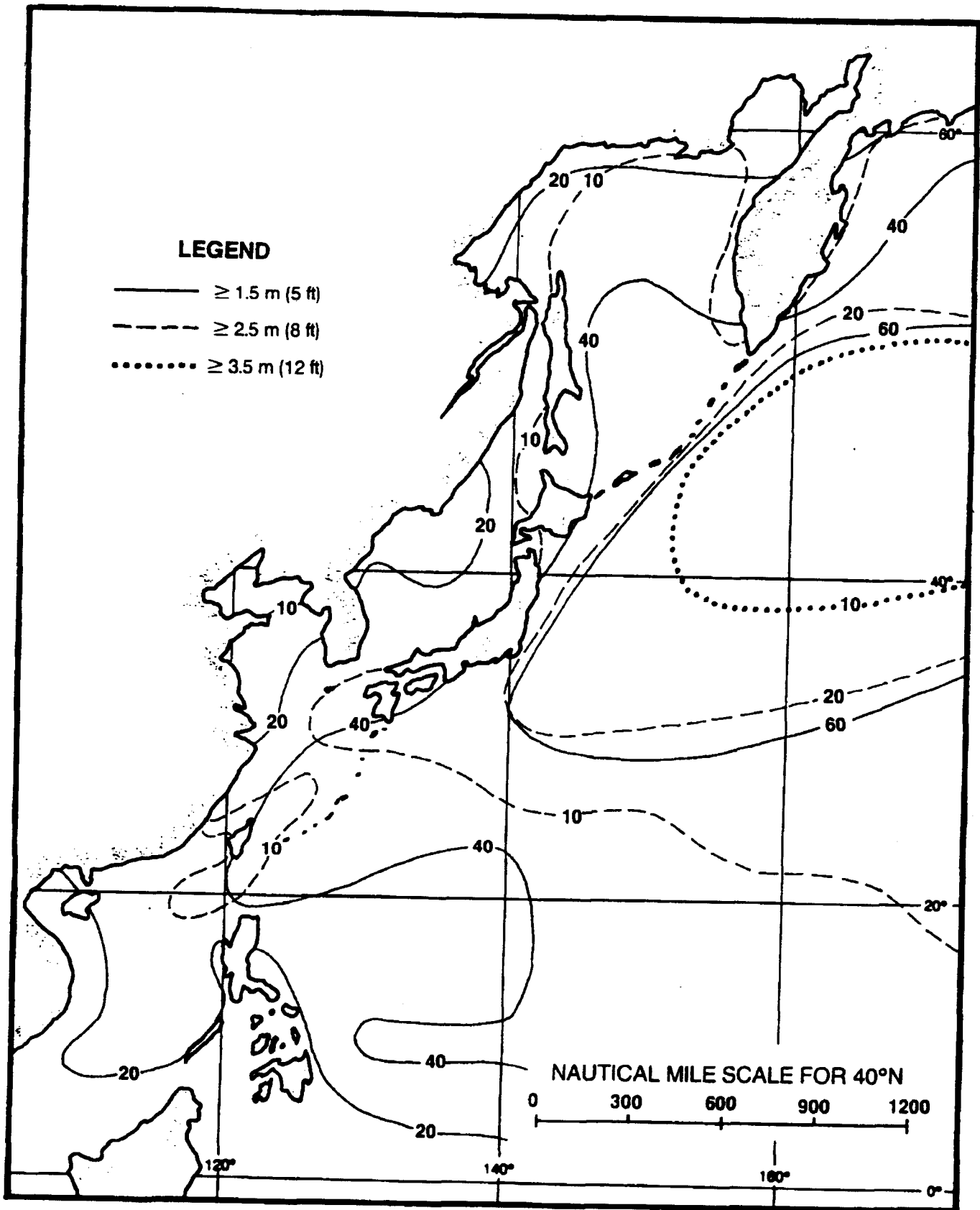


Figure 2-32. Percent frequency of occurrence of wave heights during May (adapted from U.S. Navy, 1977).

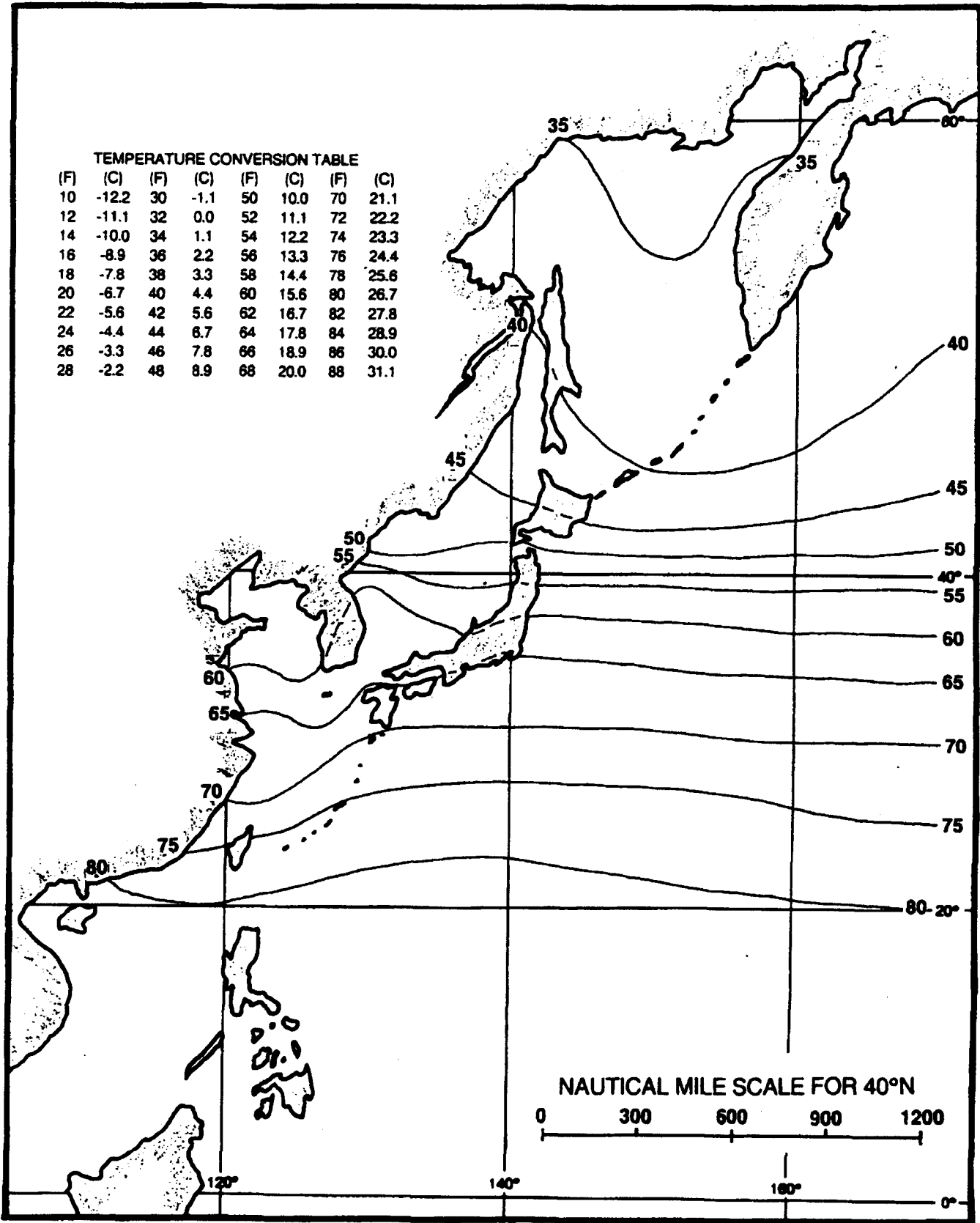


Figure 2-33. Mean surface air temperature in degrees Fahrenheit during May (adapted from Ownbey, 1973 and U.S. Navy, 1977).

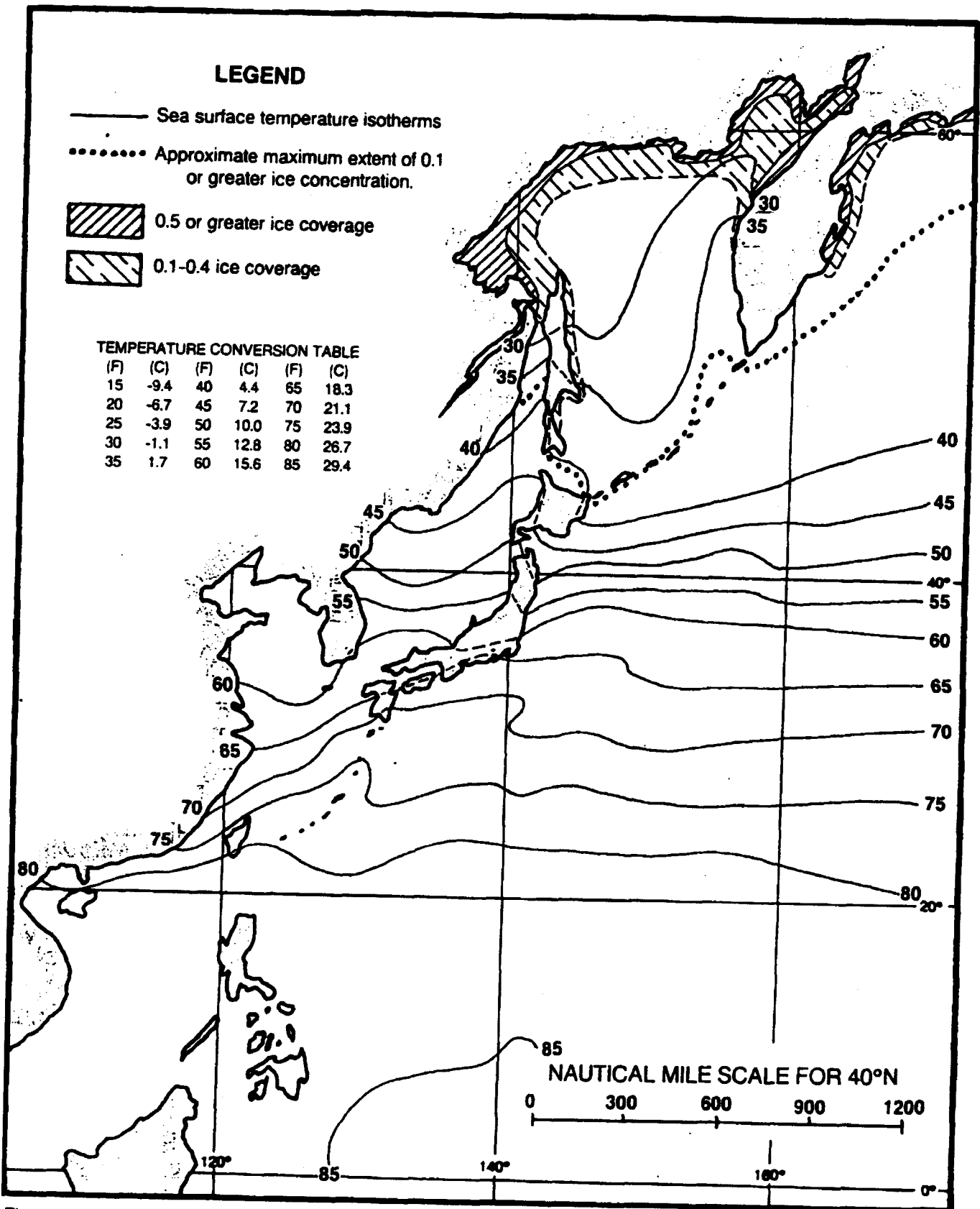


Figure 2-34. Mean sea surface temperature in degrees Fahrenheit during May, with approximate ice limits (adapted from U.S. Navy, 1967 and U.S. Navy, 1977).

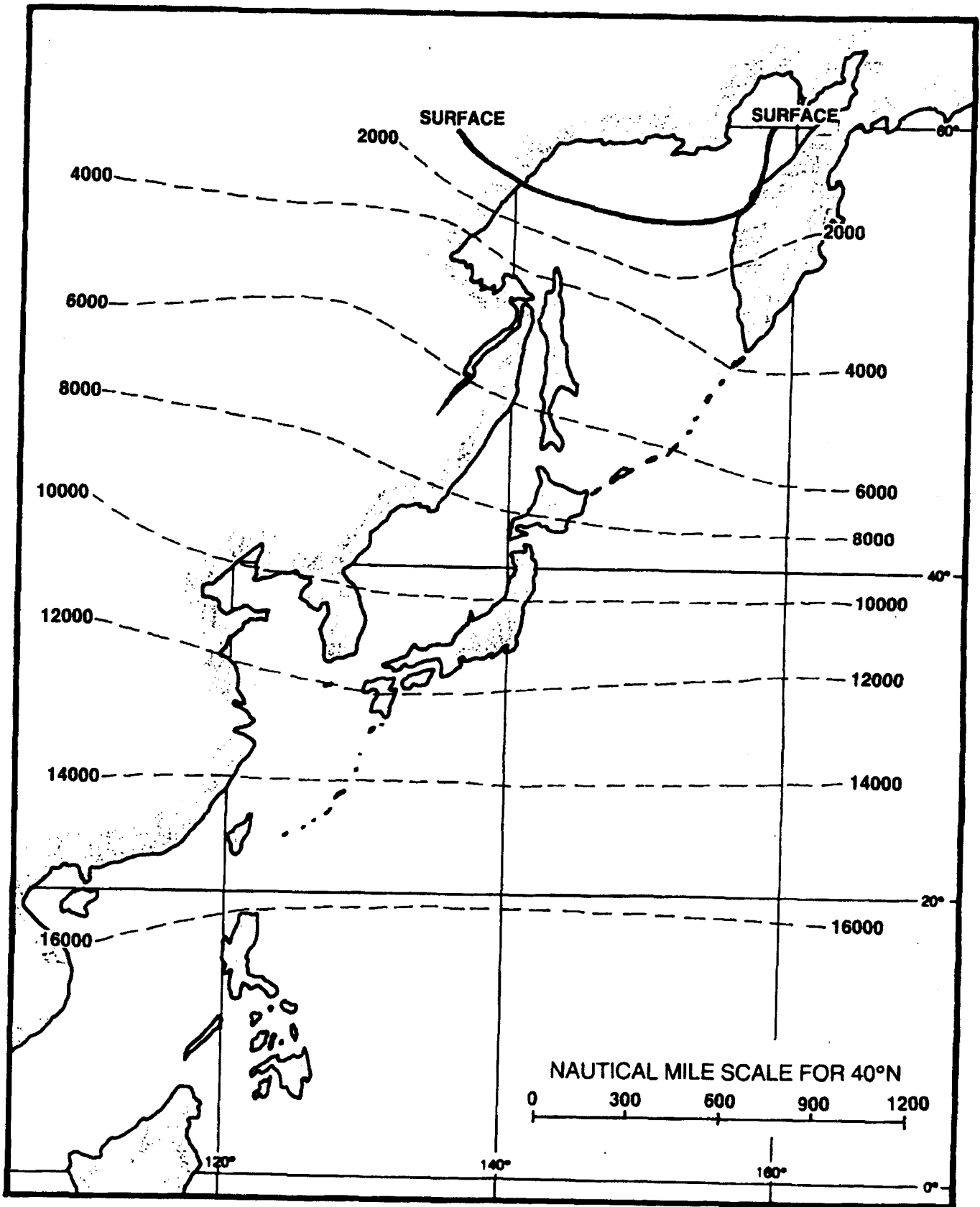


Figure 2-35. Mean altitude of the freezing level for May in feet (adapted from U.S. Air Force, 1965).

2.2.1.7 Summer (mid-June to mid-September)

At the beginning of the traditional summer season, the Polar Front is oriented east-west along southern Honshu and extends west-southwestward into China. The warm, moist air being transported northward south of the front causes warm frontal-type overrunning and usually results in extensive precipitation over Japan. This situation, called the Bai-U (or Plum Rain) season, usually persists until mid-July when the Polar Front shifts northward and establishes its summer position northwest of the Sea of Japan.

The Siberian high is weak, and usually fractured into several small high pressure cells. Most migratory lows are relatively weak and move eastward north of the central portion of Honshu. The jet stream is at its weakest during the summer with a mean position across the northern Korean peninsula, Sea of Japan, and northern Honshu (see Figure 2-36).

The monsoon trough has migrated northward, extending northwestward from the tropical north Pacific waters east of the Philippines to the East China Sea north of Taiwan, thence westward into the interior of southern China.

The most probable summer migratory low pressure systems include Lake Baikal Lows, South Mongolia Lows, and Yellow Sea Lows. Average tracks for each of the systems are shown in Figure 2-6.

Of the yearly average of approximately 57 cold fronts occurring in the Far East, only 6 (11%) occur during summer (mid-June to mid-September), a frequency of about one every two weeks (FWC/JTWC, 1969).

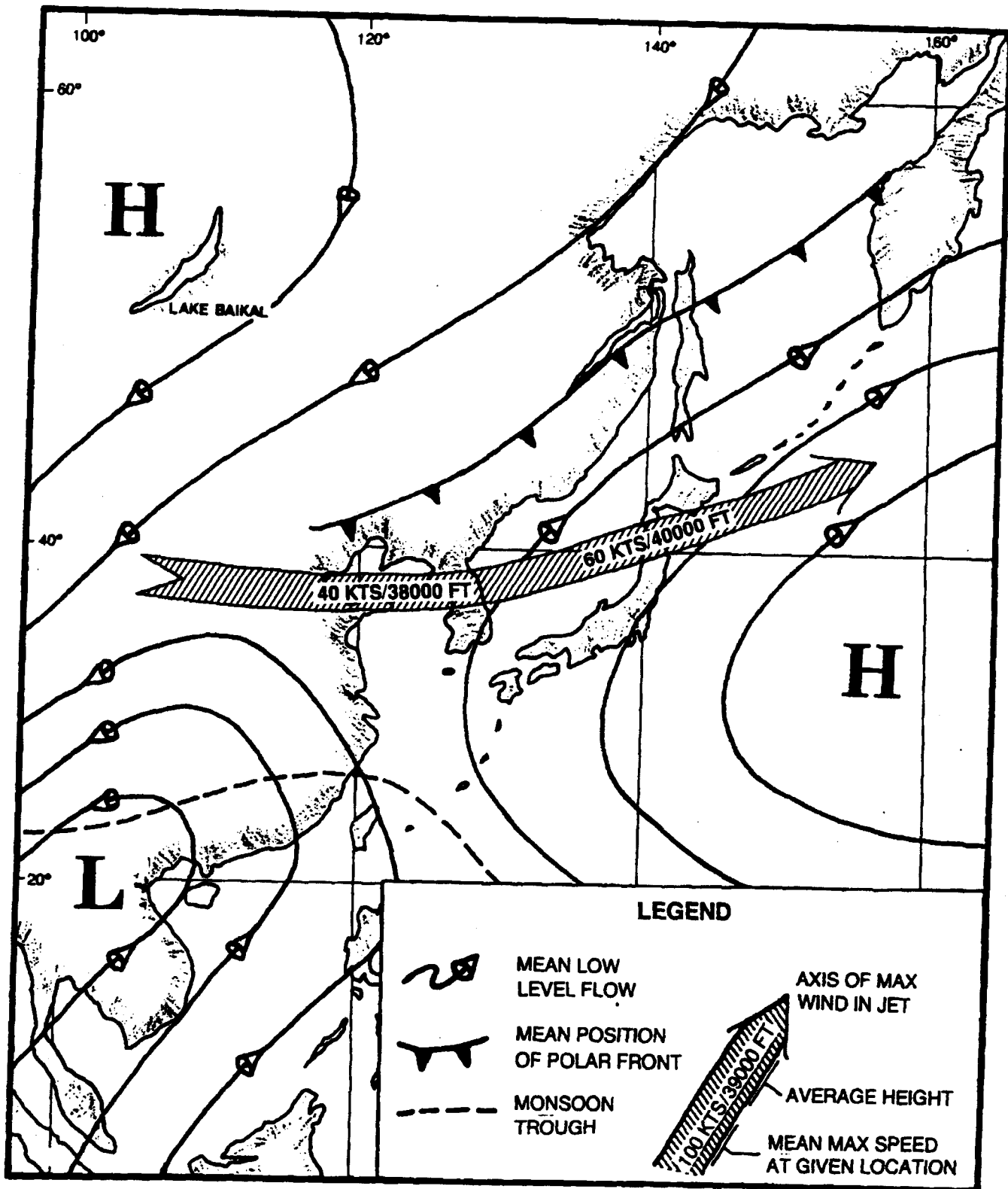


Figure 2-36. Typical atmospheric features during August: mean low level flow, mean position of polar front, mean position of monsoon trough and mean jet stream position (adapted from U.S. Marine Corps, 1967 and U.S. Air Force, 1968).

Summer brings a maximum of tropical cyclone activity to the western North Pacific and eastern Asia. Approximately four typhoons per year form in each of the months of August and September, with three forming during July (Crutcher and Quayle, 1974). Of these, a large percentage can be expected to move northwestward across the waters of the Philippine Sea or western North Pacific. Some can be expected to recurve to the northeast while south of Japan, but a significant number will move into the waters of the East China Sea, Yellow Sea, or Sea of Japan. Refer to Appendix B for tropical cyclone tracks.

Figures 2-37 through 2-49 depict various average climatic conditions that prevail over eastern Asia and adjacent waters during the month of August. A brief discussion of each of the parameters is presented in the climatology sections of the regional chapters in this handbook.

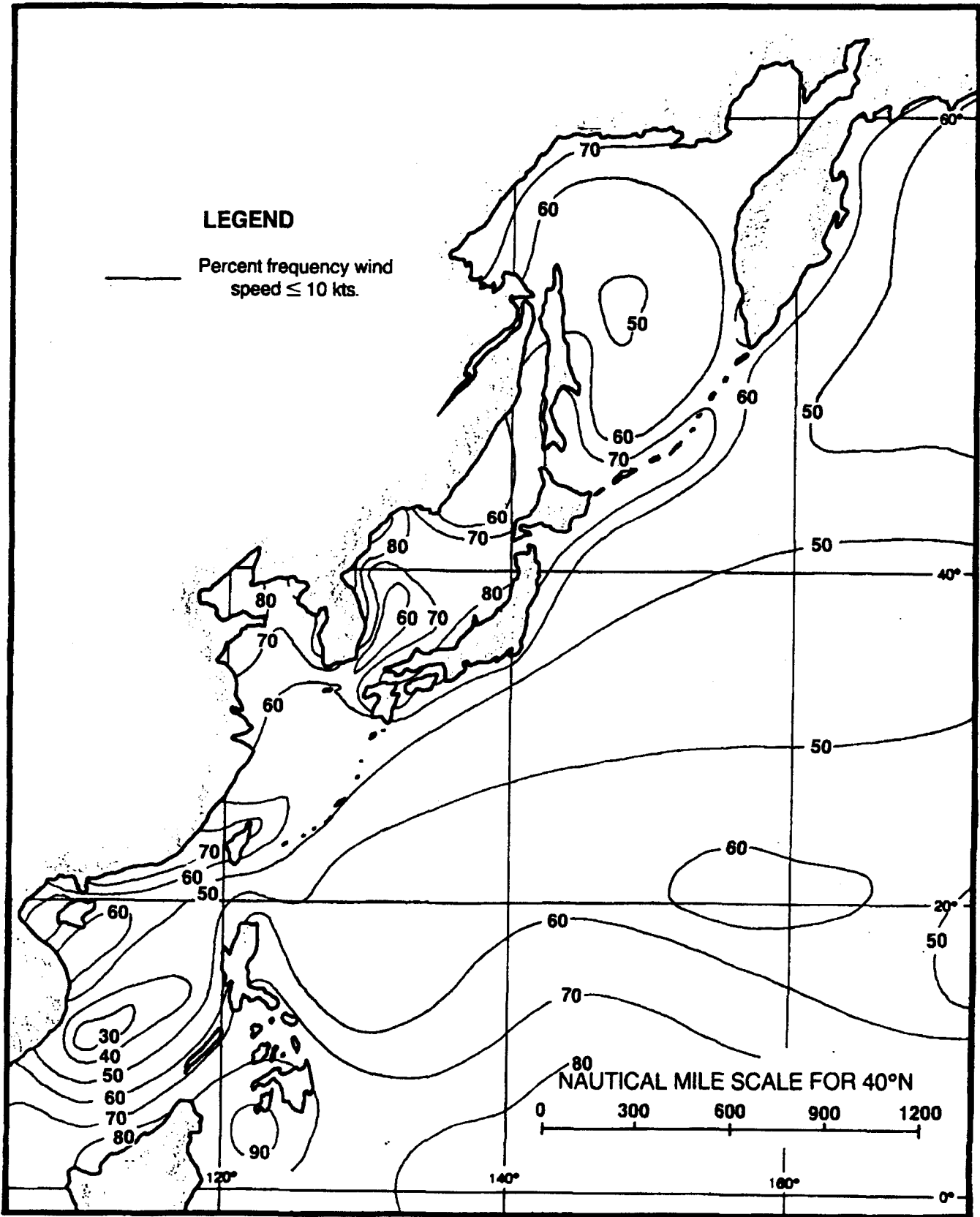


Figure 2-37. Surface winds during August (adapted from U.S. Navy, 1977).

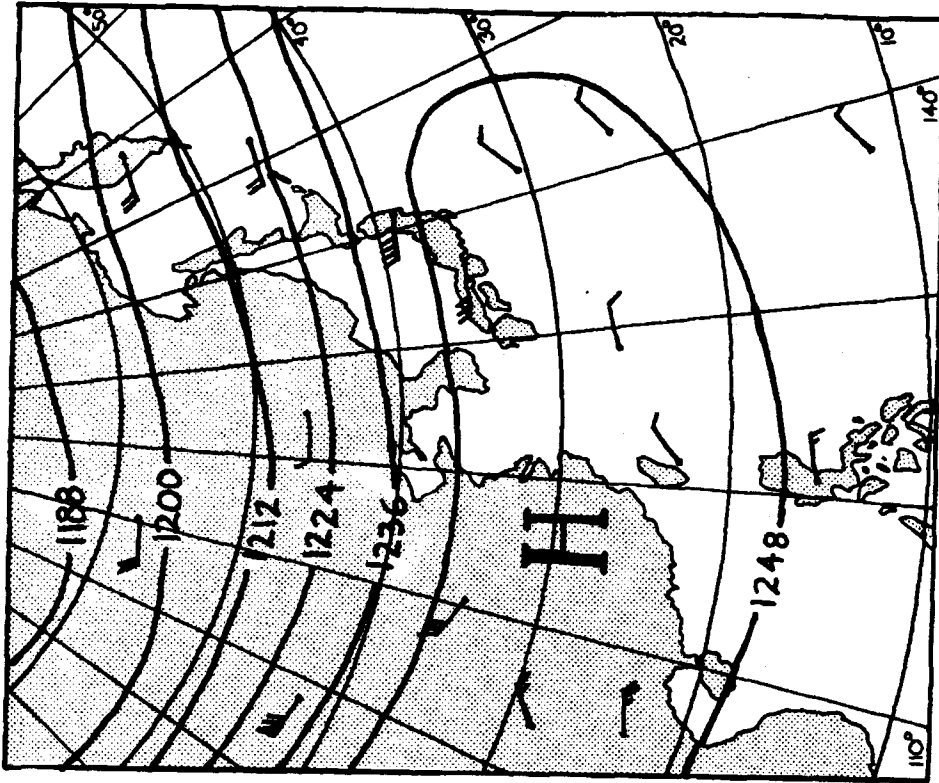


Figure 2-39. 200mb heights and winds for August. All heights in tens of gpm. (adapted from Crutcher & Meserve, 1970)

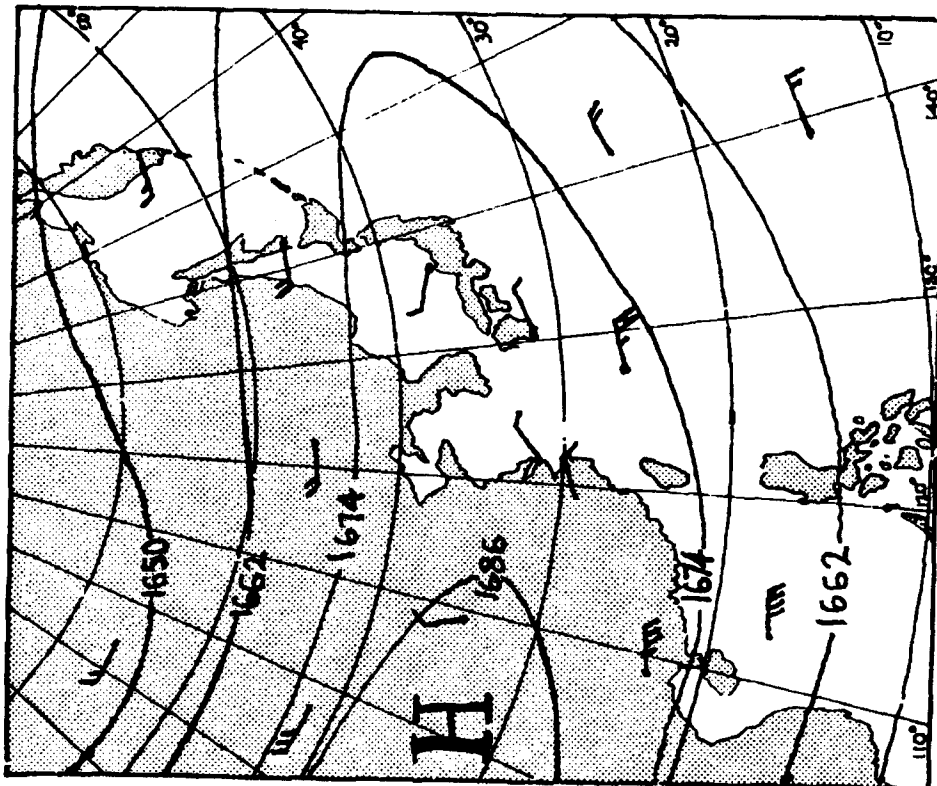


Figure 2-38. 100mb heights and winds for August. All heights in tens of gpm. (adapted from Crutcher & Meserve, 1970)

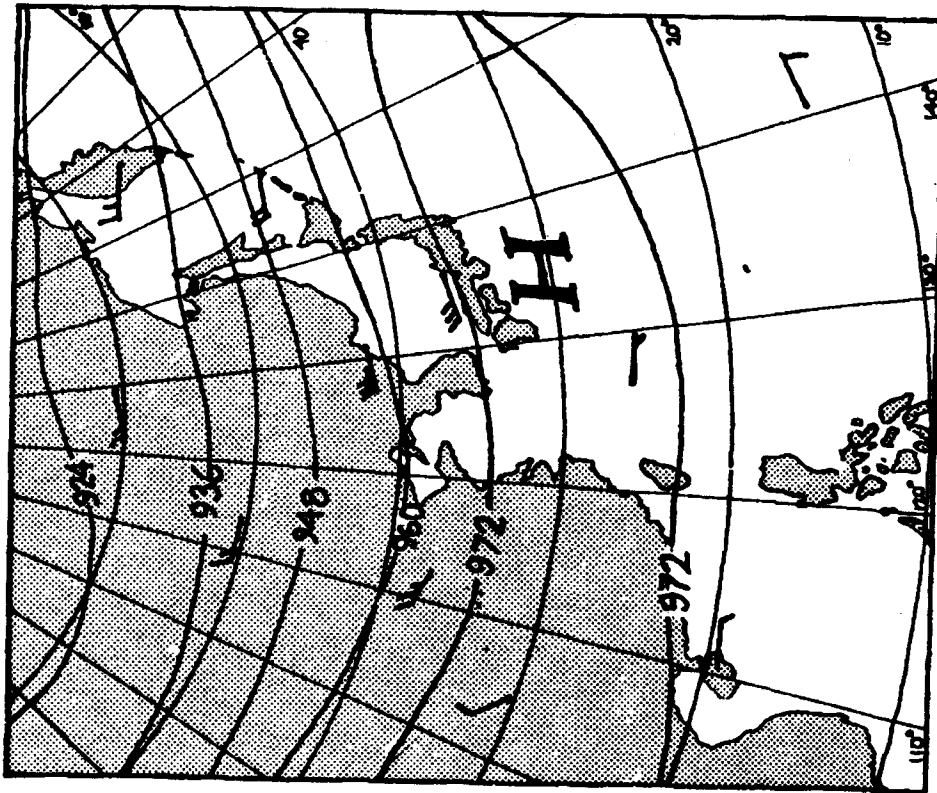


Figure 2-40. 300mb heights and winds for August. All heights in tens of gpm. (adapted from Crutcher & Meserve, 1970)

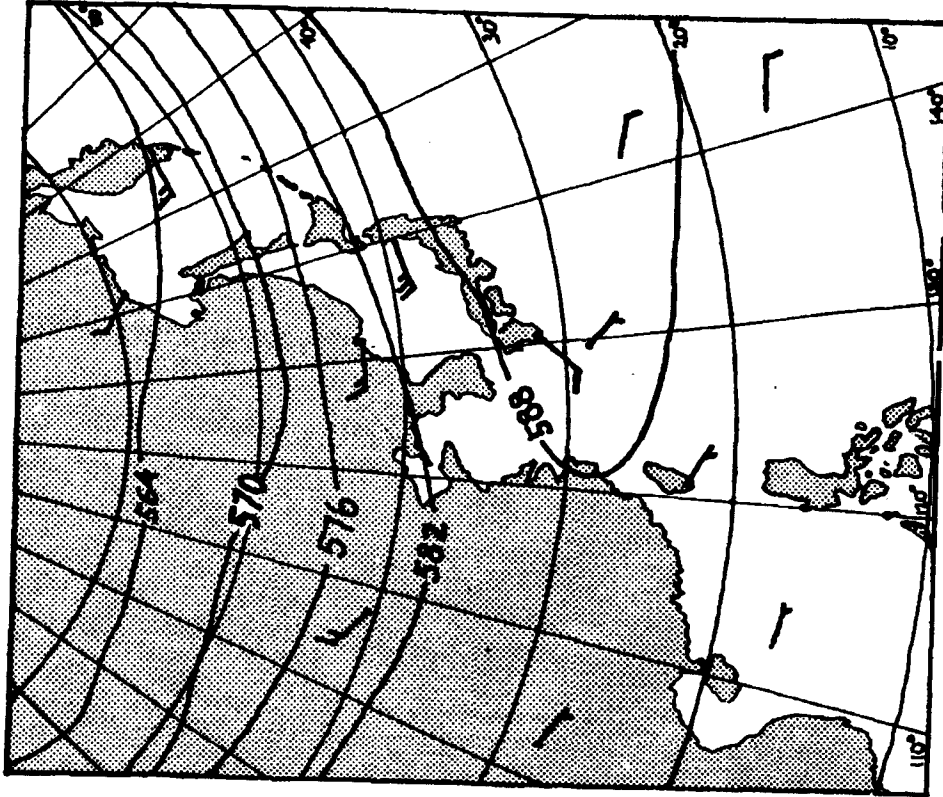


Figure 2-41. 500mb heights and winds for August. All heights in tens of gpm. (adapted from Crutcher & Meserve, 1970)

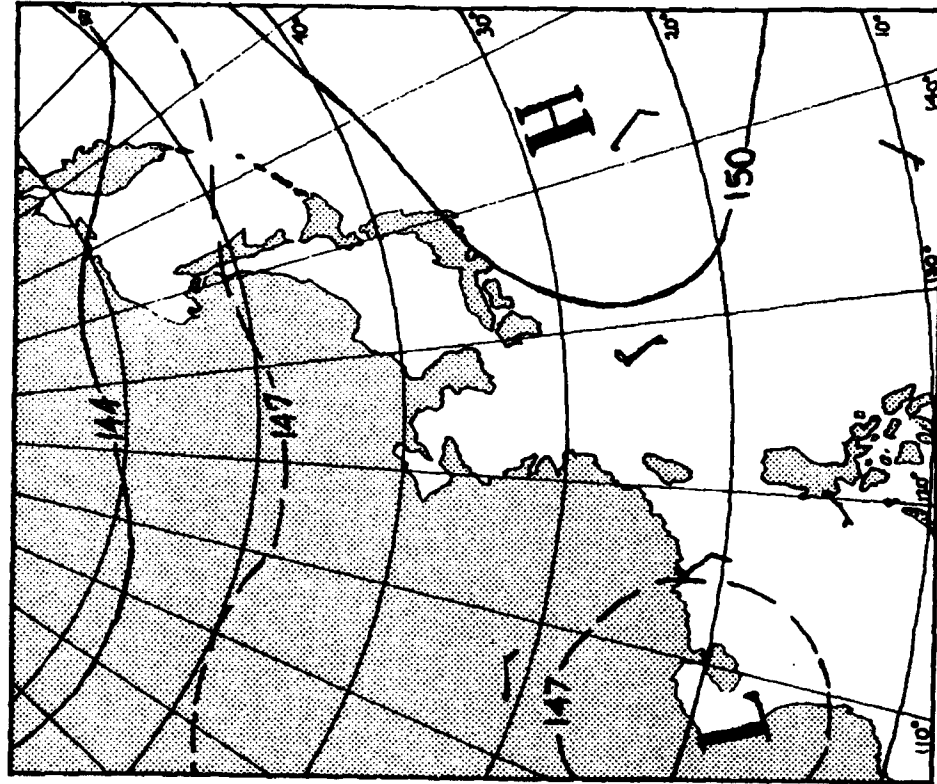


Figure 2-43. 850mb heights and winds for August. All heights in tens of gpm. (adapted from Crutcher & Meserve, 1970)

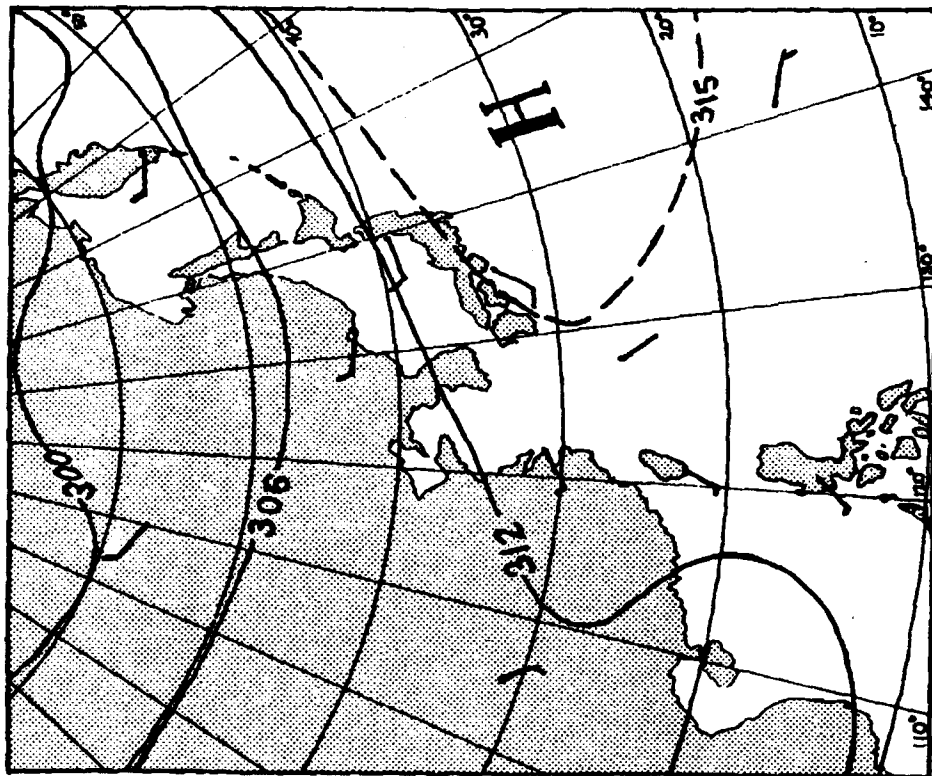


Figure 2-42. 700mb heights and winds for August. All heights in tens of gpm. (adapted from Crutcher & Meserve, 1970)

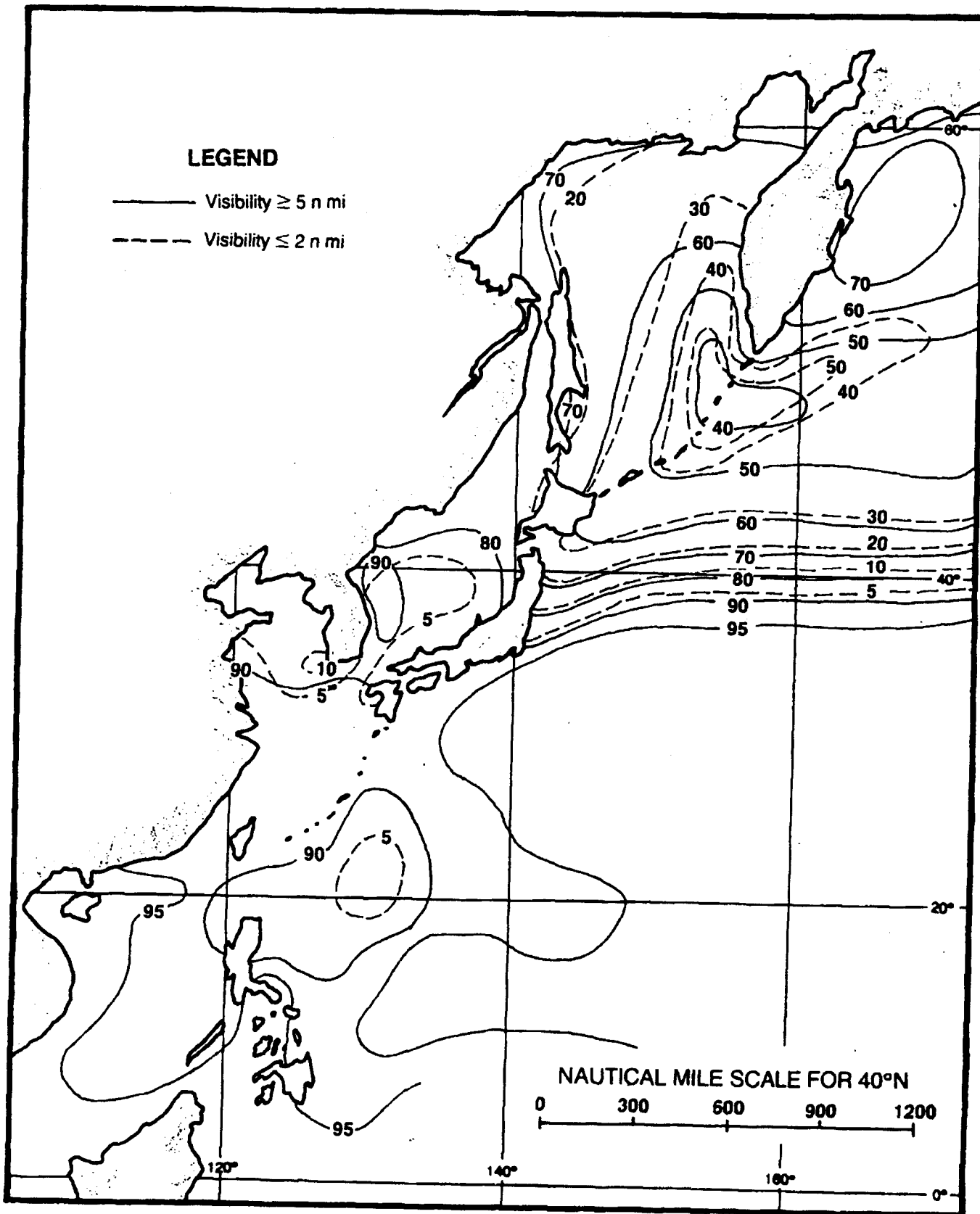


Figure 2-44. Percent frequency of occurrence of visibility limits during August (adapted from U.S. Navy, 1977).

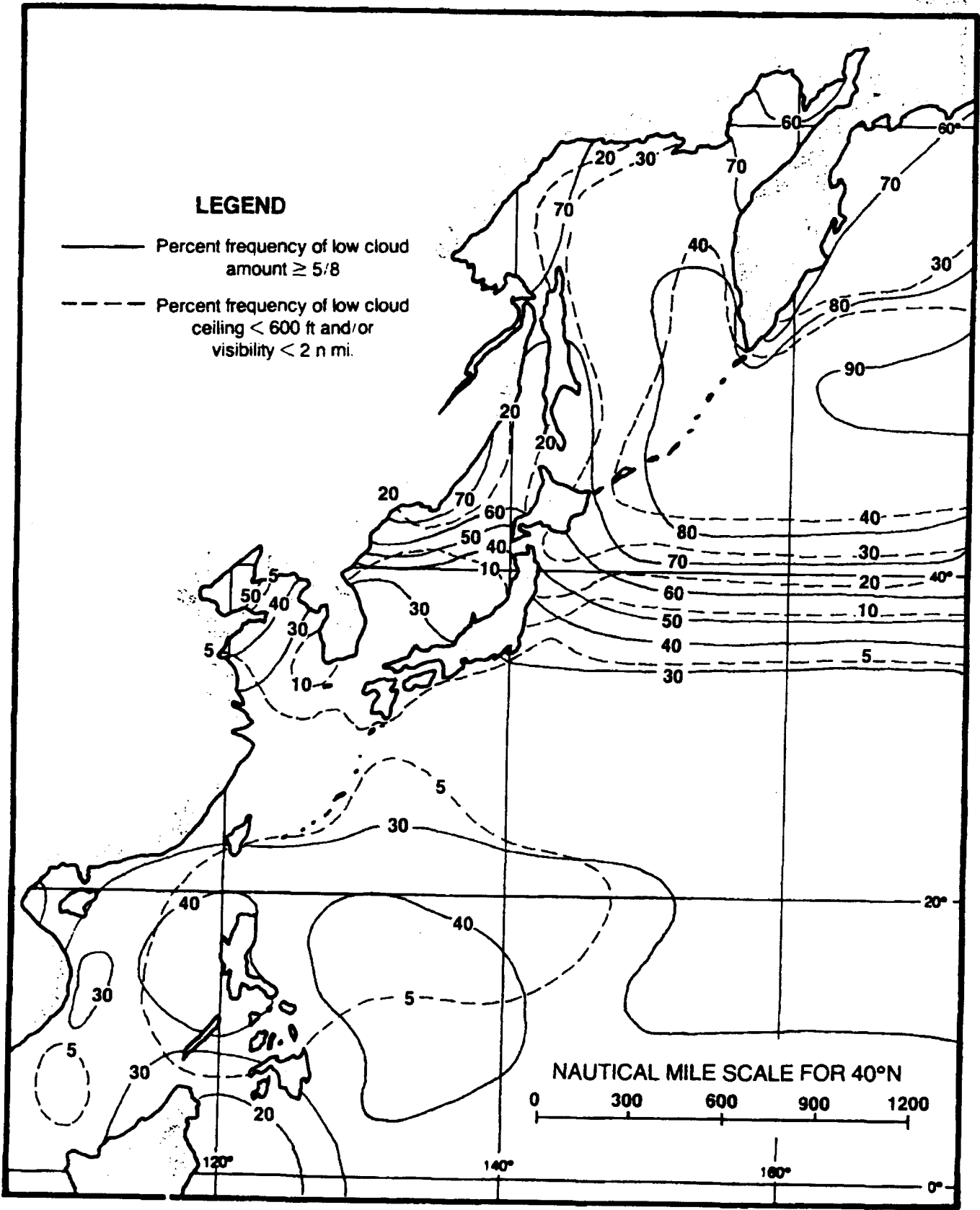


Figure 2-45. Low cloud amounts vs. ceiling and visibility during August (adapted from U.S. Navy, 1977).

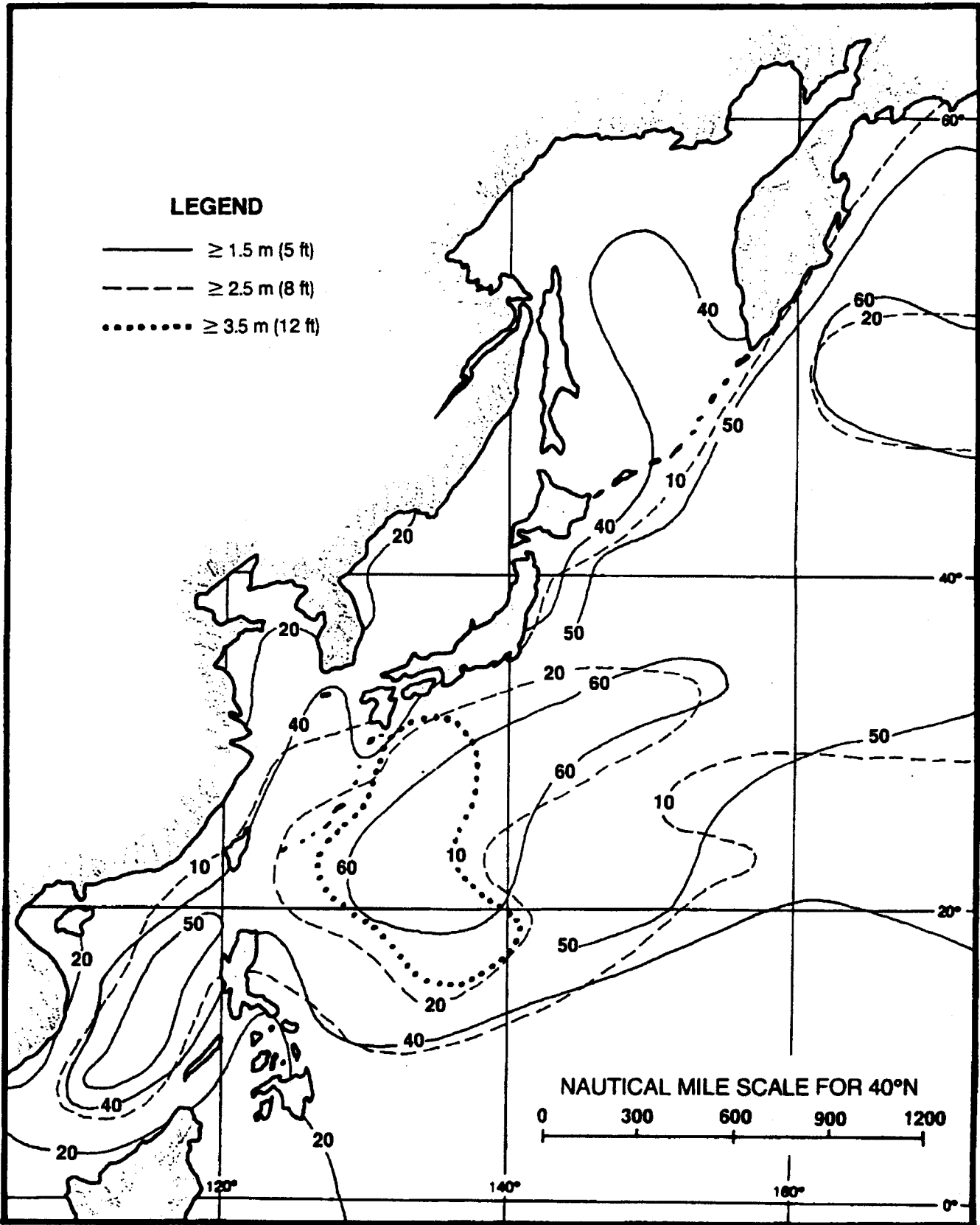


Figure 2-46. Percent frequency of occurrence of wave heights during August (adapted from U.S. Navy, 1977).

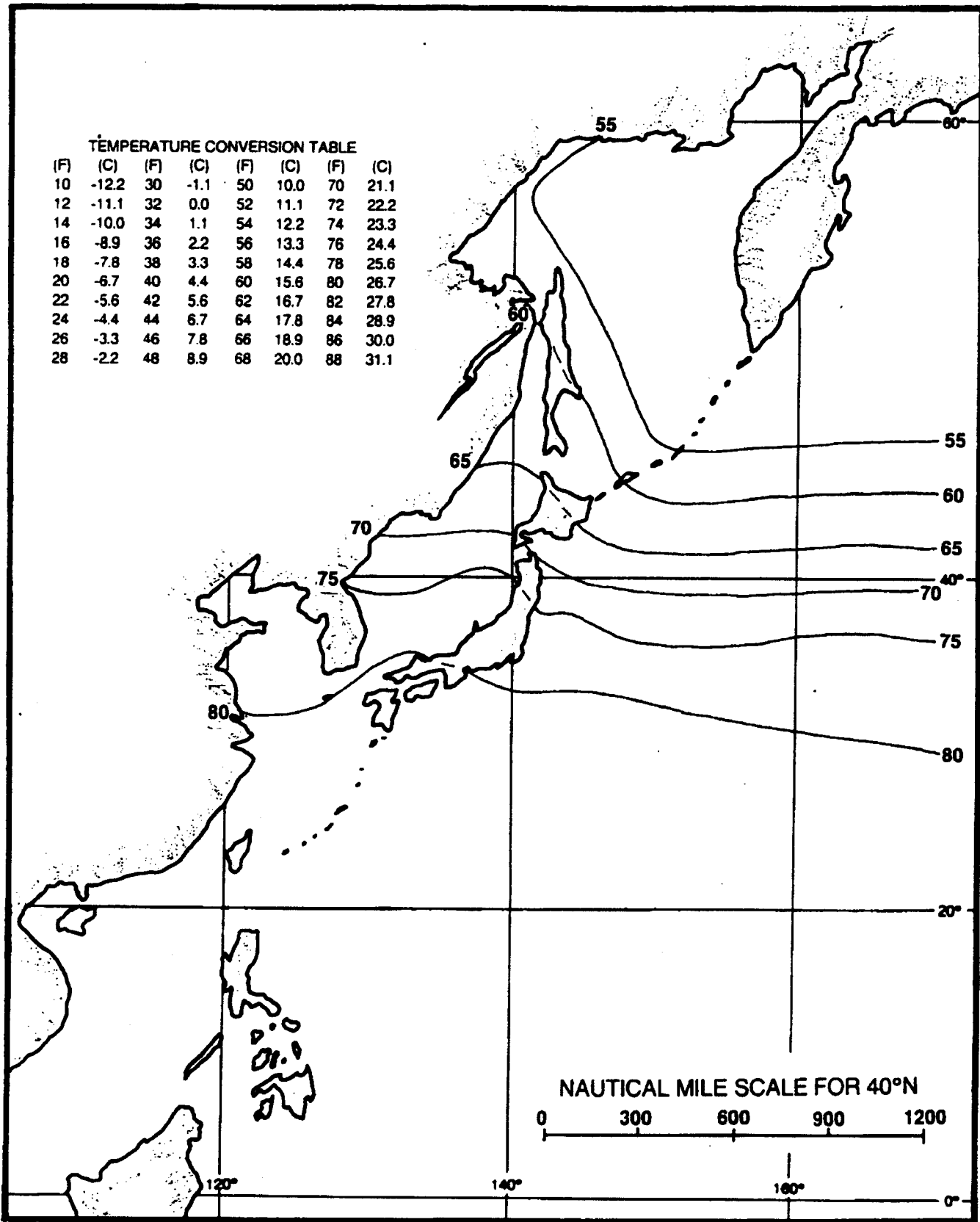


Figure 2-47. Mean surface air temperature in degrees Fahrenheit during August (adapted from Ownbey, 1973 and U.S. Navy 1977).

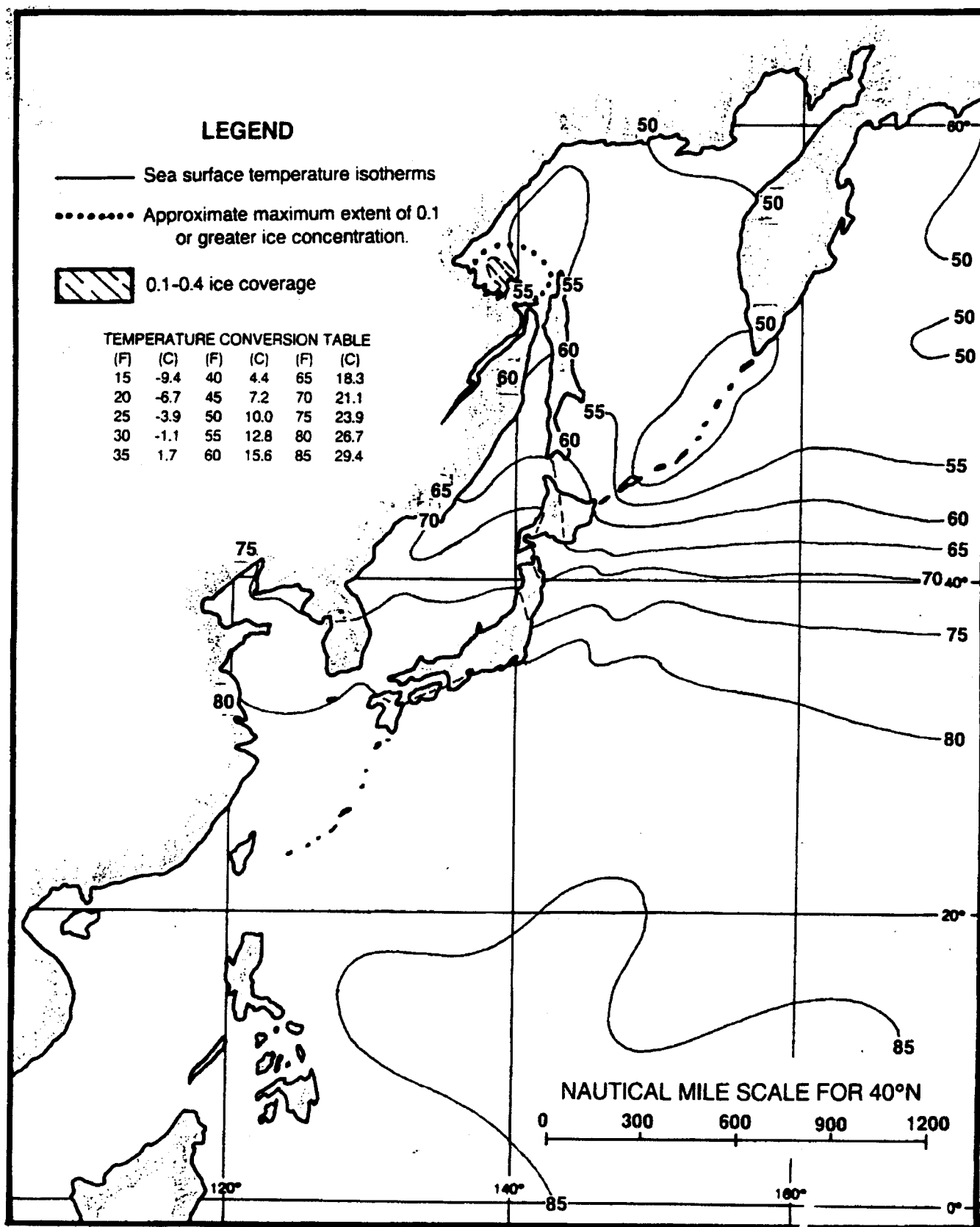


Figure 2-48. Mean sea surface temperature in degrees Fahrenheit during August, with approximate ice limits (adapted from U.S. Navy, 1967 and U.S. Navy, 1977).

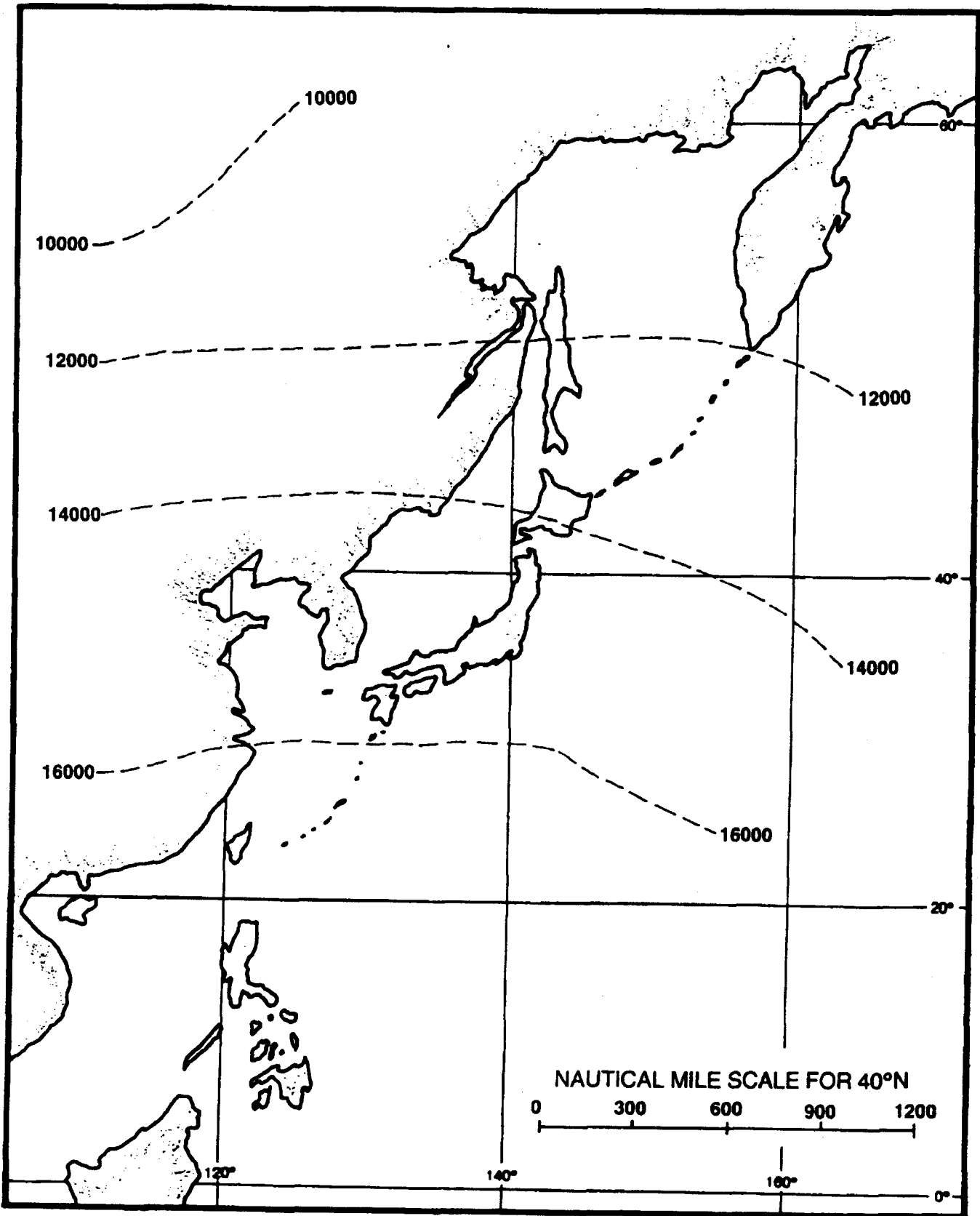


Figure 2-49. Mean altitude of the freezing level for August in feet (adapted from U.S. Air Force, 1965).

2.2.1.8 Autumn (mid-September to mid-December)

The transition from the summer season to autumn occurs rapidly. The Polar Front moves rapidly from a position north of Korea to a location south of Japan as the Siberian high pressure cell becomes the dominant weather feature over Asia. Cool, dry air invades the offshore waters as northerly flow predominates at the surface.

The rapid movement of the Polar Front southward through Japan occurs during a period called the Autumn Bai-U (or Shurin). It is similar to the Spring Bai-U in that it usually brings a period of rain and cloudy weather to the southern half of Honshu and the East China Sea due to the overrunning of the warm tropical air over the colder polar air moving southeastward from the Asian landmass. The duration of the inclement weather is shorter during the Autumn Bai-U due to the rapid southward movement of the front.

The Aleutian Low strengthens and moves to a position close to its favored winter location, and the Sea of Okhotsk low re-establishes itself during the Autumn season.

The jet stream core velocities increase, with speeds of 140 kt common over the East China Sea and Japan. As shown in Figure 2-50, the jet stream once again is split over eastern Asia as a result of the influence of the Tibetan Plateau, with the two cores merging over central Japan.

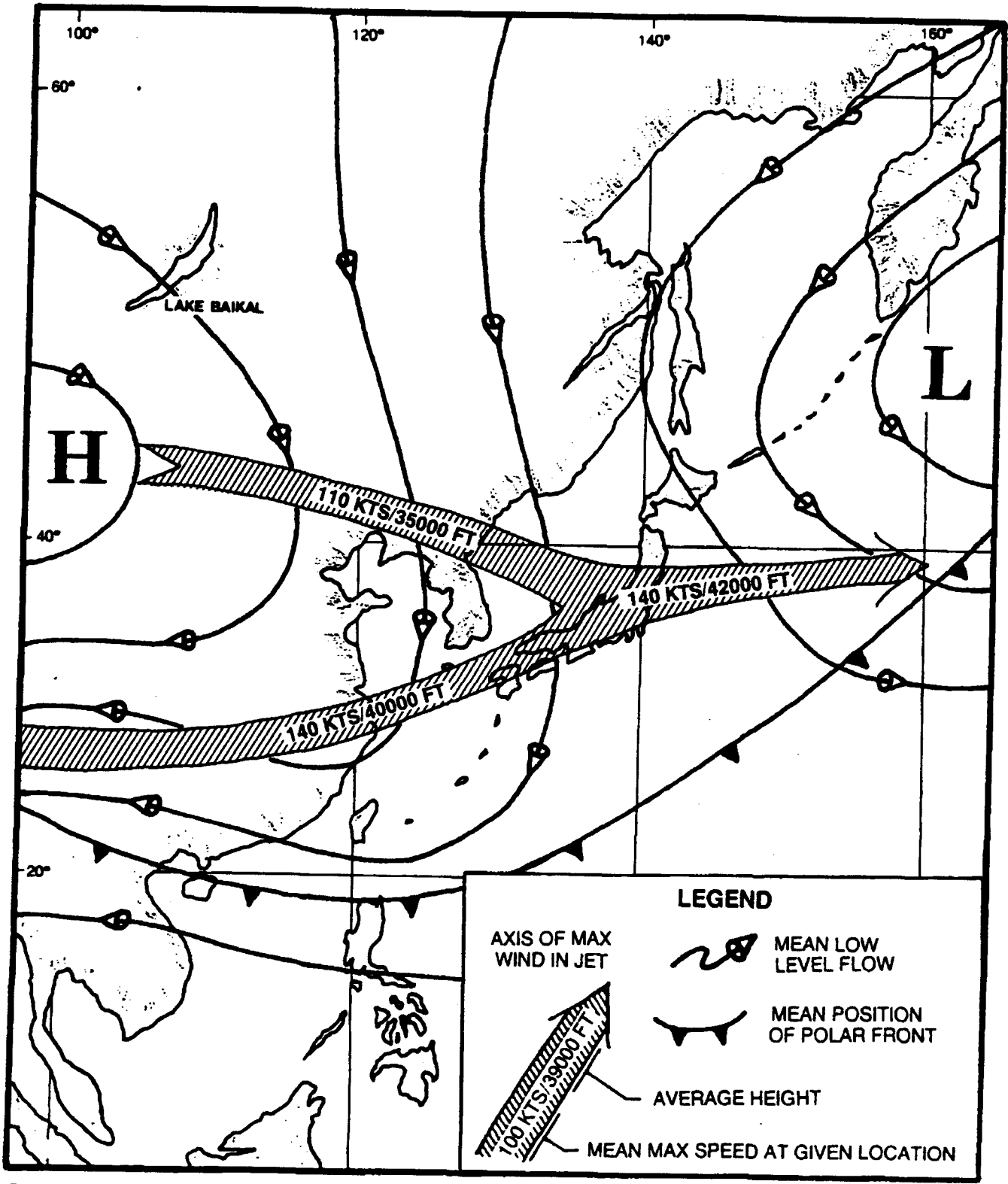


Figure 2-50. Typical atmospheric features during November: mean low level flow, mean position of polar front, and mean jet stream position (adapted from U.S. Marine Corps, 1967 and U.S. Air Force, 1968).

Figures 2-51 through 2-63 depict various average climatic conditions that prevail over eastern Asia and adjacent waters during the month of November. A brief discussion of each of the parameters is presented in the climatology sections of the regional chapters in this handbook.

The most probable types of migratory low pressure systems occurring during the autumn season include Manchurian Lows, Lake Baikal Lows, South Mongolia Lows, Yellow Sea Lows, and Taiwan Lows. Average tracks of each of the systems are depicted in Figure 2-6.

Of the yearly average of approximately 57 cold fronts occurring in the Far East, about 19 (33%) occurred during autumn (mid-September to mid-December), a frequency of about one every five days (FWC/JTWC, 1969).

From a maximum in August and September, tropical cyclone frequency declines during autumn, with an average of approximately six typhoons per year in the western Pacific (three in October, two in November, and only one during December) (Crutcher and Quayle, 1974). Early season storms pose the greatest threat to interests in the waters adjacent to eastern Asia. By December, typhoon activity is generally limited to latitudes south of 30°N. Those storms that do move north of that latitude recurve to the northeast well south of Japan. Refer to Appendix B for tropical cyclone tracks.

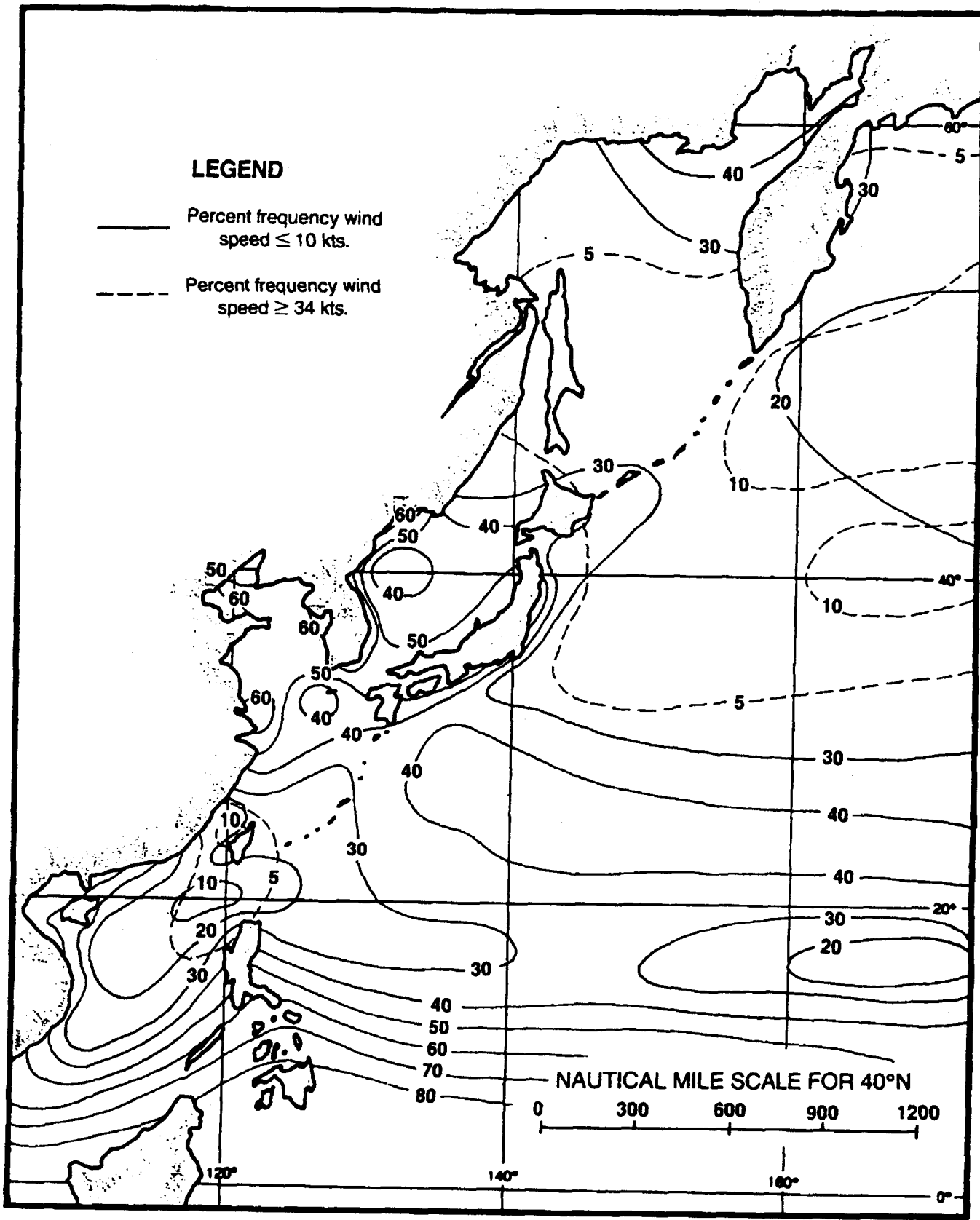


Figure 2-51. Surface winds during November (adapted from U.S. Navy, 1977).

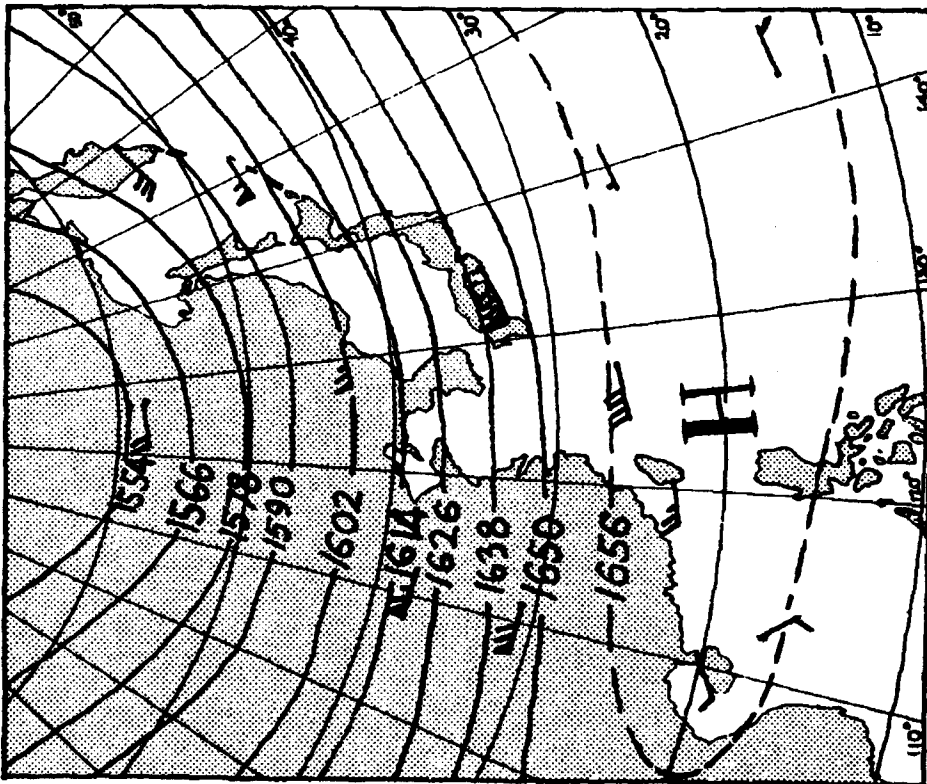


Figure 2-52. 100mb heights and winds for November. All heights in tens of gpm. (adapted from Crutcher & Meserve, 1970)

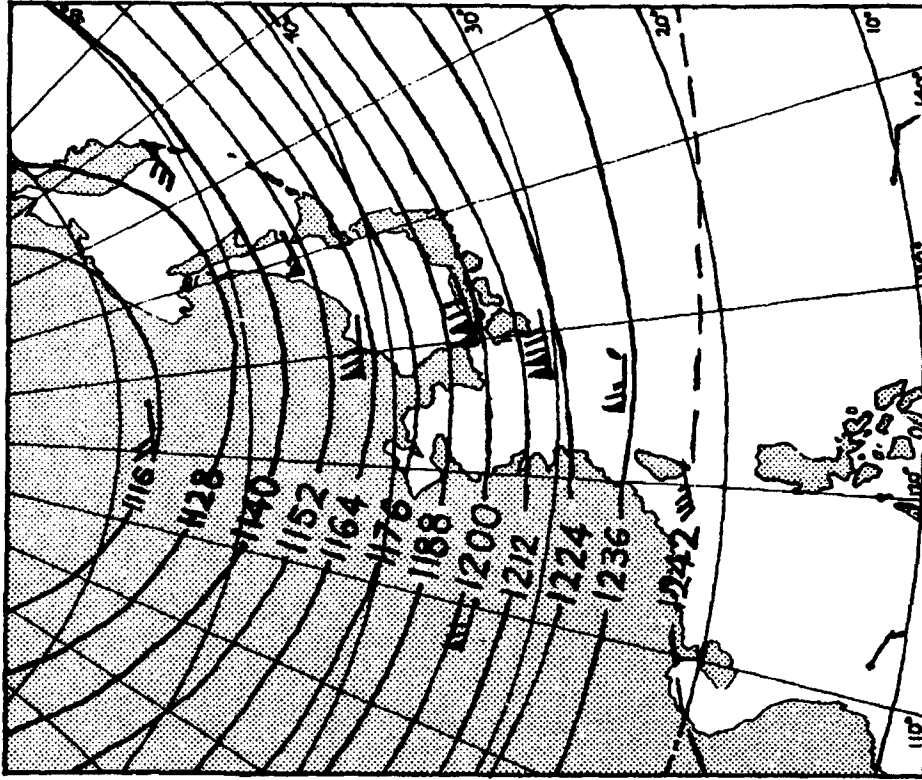


Figure 2-53. 200mb heights and winds for November. All heights in tens of gpm. (adapted from Crutcher & Meserve, 1970)

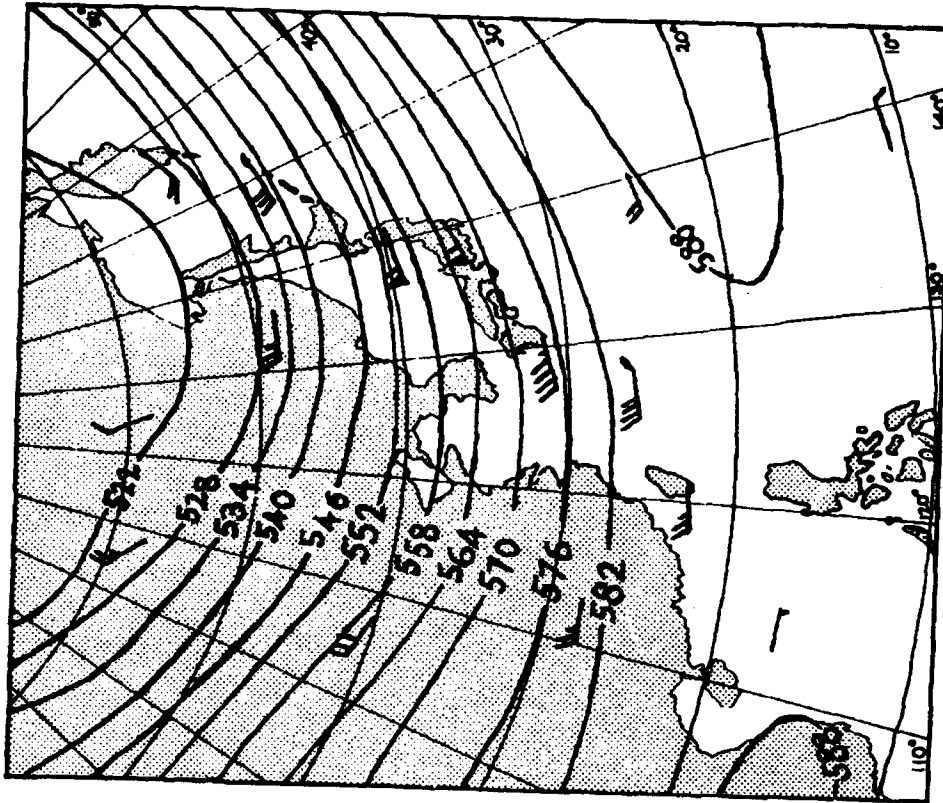


Figure 2-55. 500mb heights and winds for November. All heights in tens of gpm. (adapted from Crutcher & Meserve, 1970)

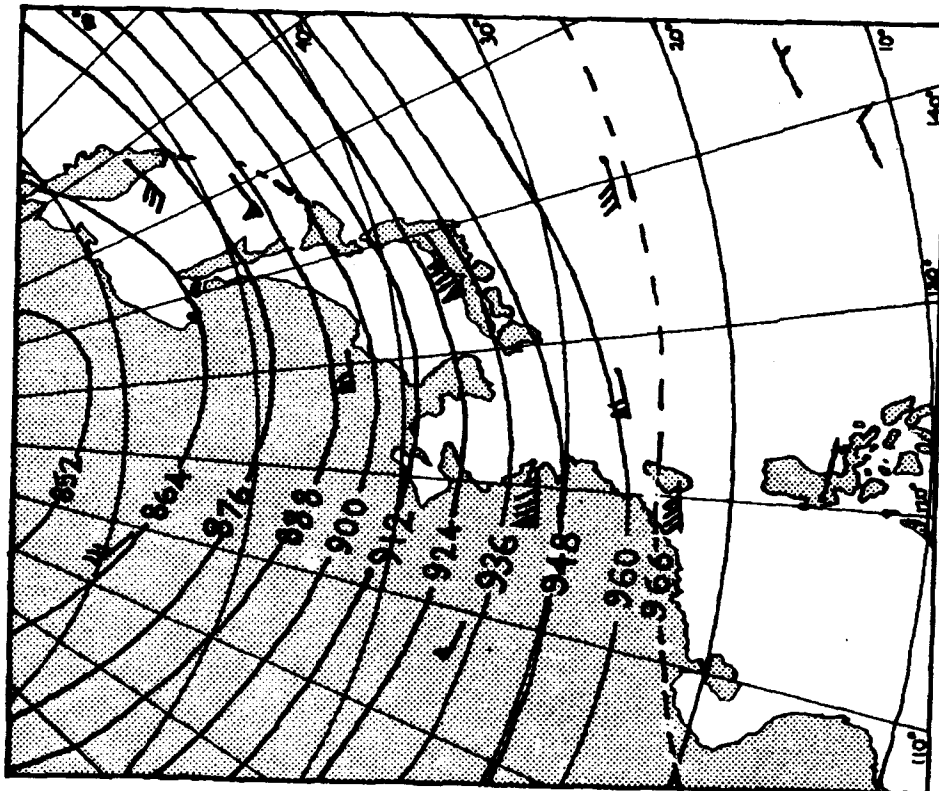


Figure 2-54. 300mb heights and winds for November. All heights in tens of gpm. (adapted from Crutcher & Meserve, 1970)

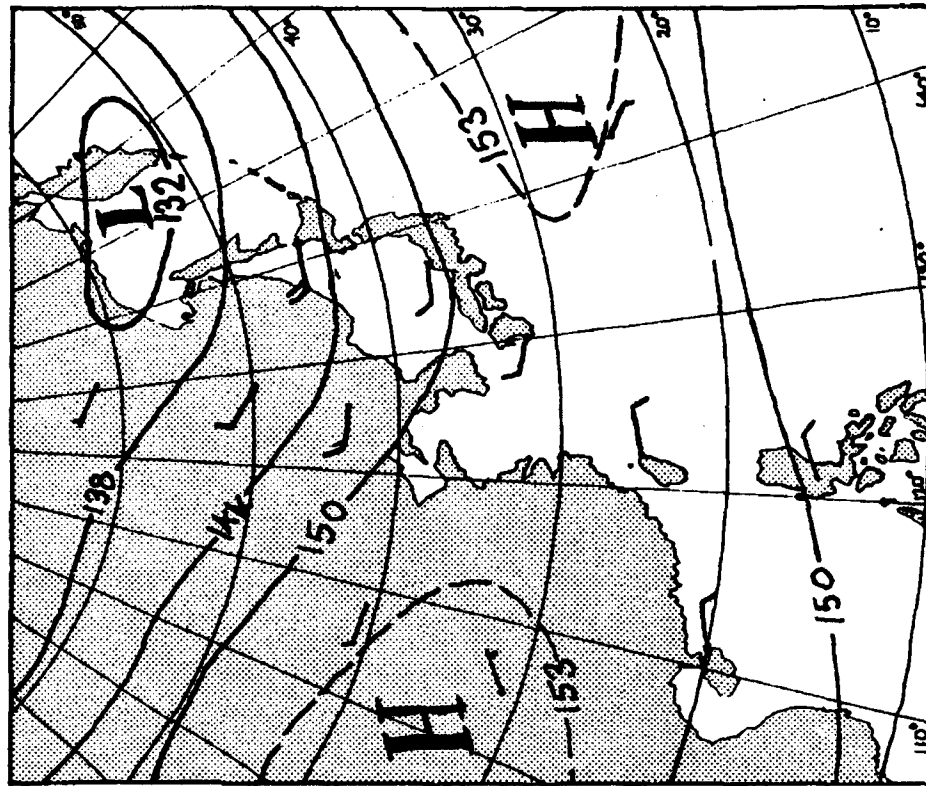


Figure 2-57. 850mb heights and winds for November. All heights in tens of gpm. (adapted from Crutcher & Meserve, 1970)

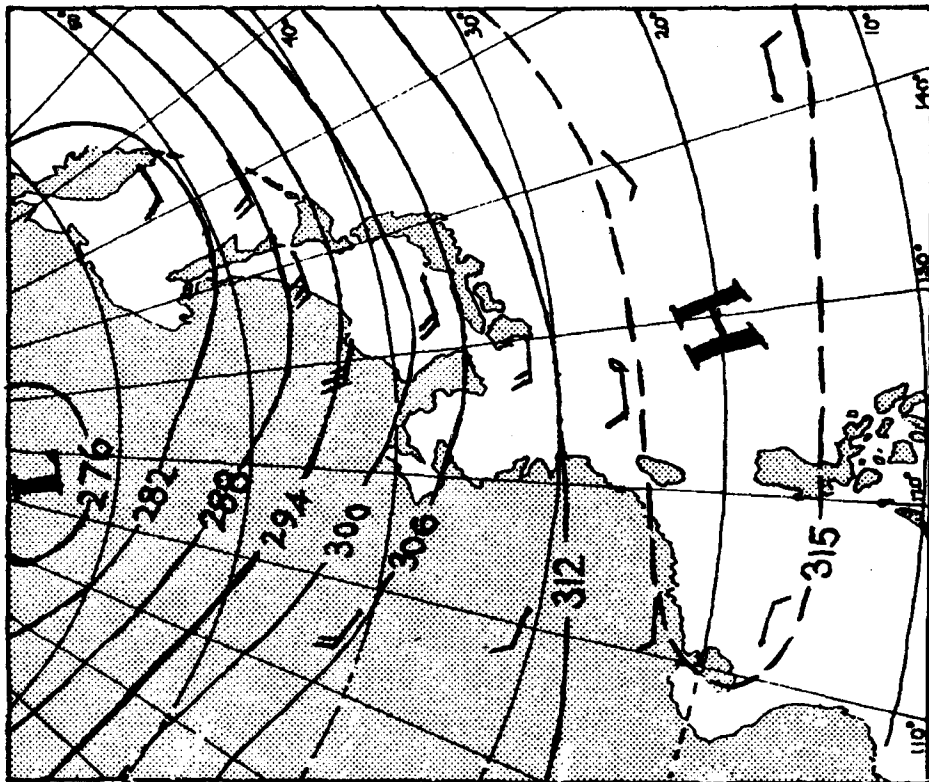


Figure 2-56. 700mb heights and winds for November. All heights in tens of gpm. (adapted from Crutcher & Meserve, 1970)

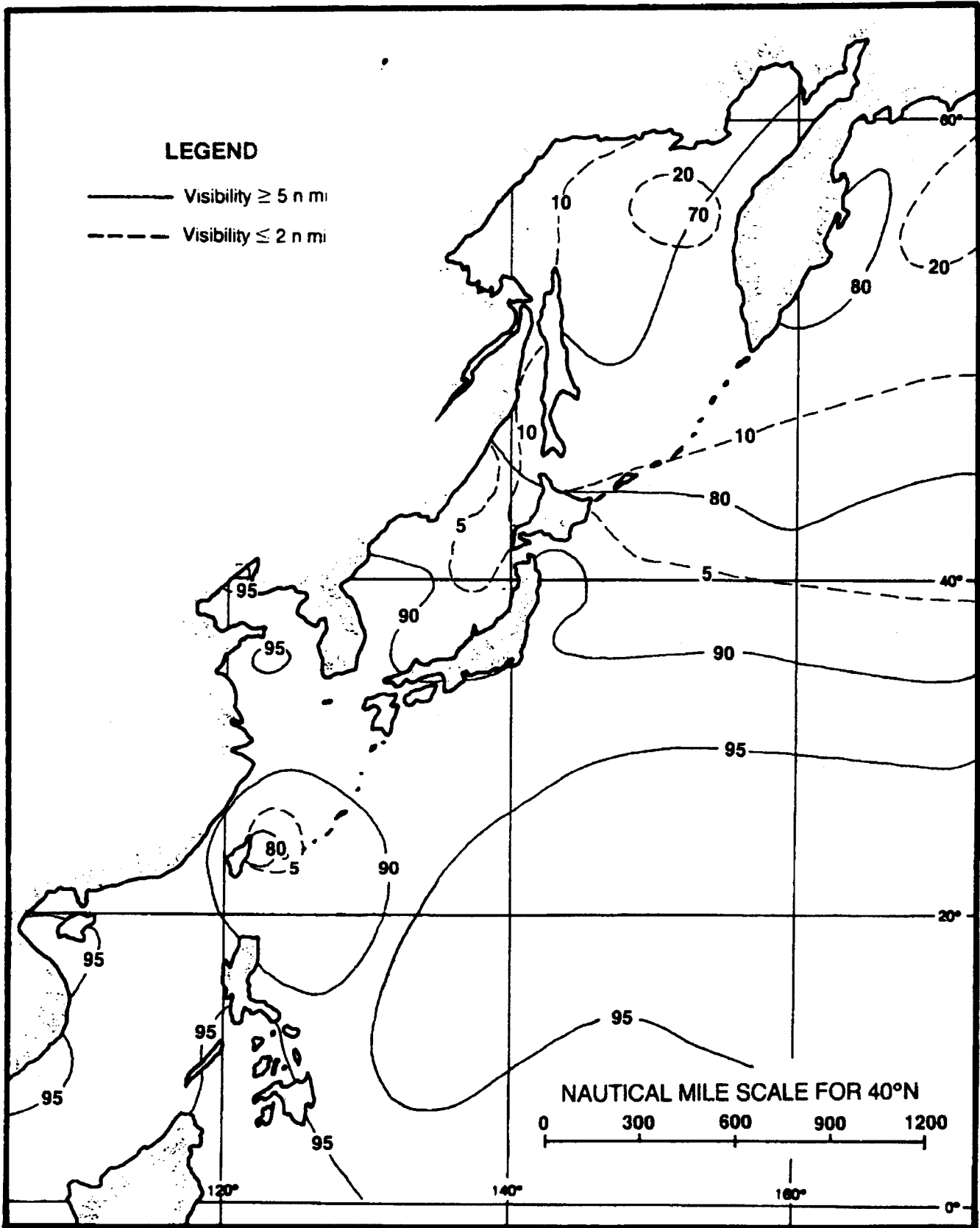


Figure 2-58. Percent frequency of occurrence of visibility limits during November (adapted from U.S. Navy, 1977).

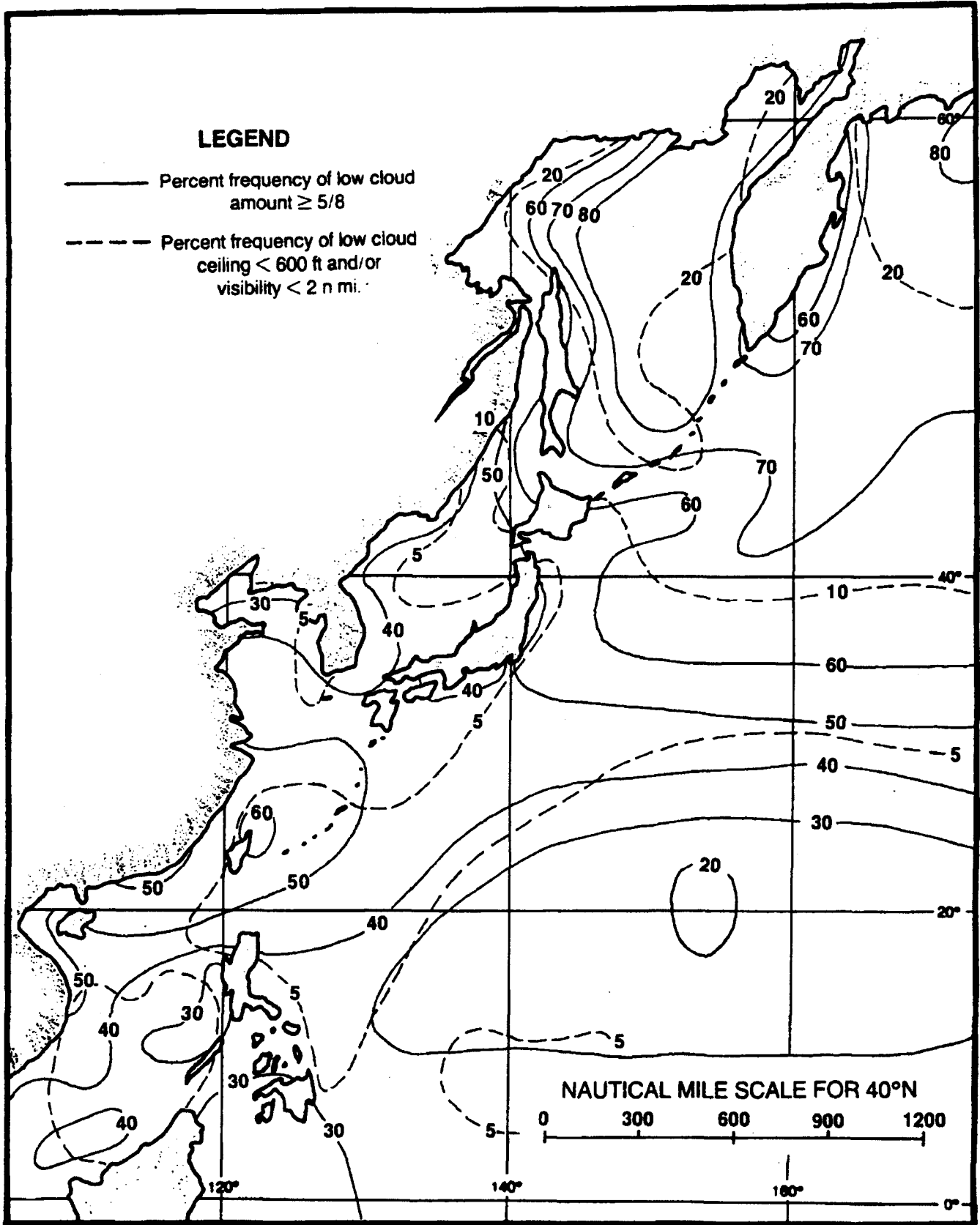


Figure 2-59. Low cloud amounts vs. ceiling and visibility during November (adapted from U.S. Navy, 1977).

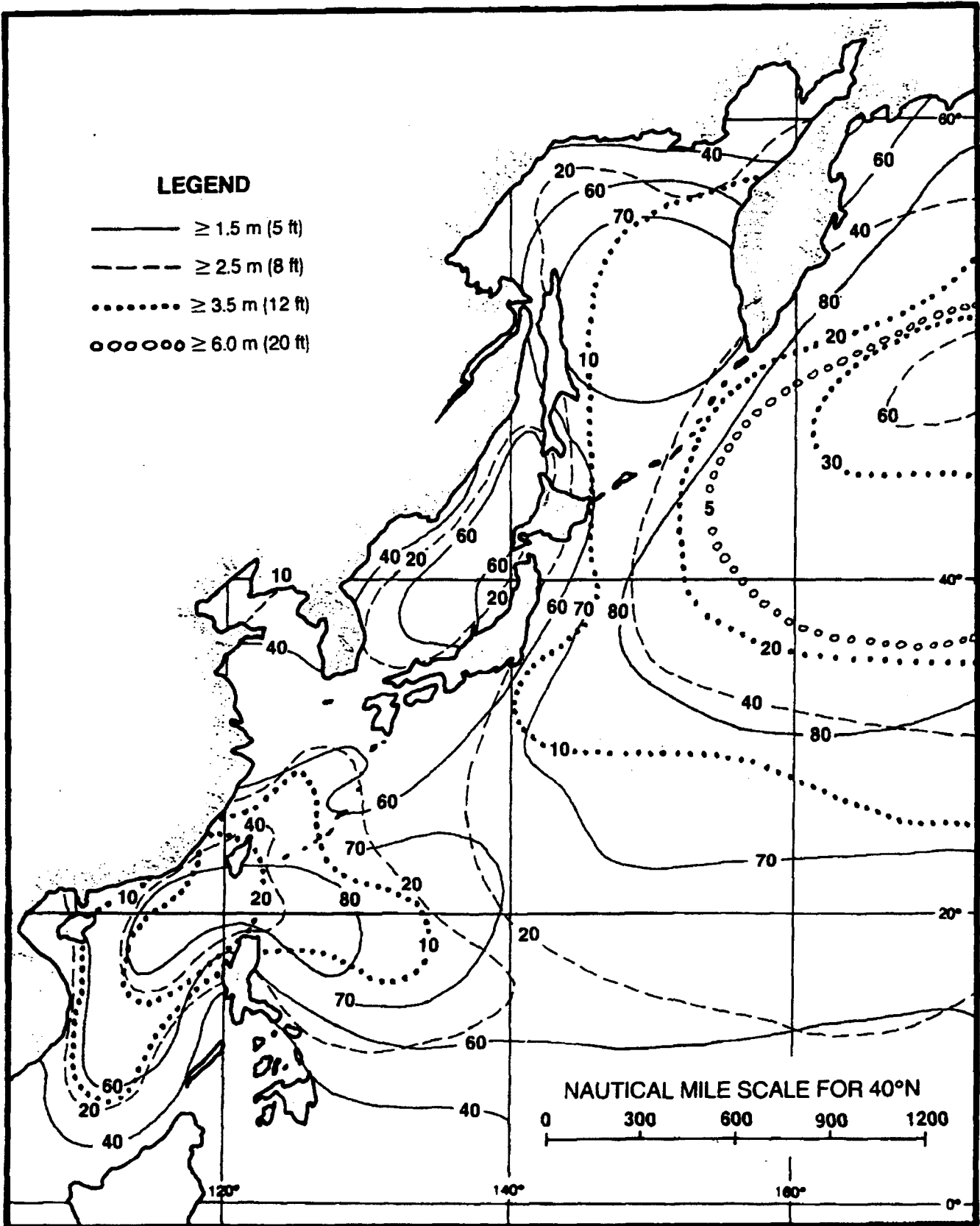


Figure 2-60. Percent frequency of occurrence of wave heights during November (adapted from U.S. Navy, 1977).

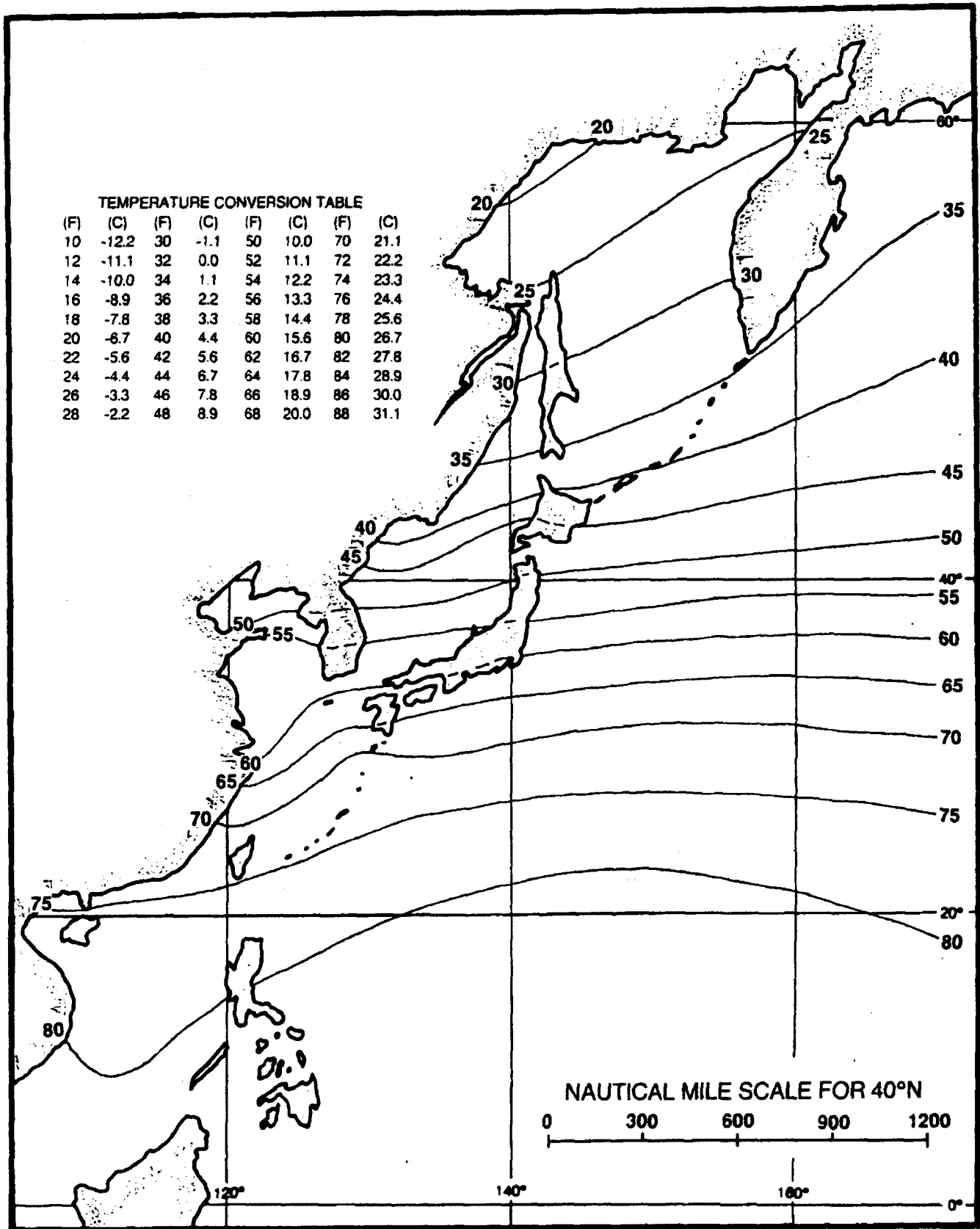


Figure 2-61. Mean surface air temperature in degrees Fahrenheit during November (adapted from Ownbey, 1973 and U.S. Navy, 1977).

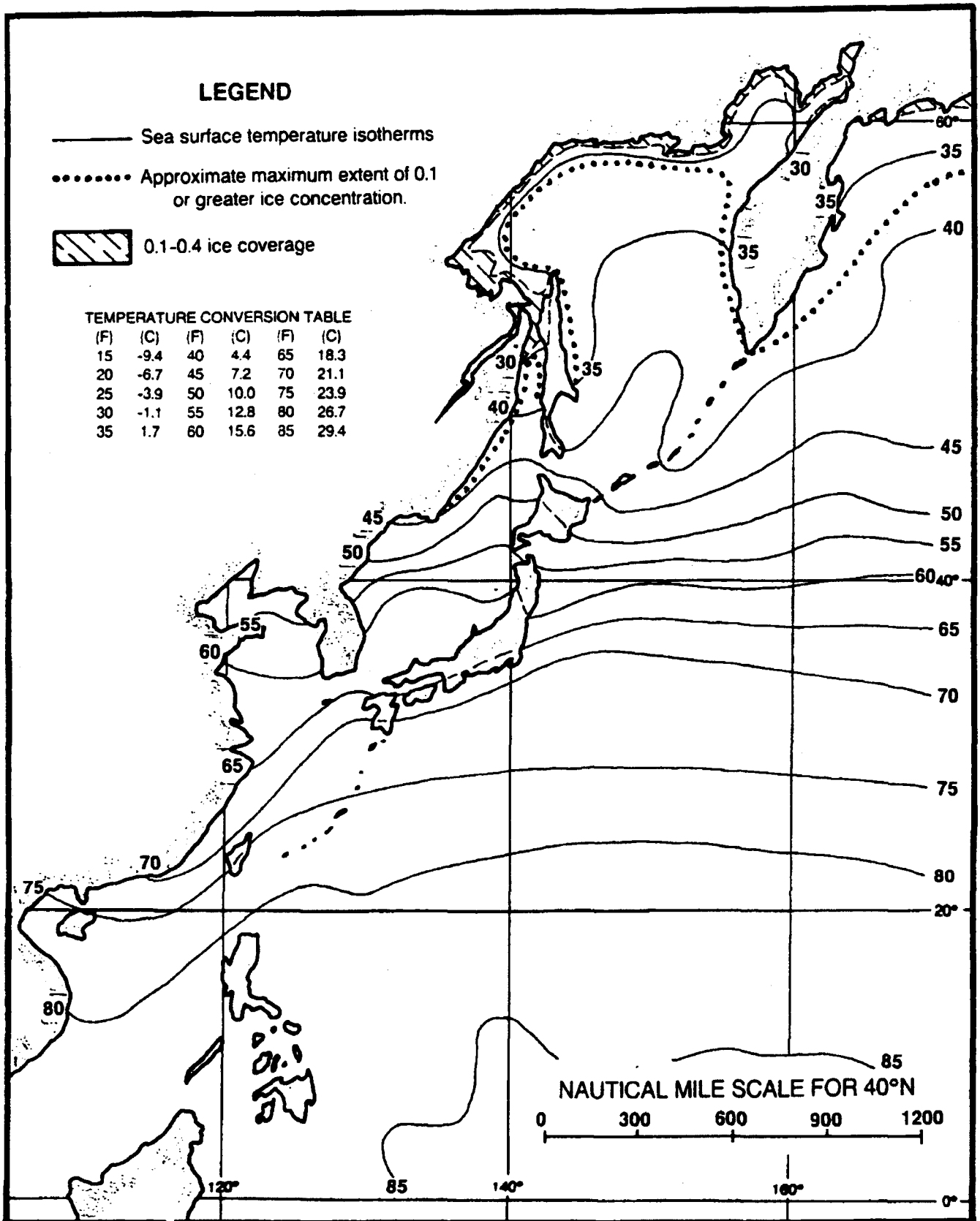


Figure 2-62. Mean sea surface temperature in degrees Fahrenheit during November, with approximate ice limits (adapted from U.S. Navy, 1967 and U.S. Navy, 1977).

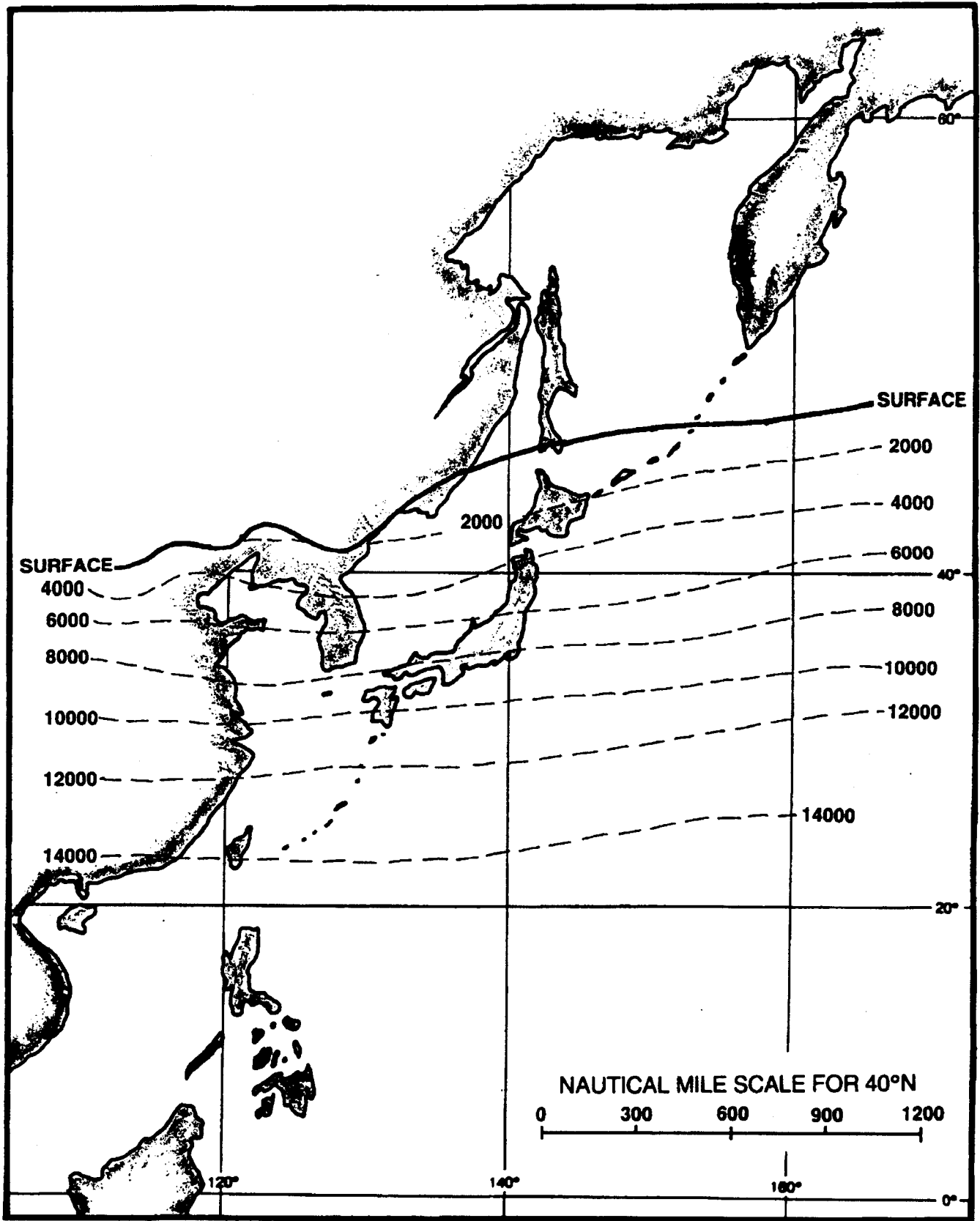


Figure 2-63. Mean altitude of the freezing level for November in feet (adapted from U.S. Air Force, 1965).

2.3 Electro-Optical and Electromagnetic Conditions

Electro-Optical (E-O) systems are playing an increasing role in U.S. Navy operational activities. Fleet environmentalists have a growing requirement to support E-O systems and therefore a need for understanding the interactions between E-O systems and the marine environment. This introduction section provides some basic background material on electromagnetic (EM) radiation, its interaction with atmospheric constituents, and general types of E-O systems of concern to fleet environmentalists. The primary sources of the information provided here are: Electro-Optical Handbook Volume I, AWS/TR-79/002, Cottrell et al, 1979, and Proceedings of Workshop to Standardize Atmospheric Measurements in Support of Electro-Optical Systems, UDR-TR-83-71, Huffman et al, 1983.

2.3.1 E-O/EM and the Atmosphere as a Medium

E-O and EM systems respond to electro-magnetic radiation as a sensed stimulus. The atmosphere interferes to various degrees with these systems because it interacts with both the source and propagation of radiation. The interaction depends on the atmospheric constituents and the radiation wavelength. This handbook addresses portions of the magnetic spectrum from visible through microwave wavelengths (0.74 micrometers through 10.0 centimeters). Table 2-1 provides categories of sensor wavelengths, general types of systems, and significance of adverse weather elements.

Table 2-1. Electro-Optical and Electromagnetic Systems and Significance of Adverse Weather Elements as a Function of Sensor Wavelength Categories (after Cottrell et al, 1979).

	MICROWAVE		FLIR				VIDICON T.V.
SYSTEMS	COMMUNICATIONS	RADAR	LASER				EYE T.V. CAMERA
WAVELENGTH CATEGORIES	MICROWAVE	MILLIMETER	INFRARED				VISIBLE
			FAR FAR	FAR	MIDDLE	NEAR	
WAVELENGTH/ FREQUENCIES	10cm-1cm 3GHz-30GHz	1cm-0.1mm	0.1mm-15μm	15μm-6μm	6μm-2μm	2μm-0.74μm	0.74μm-0.4μm
WEATHER SENSITIVITY	GENERALLY INCREASES WITH DECREASING WAVELENGTH (TO THE RIGHT IN THIS TABLE)						
CLOUDS/FOG	SIGNIFICANT		EXTREMELY SIGNIFICANT				
DRY AEROSOLS	INSIGNIFICANT		SIGNIFICANT		EXTREMELY SIGNIFICANT		
PRECIPITATION	SIGNIFICANT		EXTREMELY SIGNIFICANT				
ABSORPTION	SIGNIFICANT		CAN BE EXTREMELY SIGNIFICANT			EXTREMELY SIGNIFICANT	
SCATTERING	SIGNIFICANT		EXTREMELY SIGNIFICANT				

There are four atmospheric physical processes which affect electromagnetic (EM) radiation: reflection, scattering, absorption, and emission. The type and size of the atmospheric constituents, gaseous molecules and particulates (dust, haze, smokes, fogs, other aerosols, cloud droplets, and precipitation) affect the propagation of radiation. The influence on various wavelengths is determined by the relationship between the size of the atmospheric constituents and the wavelength of the radiation. This relationship, referred to as the size parameter, is stated as:

$$\text{size parameter} = \frac{2\pi r}{\text{radiation wavelength}}$$

where r is the particle radius.

Reflection takes place when the size parameter is greater than approximately 10, that is, when the wavelength is much smaller than the particle radius. Scattering causes such phenomenon as the blue sky on clear days and the milky sky on hazy days. The blue sky results from preferential scattering of the short visual wavelengths (blue) of sunlight by molecules in the atmosphere, known as Rayleigh scattering. Larger particles such as cloud droplets, dust, haze, and smoke particles, which have a size parameter near one with respect to visible light, scatter all the visible wavelengths and cause the sky to appear white or milky. This scattering of the sunlight is called mie scattering. Absorption takes place on the molecular scale and occurs selectively with respect to wavelengths. Each absorbing constituent of the atmosphere (mainly water vapor, carbon dioxide, ozone, and oxygen) absorbs in specific wave length intervals, which are referred to as absorption bands. Radiation at

other wavelengths is not significantly affected by that constituent. Emission is the emitting of electromagnetic radiation (for example, a flashlight beam or the heat from a household radiator). The process operates on the molecular scale, and every constituent of the atmosphere or earth emits radiation. However, emission occurs selectively with respect to wavelength, therefore the amount of energy emitted at a given wavelength may not be significant.

The bulk or fundamental atmospheric parameters of concern in E-O/EM forecasting are temperature, pressure, humidity, and wind. These elements determine the refractive index, absorption in the infrared, and the size and contribution to refractive index of atmospheric aerosols. Low-level profiles determine the atmospheric stability, which influences turbulence. Weather elements such as drizzle, rain, and snow can severely limit the performance of all of the E-O/EM systems.

Optical turbulence, which degrades laser imaging systems, results from small-scale temperature and humidity fluctuations associated with atmospheric turbulence or mixing of air of different temperature and humidity. This turbulence causes fluctuations in the optical refractive index in the atmosphere. The turbulence parameter that is related to laser system performance is known as the refractive index structure parameter, labeled C^2_w , which is a function of temperature and humidity structure parameters. The turbulence or eddies that are of concern to lasers are very small, on the order of 10 to 20 cm.

The marine atmosphere can be divided into two layers: the marine planetary boundary layer (MPBL), and the free atmosphere. The MPBL is typically on the order of 1 km thick, well mixed, and topped by a stable marine inversion. The free atmosphere is

controlled by large-scale highs and lows. The surface effects exert little influence on motion in the free atmosphere. With the exception of clear air turbulence, there is little turbulence and therefore only weak fluctuations in optical refractive index and consequently low values of C^2_N . In contrast, the MPBL is only weakly influenced by large scale patterns and is heavily influenced by surface effects. The primary surface effects are heating or cooling and friction. Surface effects cause the MPBL to be highly turbulent, and therefore large values of C^2_N are encountered. The larger the C^2_N value the greater the degradation of laser systems.

E-O systems in the visual through infrared wavelengths can be classified as either broadband or laser (narrow line) types. Broadband means to extend over a range of wavelengths, such as visual or infrared systems. A weapons system may combine both broadband and laser components e.g., a T.V. or forward looking infrared (FLIR) system used to locate a target that is then designated (illuminated and tracked) with a laser. Environmental support of combined systems would require consideration of the atmospheric parameters affecting the wavelengths of each of the systems.

2.3.2 Comments on E-O/EM Systems and Atmospheric Interactions

This section addresses some general E-O/EM systems and atmospheric interactions of concern to the fleet environmentalist.

Visual Systems: (E-O) Cameras and human eyeballs are visual systems that require cloud-free line-of-sight between the sensor and target. Furthermore, reduced visibility due to scattering and absorption by haze, fog, and precipitation limit the capabilities of

visual systems. Also, each visible system requires a minimum level of illumination.

Infrared Systems: (E-O) Lasers and Forward Looking Infrared Radar (FLIR) are active and passive systems, respectively, that operate in the infrared wavelength and require cloud-free line-of-sight to the target. Some lasers can penetrate thin cloudiness, and passive infrared systems may detect hot targets through thin clouds. Haze, fog, and precipitation degrade the transmission of energy at near infrared wavelengths. Systems operating at longer infrared wavelengths are degraded by absorption of energy by atmospheric water vapor.

Millimeter/Microwave Systems: (E-M) Radar and microwave system performance is degraded by two main atmospheric factors: Heavy cloudiness (thick cloudiness with large droplet distributions of near-precipitation-sized particles), and precipitation.

2.3.3 Specific Categories of E-O/EM Systems

2.3.3.1 High Energy Laser

Atmospheric conditions degrade High Energy Laser (HEL) system performance by reducing fluence (energy density per unit time deposited on the target) on the target in a variety of ways: aerosols and water vapor absorb energy, atmospheric turbulence spreads the beam fluence, and atmospheric turbulence also causes the beam to wander off its intended target (Burk et al, 1979).

Environmental conditions such as heavy rainfall and fog-induced low visibility can reduce the effectiveness of HEL systems

to a point that precludes operation of such systems. Goroch and Brown (1980) produced a climatology of the frequency of occurrence of adverse weather conditions which would preclude operations of the HEL system. They found that the area of the Yellow Sea, Korea, and the southern Sea of Japan experienced relatively high rates of limiting weather conditions, with fog being the most frequent factor. Their findings indicated limiting visibility conditions frequency of about 2% in winter and 10% in summer.

In general the highest rain rates occur in the tropical zones (short periods of intense rain under convection cells), while higher latitudes tend to experience longer periods of relatively light rain. The dense fog condition tendency is reversed with an increase in frequency with latitude (especially over the northwest Pacific). Local conditions related to upwelling and SST gradients, as well as the large-scale surface flow pattern, result in relatively high fog frequencies over the mid and sub-polar latitudes of the northwestern Pacific. Degraded HEL performance potential can be related to the climatology patterns of heavy rainfall and dense fog. Day-to-day performance will be influenced by these same conditions.

2.3.3.2 Forward Looking Infrared

The Forward Looking Infrared (FLIR) information presented in this handbook was taken from the Naval Environmental Prediction Research Facility (NEPRF) technical report 81-06, Climatology of Infrared Ranges in Pacific Ocean Regions of the Northern Hemisphere (Goroch and Brown, 1981). This climatology was computed for a nominal FLIR sensor attempting to detect a broadside cruiser target.

Expected range and standard deviations by month are available in this referenced report.

The basic concept of thermal sensing, such as FLIR, is the detection of a target by a thermal detector which senses or perceives a temperature difference (contrast) between the target and its background. The temperature differences result from solar heating (insolation) or cooling by the ambient wind. The sensed or perceived contrast by the detector is diminished by the atmosphere between the source (target and its background) and the receiver (the infrared detector). The loss of contrast is termed the transmittance. The strongest reduction in contrast occurs during fog or precipitation. When visibility is less than 1 km, FLIR ranges can be considered the same as the visibility.

These absorption characteristics give the FLIR ranges a close relationship to the general atmospheric circulation patterns. In general there is a latitude-FLIR range correlation (increasing range with increasing latitude) reflecting a change from the warm moist stable equatorial area, to the cooler drier but variable mid-latitudes, and finally the cold dry polar regions. Effects such as continental outbreaks, stratus and fog regimes, upwelling, and oceanic currents and associated areas of cyclogenesis result in extreme variability of FLIR ranges over near coastal waters.

In the infrared wavelengths (3.4 to 5 micrometers and 8-12 micrometers) the absorption by water vapor is generally the primary effect. Absorption by aerosol particles is normally of secondary importance. However, under conditions of atmospheric low water vapor content (low temperature and/or relative humidity) the aerosol absorption becomes dominant. The open north Pacific Ocean climatology of FLIR has the following general characteristics:

- (1) Increases from equator northward through mid-latitudes.

Winter:	Equator	10-15 km
	40-50°N	30-35 km
Summer:	Equator	10-15 km
	near 60°N	30 km
- (2) Summer equatorial type ranges extend into mid-latitudes in central and western Pacific. Reflects the northward advection of warm/moist equatorial air over western Pacific.
- (3) The variability of ranges increases with latitude and near coastlines. Reflects the variation of the general weather patterns and specifically the associated variations in temperature, relative humidity, and pressure.

FLIR climatology for the area of Japan and surrounding seas is strongly influenced by coastal, as well as seasonal and latitudinal changes. The result is significantly large variations in FLIR ranges over most of this area on both seasonal and daily or synoptic time scales. FLIR ranges and variations over the area south of about 40°N correlate highly with the monsoon patterns. Equatorial values, near 15 km with about 2 km variations, occur during July and August under the fully developed Southwest Monsoon. Mid-latitude ranges of 25 to 30 km with variations of 10 to 20 km are found during December through March reflecting the Northeast Monsoon and migratory systems. North of about 40°N the FLIR ranges reflect the general middle and high latitude patterns averaging from 20 to 30 km, but are extremely variable with variations approaching the average values.

2.3.3.3 Radar and Microwave

The problems associated with atmospheric refraction and anomalous propagation of radar and radio waves have long been recognized by the U.S. Navy. The development of the computer-based

IREPS (Integrated Refraction Effects Prediction System) by the Naval Ocean System Center (NOSC), originally on Hewlett-Packard 9845 computers aboard selected ships, has significantly enhanced refraction index forecasting. General discussion of refraction and related conditions are addressed in several Navy standard training manuals including the Aerographic's Mate 1 & C training manual.

The refractive index N is defined as the ratio of the speed of propagation of an electromagnetic (EM) wave in a vacuum to that in the actual atmosphere. Refraction is the bending of waves due to a change in density of the medium through which they are passing, the atmosphere for our purposes. Under standard, or "normal", conditions the density of the atmosphere decreases at a gradual but continuous rate with altitude. This density change is a function of decreasing temperature, humidity, and pressure and results in a rate-of-change of N of 12 units/1000 ft. When non-standard temperature and humidity vertical distributions occur the rate-of-change of N becomes non-standard too.

The speed of propagation of an EM wave in a vacuum is greater than in air. Therefore, under normal conditions with decreasing density with height, EM waves travel faster at higher levels in the atmosphere than at lower. The result is that as a wave front, with some vertical extent, moves through the atmosphere the upper portion moves fastest and results in a downward bending or refraction of the wave front. The standard refraction rate however, is less than the curvature rate of the earth's surface. The end result is that under standard atmospheric conditions the wave front gradually moves away from (to higher altitude) the earth's surface but at a lesser rate than a line tangent to the earth's surface.

In the real world the atmosphere is seldom, if ever, standard. The actual refraction is typically slightly greater (super refraction) or less (subrefraction) than standard. Certain conditions occur which disrupt the standard temperature and humidity distributions to the extent that a significant degree of EM wave bending occurs and the wave becomes trapped within a layer of the atmosphere. This occurs under conditions of increasing temperature or sharply decreasing humidity with increasing altitude (as with an inversion). Anomalous propagation (AP) of the radar or microwave energy will then take place. The energy trapped within the layer will provide extended ranges in the layer or duct, but reduced ranges will result in the region which the waves were refracted away from.

There are three general types of ducts: 1) elevated ducts, 2) surface-based ducts that extend down from elevated trapping layers, and 3) evaporation ducts.

Elevated ducts primarily affect airborne operations. They are the result of moisture layers and/or elevated temperature inversions. They may be found anywhere from the surface to 20,000 ft or more, but are most common below 10,000 ft.

Surface-based-ducts can result in extended detection, intercept, and communication ranges for all frequencies above 100 MHz (Petit and Hamilton, 1984). These extended ranges presuppose that both the transmitter and receiver are in or near the duct. Surface ducts typically are found under the southeast quadrant (northern hemisphere), northeast quadrant (southern hemisphere) and near the center of high pressure systems.

Evaporation ducts are created by strong negative vertical water vapor gradients (i.e., water vapor rapidly decreases with

height). Normally they occur within 100 ft of the surface and tend to extend ranges for surface-to-surface systems operating above 3 GHz.

Meteorological factors affecting evaporation duct height climatology for 10 Atlantic ocean weather stations was studied by Sweet (1980). Some general observations from this study are considered applicable to the general problem.

- (1) Evaporation duct heights are normally within 100 ft of the sea surface.
- (2) Evaporation duct heights increase as latitude decreases. Median annual duct heights (the height exceeded half the time during the year) ranged from about 50 ft at 35°N to about 20 ft at 55°N and remained nearly constant to 62°N, the northernmost station in the study.
- (3) Increased air and sea surface temperatures result in higher duct heights.
- (4) In mid-latitude, maximum duct heights occur during late fall and early winter. Minimum duct heights occur in late spring and early summer.
- (5) Stronger winds result in higher duct heights.
- (6) Sea surface temperatures greater than air temperatures result in higher duct heights.

Helvey and Rosenthal (1983) conducted a study to define ways of inferring refraction conditions from synoptic parameters. Considerable scatter or variation in duct conditions was found when attempting to correlate synoptic conditions with refractive conditions, resulting in an acknowledgement in the report that the procedures developed should be considered tentative interim guidance.

Seasonal histograms of duct heights (taken from the Tactical Environmental Support System (TESS) data base) are included for each geographic area.

2.3.4 Forecast Aids for Elevated and/or Surface Based Ducts

The following synoptic features and inferred elevated trapping layer (ETL) indicators are provided for assistance in forecasting ETL conditions for the current time at remote sites. When coupled with forecasting of synoptic or climatological patterns, these inferences can also be helpful in forecasting future ETL conditions.

(1) The strongest and most persistent inversions and associated refractive layers occur in the equatorward half of subtropical oceanic highs, particularly the southeast quadrant in the northern hemisphere and northeast quadrant in the southern hemisphere.

(2) Tracking westward under the equatorward half of the subtropical highs, convection related to warmer SST results in a progressively higher and weaker inversion (and refractive layer) with a correspondingly deeper marine layer.

(3) Changes from fog through low stratus areas to higher stratocumulus and cumulus areas infer a higher and weaker inversion.

(4) Ocean currents influence the thickness of the marine layer. Warm currents, such as the Kuroshio of the western north Pacific weaken and increase the thickness of the marine layer while the cold currents of the northwestern and eastern portion of the north Pacific intensify and reduce the thickness of the marine layer.

(5) Because inversions and ducting are associated with subsidence and stable layers, therefore highs rather than lows, the frequency of ducting shows a strong correlation with SLP. When the SLP is below 1000 mb, the probability of ducting is very low (<10%) while with SLP >1020 the probability approaches 50%.

(6) Duct frequency versus surface wind direction is at a minimum for S through WNW winds and a maximum for NNW through SE winds.

(7) Duct frequency increases as the temperature difference between the surface and 700 mb decreases. Small differences indicate a stable atmosphere (high frequency of inversion and ducts) and large differences indicate an unstable atmosphere and convective activity (low frequency of inversion and ducts).

Forecast Aids for Prediction of Standard Refractive Conditions

- (1) Area of concern is located within the northwest quadrant of subtropical highs or northern half of migratory highs.
- (2) Under or immediately following an active front.
- (3) Area of cyclonically curved isobars.
- (4) Close to a low pressure center.
- (5) Surface pressure less than 1000 mb.
- (6) Cold air aloft, 700 mb temperature less than -10C.
- (7) Presence of cumulus and deep convective clouds.
- (8) Unstable, windy conditions.
- (9) Open celled clouds behind frontal systems.

Forecast Aids for Duct Height

- (1) The maximum frequency of oceanic ducts occurs in the 4,000 to 6,000 ft layer.
- (2) A secondary frequency maximum occurs between the surface and 2000 ft when the SLP is >1018 mb and surface winds are <6 kt (near centers of highs).
- (3) When a migratory upper-level trough replaces a anticyclone, strong low-level ducts are likely to become weak ducts near 10,000 ft within a 48-hour period.
- (4) Within oceanic anticyclones, duct heights vary by about 3000 ft from the lowest level in the SE quadrant to the highest in the NW quadrant.
- (5) In addition to synoptic variations there are general latitude variations. On the average ducts are higher in lower latitude (over warmer water) and lower towards the poles (over colder water).
- (6) There is a tendency for the mean elevated duct heights to increase with increasing SST. Table 2-2 provides approximate mean duct heights for areas within 300 n mi of the center of highs for SST intervals.

Table 2-2. Approximate Mean Elevated Duct Heights (Z_D) for areas within 300 n mi of highs for Specified Sea Surface Temperature Intervals (Helvey and Rosenthal, 1983).

Sea Surface Temperature (SST)		Height MSL (Z_D)	
(C)	(F)	(m)	(ft)
5- 7	41-45	1000	3300
8-10	46-50	1200	3900
11-12	51-55	1300	4300
13-15	56-60	1400	4600
16-18	61-65	1500	4900
19-21	66-70	1600	5200
22-24	71-75	1700	5600
25-27	76-80	1800	6200
>27	>80	2000	6600

(7) A best fit linear regression for optimum coupling height (OCHT), where OCHT is defined as the altitude at which electromagnetic energy is most effectively "coupled" into the duct, is:

$$\text{OCHT (m)} = 42 (\text{SST in } ^\circ\text{C}) + 743$$

Example: SST = 20°C

$$\text{OCHT} = 1583 \text{ m}$$

Based on 5 year study by Ortenburger, L. N. et al. (1978) of GTE, Sylvania, Electronic Systems Group, Western Division, Mountain View, California.

Forecast Aids Based on Satellite Interpretation

(1) The areas of open cells, to the rear of fronts, indicate unstable conditions and therefore are likely to have near-standard propagation conditions.

(2) Areas of closed cells indicate stable conditions, and inversions and ducting are probable.

(3) Areas of smooth low-level stratus are likely to be topped by a low-level inversion, and ducting is likely (may be surface-based).

(4) The appearance of ship condensation trails indicates a strong shallow marine layer and probable surface-based ducts.

(5) Frontal bands imply strong winds, well mixed atmosphere, and near-standard propagation conditions.

(6) Over the region where the closed cells become smaller and change to smooth continuous structures the inversions and duct heights will be lowering.

(7) In regions of offshore flow where clear conditions extend seaward and change to lighter gray shade areas and then smooth stratus type clouds, surface-based ducts are likely. These areas are under the influence of high pressure and subsidence.

(8) In regions of offshore flow where distinct cloudlines are seen forming, near-standard propagation conditions are probable. The areas generally have well mixed and unstable atmospheric conditions.

(9) Improved visibility, EM ranges, and weakened low level inversions are typically found in the lee of mountainous islands. In visual imagery then areas will appear darker than surrounding areas, unless they are in a sunlint area in which case very bright return will be seen if surface winds are light.

(10) Cornering effects result in increased winds, convergence, cloud development, and typically degraded visibility and EM conditions. Cornering effects occur where moderate or stronger winds blow around islands or points of land.

(11) Increasingly lighter gray shades over water areas imply increased atmospheric humidity and/or aerosols and reduced visibility and EM ranges.

(12) When smoke plumes from coastal facilities can be seen extending for some distance in satellite imagery or by eye, a temperature inversion is likely near the top of the smoke plume level.

(13) The SST pattern in shallow coastal water areas will exhibit a strong seasonal reversal relative to the deep water SST. Coastal waters tend to be hot in summer and cold in winter and will modify the atmosphere above it and the EM conditions. Summer heating provides well mixed and near normal conditions. Winter cooling will stabilize the lower levels resulting in low level inversions and generally reduced EM ranges.

2.4 Ocean Acoustics

A complete review of ocean thermal and acoustic properties and resulting sound propagation characteristics is beyond the scope of this handbook. The subjects are addressed in a number of training and information manuals, including general information in the Aerographer's Mate Training manuals and area specific information in Special Publication 3160-NP7. Application programs are also available on the Tactical Environmental Support System (TESS).